CFD ANALYSIS ON AERODYNAMIC EFFECT OF SPOILER ON TOYOTA HIACE MIDIBUS CAR

Bisrat Getachew Agonafir

A Thesis Submitted to

The Department of Mechanical Systems and Vehicle Engineering

School of Mechanical, Chemical and Materials Engineering

Presented in Partial Fulfillment of the Requirement for the degree of Master of Science in Automotive Engineering

Office of Graduate Studies

Adama Science and Technology University

August, 2021 G.C

Adama, Ethiopia

CFD ANALYSIS ON AERODYNAMIC EFFECT OF SPOILER ON TOYOTA HIACE MIDIBUS CAR

Bisrat Getachew Agonafir

Advisor: N. Ramesh Babu (PhD)

A Thesis Submitted to

The Department of Mechanical Systems and Vehicle Engineering

School of Mechanical, Chemical and Materials Engineering

Presented in Partial Fulfillment of the Requirement for the degree of Master of Science in Automotive Engineering

Office of Graduate Studies

Adama Science and Technology University

August, 2021 G.C

Adama, Ethiopia

DECLARATION

I hereby declare that this Master Thesis entitled "**CFD Analysis on Aerodynamic Effect of Spoiler on Toyota Hiace Midibus Car"** is my original work. That is, it has not been submitted for the award of any academic degree, diploma or certificate in any other university. All sources of materials that are used for this thesis have been duly acknowledged through citation.

Bisrat Getachew	________________	________________
Name of the student	Signature	Date

RECOMMENDATION

I, the advisor of this thesis, hereby certify that I have read the revised version of the thesis entitled “CFD Analysis on Aerodynamic Effect of Spoiler on Toyota Hiace Midibus Car” prepared under my guidance by Bisrat Getachew submitted in partial fulfillment of the requirements for the degree of Master’s of Science in Automotive Engineering. Therefore, I recommend the submission of revised version of the thesis to the department following the applicable procedures.

N. Ramesh Babu (PhD)	________________	________________
Major Advisor	Signature	Date

APPROVAL PAGE

I, the advisors of the thesis entitled "CFD Analysis on Aerodynamic Effect of Spoiler on Toyota Hiace Midibus Car" and developed by Bisrat Getachew, hereby certify that the recommendation and suggestions made by the board of examiners are appropriately incorporated into the final version of the thesis.

N. Ramesh Babu (PhD)	____________________	____________________
Advisor	Signature	Date

We, the undersigned, members of the Board of Examiners of the thesis by Bisrat Getachew have read and evaluated the thesis entitled "CFD Analysis on Aerodynamic Effect of Spoiler on Toyota Hiace Midibus Car" and examined the candidate during open defense. This is, therefore, to certify that the thesis is accepted for partial fulfillment of the requirement of the degree of Master of Science in Automotive Engineering.

Chairperson	Signature	Date
Internal Examiner	Signature	Date
External Examiner	Signature	Date
Head of the Department	Signature	Date
School Dean	Signature	Date
Post Graduate Dean	Signature	Date

ACKNOWLEDGEMENT

First of all, I would like to thank immensely my Lord for all His Provisions and Blessings throughout my life and the thesis work. I would also like to thank my parents Getachew Agonafir and Aster Haile, and my Family for their support and encouragement. I would like to express my sincere gratitude for my Advisor N. Ramesh Babu (PhD) for his excellent guidance, moral support and constructive criticism. Finally, I thank my friends and co-workers for their suggestions and helps they provided for me.

TABLE OF CONTENTS

CONTENTS **PAGE**

LIST OF TABLES

TABLE **PAGE**

LIST OF FIGURES

ACRONYMS AND SYMBOLS

AFC	Active Flow Control
BC	Boundary Condition
BL	Boundary Layer
BEM	Boundary Element Method
CAD	Computer Aided Drafting
CFD	Computational Fluid Dynamics
DNS	Direct Numerical Simulation
FVM	Finite Volume Method
FEM	Finite Element Method
LBM	Lattice Boltzmann Method
LES	Large Eddy Simulation
OLD	Outer Layer Device
RAM	Random Access Memory
RANS	Reynolds-Averaged Navier-Stokes
RNG	Re Normalized Group
SST	Shear Stress Transport
3D	Three Dimensional
VG	Vortex Generator
C	Specific Heat Capacity
C_l	Lift Coefficient
CPU	Central Processing Unit
Cop	Coefficient of Pressure
C_d	Drag Coefficient
C_p	Pressure Drag
F_f	Friction Drag
F_l	Lift Force
F_d	Drag Force
Ps	Static Pressure
P_d	Dynamic Pressure
P	Pressure

T	Temperature
V	Speed
kmph	Kilometer per hour
g	Gravity
K	Coefficient of Thermal Conductivity
mm	Millimeters
m/s	Meter per Second
ρ	Density
ε	Epsilon
Φ	Viscous Dissipation Function
μ	Viscosity
%	Percentage

ABSTRACT

Most of the vehicle in modern time have a problem in high-speed driving in which car balance, fuel efficiency, better environment is a major criterion for car manufacturers. When a vehicle travels from place to place the fuel consumption is affected by the aerodynamic drag, lift weight, side forces and thrust. A large percentage of the usable fuel is employed in overcoming the aerodynamic at highway speeds and therefore if reduced could produce a large reduction in the total fuel consumption and reduce the negative environmental effects. There are many vehicles used in Ethiopia for transporting goods and peoples from place to place. Toyota HiAce midibus (dolphin) is one of the many vehicles that are used in Ethiopia for transportation. The main objective of this thesis work is to study the effect of spoiler on aerodynamic performance of the Toyota HiAce midibus(dolphin) in order to improve the overall aerodynamic behaviour of the vehicle. The analysis were performed using spoiler with different angle of inclination by computational fluid dynamics (CFD). A baseline model of the vehicle modeled with solid works with scale of 1:12 was analyzed at various speeds and improvement in drag coefficient and lift coefficient were obtained in models with spoiler when compared to the baseline model without any Add-on device. A drag reduction of 15.21%, 3.44% and 2.02% was achieved on spoiler with 0 , 8, 12 angle inclination respectively when compared to the baseline model. Because of the reduced drag, the fuel consumption was reduced by 9.12%. The lift coefficient of the baseline was also reduced by 65.9%, 33.87% and 26.43% for spoiler with 8 ,12, 0 angle of inclination respectively at 120 kmh. This reduction in lift coefficient increases the vehicle stability at higher speed. The overall aerodynamic performance of the vehicle improved using spoiler as an Add-on device which lead to better fuel economy and stability of the vehicle.

Keywords: Add-on device, Aerodynamics, CFD, Drag and Lift coefficient, Spoiler.

CHAPTER ONE
INTRODUCTION

In this chapter background of the study, statement of the problem, objective of the study, scope of the study, significance of the study, beneficiaries, and structure of the study are included.

1.1. Background

The subject "Aerodynamics" studies with air flow passing over the automobile and also the behavior of air flow with the help of experimental setup like as Wind Tunnel as well as theoretical (analytical or semi analytical) and computational fluid dynamics (CFD) approaches respectively. It primarily the way of flowing gaseous medium which might be air, helium or any other gas that depends on the condition. Anything is passing through air then effect of aerodynamic is shown, like rocket launching, kite flying in sky. Even cars passing through air is also affected by aerodynamics effect. CFD analysis is only reliable device to evaluate particular design parameter of a generic shape of automobiles. CFD is a branch of fluid mechanics that is used in analysis of numerical methods and algorithms that involves fluid flows the study of the system is related in way of computer-based simulation.

Nowadays around 50% of fuel is consumed by ground vehicle all over worldwide and affected 60% greenhouse gas affected by the emission of gases from consuming fuel. In recent times increasing the greenhouse effect in global warming world to reduce CO_2 emission with the help increasing the performance of automobile by lowering the coefficient of drag by using the various methods like passive flow control system ex. Ahmed body, Add-on Device, VG is concluded (Shinde & Shende, 2017). The effect of aerodynamic design is increasing fuel efficiency, reducing drag and also improving the stability of automobile in high speed (Cheah et al., 2007). In our country Ethiopia road traffic accident that occurs due to passenger cars is 35% (Abegaz & Gebremedhin, 2019).

When a driver drives at higher speed which is above 110 kmph especially at high ways the vehicle can have a tendency to lift over. This happens because there is a high pressure Infront of the wind shield causing the pressure to drop. Then when the lower pressure passes the top part of the vehicle causing higher pressure at lower part of the vehicle. Which in turn affects the performance of the vehicle. So, efforts in research have been employed for better fuel economy and performance of road vehicles.

It's important to add extra parts to the body of a vehicle like rear spoilers, lower front and rear bumpers, air dams and many more aerodynamic aids as the performance handling, safety and comfort of a vehicle is majorly affects the aerodynamic properties of the vehicle. And this extra part designed in lowering drag of the vehicle which is important to increase stability. Rear spoiler is a component which is used to decrease the overall drag, and also to increase downward force of a vehicle especially passenger car. It is an aerodynamic device that is designed to 'spoil' unimportant air motion across a car body. Main fixing location is at rear portion, depends on shape of the rear portion either the car is square back, notchback or fastback because not all rear spoiler can be fixed at any type of rear portion of a car. However, spoiler can also be attached to front/rear bumper as air dam. The use of rear spoiler can contribute to the reduction of drag. Lowering drag force can save fuel; Moreover, spoiler can also be used to control stability at cornering. Besides reducing drag, it can reduce rear-axle lift.

1.2. Statement of the Problem

Now a days vehicle manufacturers companies' priorities are vehicle stability in high speed, fuel consumption and etc and one way of doing this is by reducing drag and lift on vehicles with different add-ons on the vehicles. And in our country Ethiopia, there are different kinds of passenger cars, one of them is called passenger car (locally called dolphin) vehicle. Dolphin passenger car which is used in Ethiopia for transportation of the goods and people causes accidents due to lack of stability at higher speeds due to the development of lift-over tendency. When a driver drives at higher speed which is 110 kmph especially on high ways the vehicle can have a tendency to lift over. This happens because there is a high pressure Infront of the wind shield causing the pressure to drop. Then when the lower pressure passes the top part of the vehicle causing higher pressure at lower part of the vehicle. Which in turn affects the performance of the vehicle. To overcome this problem spoiler was added at various angle of inclination at top back of the vehicle and investigated by using CFD.

1.3. Objectives

1.3.1. General Objective

The general objective of this study is to investigate aerodynamic effect of spoiler on dolphin car by using CFD.

1.3.2. Specific Objectives

The specific objectives are: -

- To model the vehicle by SOLIDWORKS.
- To model the spoiler’s using CAD.
- Meshing the models using ANSYS meshing.
- To investigate the vehicle by CFD with and without spoiler at different speeds (kmph)
- To estimate the drag and lift with varying shape and angle of spoiler using CFD

1.4. Significance of the study

The result of this thesis can be significantly useful for individuals, researchers and manufacturers who are engaged in vehicle body design, to reduce the drag and lift forces. It is true that aerodynamics can be improved by properly designing various component profiles.

1.5. Beneficiaries of the study

Vehicle manufacturer, researchers, vehicle owners, society and country as a whole benefitted with this work.

1.6. Scope of the study

The thesis work includes the modeling of the Dolphin car with and without spoiler and investigating the influence of spoiler on aerodynamic behavior of the car. Study on the effect of varying shape and angle of spoiler on lift and drag acting on the car using CFD is also included in this work.

1.7. Limitations

In the automotive industry, aerodynamic analysis is carried out in two ways: Experimentally (Wind-tunnel test) and Numerically using ANSYS Fluent software. To perform the numerical analysis, it’s necessary to use a high-performance computer to obtain accurate results. Moreover, there are no large-sized powerful Wind-tunnels and high cost of preparing a 3D model of Dolphin vehicle are the main limitations. The study also focus on a simplified 3D model of Dolphin vehicle aerodynamic performance excluding parts such as side-view mirrors, windscreen wipers while designing the models.

1.8. Structure of the report

This thesis report consists of five chapters. The first chapter begins with introduction about the study. It includes the background of study, statement of the problem, objectives, scopes, significant of the study, beneficiaries and structure of the report. Chapter two focuses on different literatures which emphasize on study of vehicle aerodynamics. Chapter three describes materials and methodology used to complete this work. The results and discussions are presented in chapter four. The generated data of pressure force, lift force, drag coefficient and lift coefficient are presented in form of tables and graphics for quantitative and qualitative discussion. The contours of flow are also discussed to understand the best design characteristics. The final chapter of this thesis consists of conclusion, recommendations and future scope of the work.

CHAPTER TWO

LITERATURE REVIEW

To understand the study of aerodynamics and CFD analysis, reviewing different literature is very important to fully understand the aerodynamics of different vehicles. Literature review mainly include different researches on aerodynamics. It also includes reviewing previous aerodynamic studies and analysis on different vehicles.

2.1. Previous Investigations

Studies on aerodynamic drag of Skoda car and successfully simulated with ANSYS fluent solver the analysis shows aerodynamics drag in term of drag forces or drag coefficient proportionally increased to the square of velocity for car body and the drag is reduced from 0.325 to 0.305 in our CFD analysis. On this investigation modification on exterior body of a car can increase aerodynamic performance which in return reduces coefficient of drag. Reducing drag have impact on fuel consumption (Socrates et al. 2018).

On the study using sedan car with out changing the outer profile of the car by using vortex generator as add-ons device to reduce drag and lift forces. The outer profile of the sedan car was generated using 3d modelling software. Therefore, without modifying the car profile the reduction of 6% of drag and negative lift force can be attained by adopting vortex generator as an aerodynamic add on device (Selvaraju et al. 2015).

This study implies there is a possibility of drag reduction in exterior body modification. For estimation of drag and lift forces achieved successfully by using CFD and aerodynamic drag for car body profile is simulated using ANSYS fluent solver, the analysis shows aerodynamics drag in term of drag forces or drag coefficient proportionally increased to the square of velocity for car body. These modifications are helpful in reducing the coefficient of drag i.e. Cd which effects the fuel consumption. By these modifications the coefficient of drag is reduced by approximately 2.18% (Velagapudi et al. 2015).

On the study of design and aerodynamic analysis to improve the performance of the vehicle, Toyota fortuner was analized using solidwork on outer parts only. The car was assumed to move at speed of 100km (30m/s). when investigated at this speed the car may rollout at higher speed or serious conditions. So to improve this problem external body modification and optimization has been carried out. And the result was better than the previous one when optimized and increased performance (Siva & Loganathan, 2016).

On this study different kinds of spoiler angles are used for reduced drag and lift forces. On the analysis six (6) different modification was used. And the 12 degree inclination is better and creates 1.56% extra CD than 4 degree inclination and minimum CL is maintained for the sake of high speed cars (Das & Riyad, 2017).

Analysis was carried out using computational fluid dynamics (CFD) by using ANSYS Fluent. A passenger sedan car was used for rear spoiler at high speed. From the analysis using rear spoiler increases the drag from 0.001 to 0.0045, which is a 350% increase, while the lift coefficient reduces from 0.0005 to -0.006 which is a 1300% lift reduction. For high speed vehicles reduction in lift coefficient is very important b/c of stability, in producing tire capacity in cornering and improves braking performance. In general they investigated and come to conclusion , for passenger cars its important having drag reduced b/c the priority is driving safely and for high speed cars reduction in coefficient of lift is important b/c of the above mentioned points (Ipilakyaa et al. 2018).

CFD analysis was carried out on production vehicles. Diffuser was added in rear end of the vehicle with 8 degree inclination. The lift coefficient was reduced by 34% while the drag slightly increased by 0.5%. Also by increasing the angles to 10 degrees, 15 degrees, reduces the lift coefficient but increasing drag reduction. The addition of a diffuser at 8 degree to the original vehicle reduces lift coefficient with negligible increase in drag. In conclusion such modification in selected cars improves stability which is handling capability in high speed (Parab et al. 2014).

Another study was conducted in evaluating the concept of aerodynamic effects using rear spoilers in small vehicles. On this analysis rear spoiler can be beneficial in reducing coefficient of lift force. Also raising deck height without affecting aesthetic of the vehicle can get rid of small vortex generator. By understanding wake region phenomenon and modifying it can be used in reducing drag and increasing fuel efficiency (Ghanegaonkar & Hiwase, 2014).

A simplified hatchback model was analogized using RANS-based CFD simulation on rear-roof spoiler on aerodynamic drag performance. Increasing the pitch angle can increase coefficient of drag but within the range of 0 degree to 5 degree the result shows the simple strip-type spoiler is beneficial. And also, on this analysis spoiler relies on two mechanism in reducing aerodynamic drag. The first is preventing the air flow from accelerating at the leading edge of the slant section and the second is preventing the formation of longitudinal vortices of side edge of the slant section (Kane et al. 2016).

On this analysis Modeling of sedan kind of automobile is completed using SOLIDWORKS. Analysis of effect of the rear spoiler in the automobile is completed using ANSYS FLUENT style software system. The Analysis and Modeling of automobile without the rear spoiler and therefore the CD (Coefficient of drag=1.294) was solved. The Analysis and Modeling of automobile with a rear spoiler and also the CD (Coefficient of drag=0.988) was calculated (Bhalerao et al. 2019).

On this study it can be judged that aerodynamic drag is the most important factor which is responsible for Fuel consumption, power loss and top speed in a vehicle. It is also concluded that the external design features of a vehicle account highest in reducing the effects of drag in a vehicle (Sarkar et al. 2019).

On this study the analysis was drag reduction with or without add-on devices on the passenger car with CFD simulation. Ansys-fluent was used on the analysis and the result was drag reduced up to 4.32% and coefficient of lift is reduced up to 18.83% due to addition of spoiler with vortex generator. With add-ons devices installed on the passenger cars aerodynamic drag and lift can be reduced to increase fuel efficiency and stability of the vehicle (Bansal & Sharma, 2014).

Investigation on CFD analysis of aerodynamics of a car which results in pressure difference between front end and rear end by introducing a duct on the roof of the vehicle but there is no significant drag reduction on the vehicle after applying a duct on the roof of the vehicle (Varma et al. 2018).

The analysis conducted shows that there is an increment in the drag coefficient of the car of 47.20% when attached with a spoiler. However, the lift coefficient value shows a tremendous declination from 0.03957 to -0.16254. The result of this study show that an attached spoiler could increase the drag coefficient and decrease the lift coefficient of a car. The best spoiler should have a least increment in the drag coefficient and considerable decrement in the lift coefficient (Nawam et al. 2018).

This study found that ERC model with spoiler would have better aerodynamic efficiency compared to ERC model without spoiler. Also, S1223 at -6 degrees was identified as the optimized configuration as it generates the highest downforce. Even though the drag coefficient at this setting angle is slightly higher, but in terms of stability and handling IT is at its best (Eftekhari et al. 2020).

In this study paper the variations of coefficient of lift and drag with and without vortex generators (VG) on the roof of a generic passenger car have been studied at varying yaw angles of VG. The yaw angles used are 10°, 15° and 20°. To measure the effect of altering the vehicle body, wind tunnel tests have been performed with 1:15 scaled model of the utility vehicle with velocities of 2.42, 3.7, 5.42 and 7.14m/s. This analysis shows that a great improvement of the aerodynamic drag force reduction can be achieved with vortex generator (Sharma & Bansal, 2013).

In this paper the effect of spoilers on aerodynamic characteristics of an airfoil were observed by CFD.As the experimental airfoil NACA 2415 was chosen and spoiler was extended from five different positions based on the chord length C. Airfoil section is designed with a spoiler extended at an angle of 7 degree with the horizontal. The spoiler extends to 0.15C.The geometry of 2-D airfoil without spoiler and with spoiler was designed in GAMBIT. The numerical simulation was performed by ANSYS Fluent to observe the effect of spoiler position on the aerodynamic characteristics of this particular airfoil. The results obtained from the computational process were plotted on graph and the conceptual assumptions were verified as the lift is reduced and the drag is increased that obeys the basic function of a spoiler (Mashud et al. 2012).

In this study, two different types of simulations were made, one for the flow around a simplified high speed passenger car with a rear-spoiler and the other for the flow without a rear-spoiler. The standard k-! model is selected to numerically simulate the external flow field of the simplified Camry model with or without a rear-spoiler. Through an analysis of the simulation results, a new rear spoiler is designed and it shows a mild reduction of the vehicle aerodynamics drag. This leads to less vehicle fuel consumption on the road (Hu & Wong, 2011).

2.2. Passenger vehicle aerodynamics

Modeling of Honda Civic R 2009 is done using SOLIDWORKS. Analysis of effects of rear spoiler in automobile is done using AUTODESK flow design software. The Modeling and analysis of Honda Civic R 2009 car without rear spoiler and the CD (Co efficient of drag=0.28) was calculated. The Modeling and analysis of Honda Civic R 2009 car with rear spoiler and the CD (Co efficient of drag=0.21) was calculated (Ganesh & Vasudevan, 2015).

In this paper, the effects of installing a rear spoiler on performance of an EV were investigated through simulations and practical test. All components of an EV were modeled and it was shown that installing a rear spoiler reduced the drag coefficient up to 7 per cent which in turn reduced the energy consumption of vehicle. Furthermore, the lift coefficient decreased from 0.008 to -0.036. These reductions also entail another benefit which is the reduction of emission in ICE cars, but, in EVs the benefits are not limited just to abovementioned items (Tousi et al. 2015).

CFD study on aerodynamic effcts of a rear wing/ spoiler on a passenger vehicle, When the vehicle is moving at a certain velocity, the viscous effects in the fluid are restricted to a thin layer called boundary layer (Cakir, 2012).

CFD Analysis of Automobile Rear Dynamic Spoiler From the analysis part the maximum downward pressure created at an angle 20^{o} and at angle 8^{o} where the minimum pressure has been produced. The stopping distance of the car model with spoiler has been reduced at an angle20^{o} . When the car is in running, at initial condition the spoiler angle kept is 8^{o} and the spoiler moves to angle 20^{o} when the brake is applied which is manually attached to break pedal. The effect of spoiler has become effective when the angle of spoiler increases downward. The stopping distance of car has been reduced to 4.52 % at a speed of 150 km/hr, and the friction between the tire and road has been increased due to the pressure acting downward which is considered as mass acting on rear of car at particular condition (Sivanesh Prabhu. M, Arulvel. S, 2017).

This paper the aerodynamics of vehicle was analyzed at constant velocity for various spoiler angles with respect to ground. The comparison between the vehicle with spoiler and without spoiler is also done. The computational results with spoiler are compared with the experimental data. The results of the CFD analysis are somewhere very close to exact but are approximate as we had done 1000 iterations. In the analysis we the used spoiler at various angle i.e. 0, 10, 20 and 30 degree. In the analysis we got the results for coefficient of drag and drag force (Tomar et al. 2019).

This study observing the CFD analysis results the pressure drop and velocity, drag force, lift force and mass flow rate will be increases by increasing the speeds. The drag forces decreases at modified model by the speed 70 km/hr. lift force will increases at modified model by the speed 110 km/hr. So it can be concluded the lift force more for modified model by the speed at 110 km/hr so modified model of spoiler is better model (Kumar, 2017).

This paper investigates the effect of rear spoiler on sedan and front spoiler above windshield of a hatchback model. The comparison is done on both with and without spoiler. The CFD investigations are done with 3 turbulence models which show that the drag marginally increases, but there is reduction in lift which implies increase in down force. Some researchers have found marginal reduction in drag also. However the benefits of increased down force and road traction should offset the increment in drag. Moreover the spoiler does its function at higher speeds .Movable flaps are used in aerospace applications to counter transient conditions, however these devices need additional power from prime mover which is not justifiable in case of road vehicles (Yakkundi & Mantha, 2018).

This paper It is found that the coefficient of drag, coefficient of lift, wake region is affected with the addition of spoiler. Following conclusions can be drawn from the above analysis, Coefficient drag was increased by 8.33% with the addition of spoiler, Coefficient of lift was reduced by 59.09% with the addition of spoiler and It is found that the flow was attached for a longer length of rear end of car without spoiler due to which wake region was smaller. With the introduction of spoiler the flow was separated at the spoiler which resulted in increased wake region (Kazi et al. 2016).

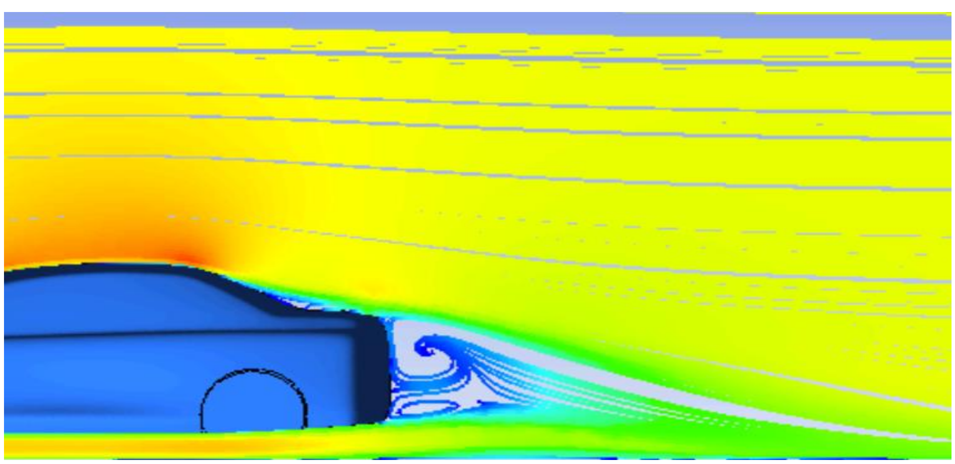

Figure 2.1. stream line on external flow over vehicle

Figure 2.1, shows the streamline of an external flow around a stationary vehicle. When the vehicle is moving at a certain velocity, the viscous effects in the fluid are restricted to a thin layer called boundary layer. Outside the boundary layer is the inviscid flow. This fluid flow imposes pressure force on the boundary layer. When the air reaches the rear part of the vehicle, the fluid gets detached. Within the boundary layer, the movement of the fluid is totally governed by the viscous effects of the fluid. The Reynolds number is dependent on the characteristic length of the vehicle, the kinematic viscosity and the speed of the vehicle. The fluid moving around the vehicle is dependent on the shape of the vehicle and the Reynolds number. There is another important phenomenon, which affects the flow of the car and the performance of the vehicle. This phenomenon is commonly known as 'Wake' of the vehicle. When the air moving over the vehicle is separated at the rear end, it leaves a large low-pressure turbulent region behind the vehicle known as the wake. This wake contributes to the formation of pressure drag, which is eventually reduces the vehicle performance.

2.3. Flow control

Flow control have been used for many years to control the fluid flow, and some employ different concepts to serve this purpose in last decades. The ability to manipulate a flow passively or actively is of immense technological importance (Jahanmiri, 2010). The classification of flow control methods are given in Figure 2.2.

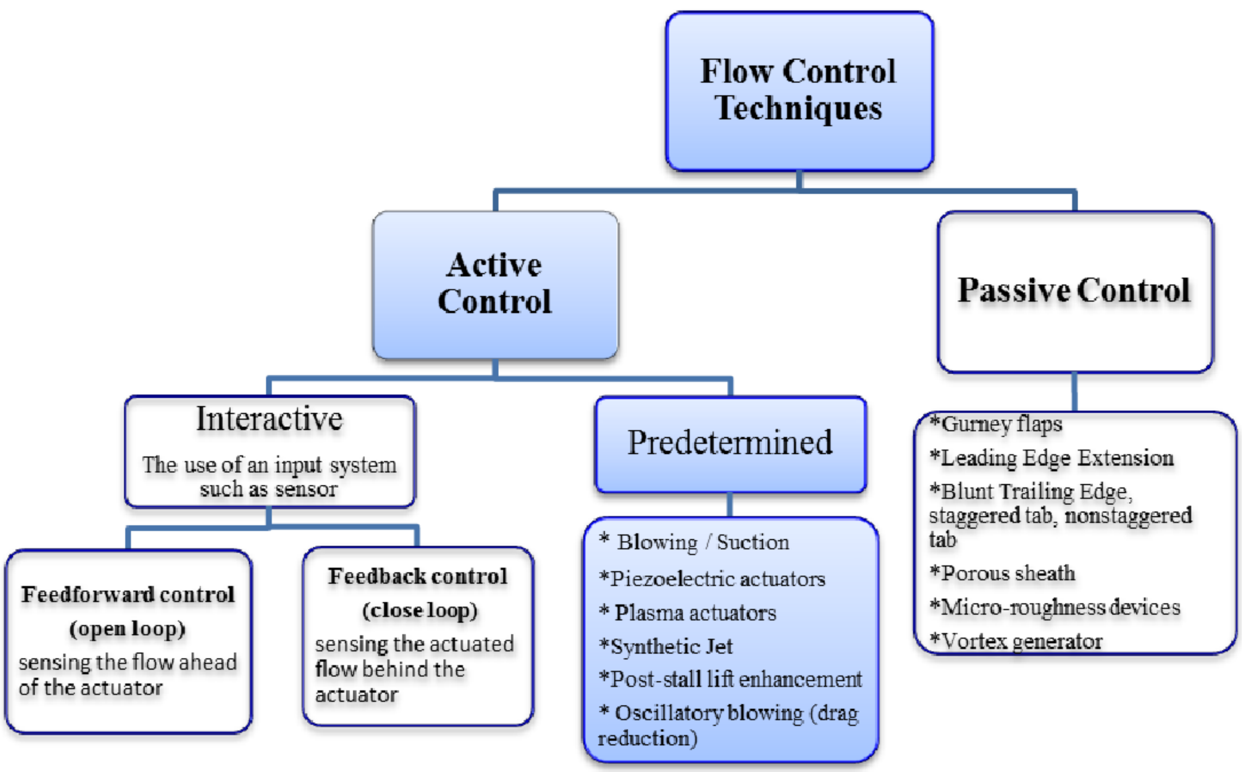

Figure 2.2. Flow control methods

2.3.1. Active flow control

Active flow-control (AFC) is a fast growing multi-disciplinary science and technology aimed at altering a natural flow state or development path into a more desired state (or path). The theory of AFC is of limited scope due to the inherently nonlinear nature of the leading physical processes. Still, significant insight can be gained by considering linear stability analysis of simplified problems, as a first-order approximation helping identify unstable mechanisms that can enhance performance, isolate optimal leading parameter ranges and increase efficiency. Significant progress has been made in control theory for optimal and automated design of closed-loop controllers that can be applied to AFC systems given a sufficiently accurate and efficient model of the system. Likewise, progress made in computer capabilities(processing speed, memory, storage, and parallel processing)has been accompanied by similar efforts to resolve modeling issues (of turbulence and algorithms) and arrive at efficient and validated numerical tools for unsteady flow computations at relevant Reynolds numbers (Jahanmiri, 2010).

2.4. Control Application

To successfully apply active flow control, several basic questions should be answered. First the control objective to be achieved is specified (e.g., increased lift). Secondly, the flow phenomenon to be controlled or leveraged is identified (e.g., boundary layer separation). Flow physics is key to scaling and determining influential parameters. An appropriate actuation strategy is then selected (e.g., predetermined open-loop control or feedback control). Finally, a range of operation for the key control parameters is determined (e.g., forcing frequency and amplitude). Several recent successful applications of active flow control are highlighted. The review is intended to provide a sampling of some of the ongoing research in this burgeoning area of fluid mechanics. But before elaborating the examples of AFC, the roadmap to apply different control methods is explained (Jahanmiri, 2010).

2.4.1. Control of jets

For the reasons like increasing mixing, reduce jet engine noise, and ―vector‖ the jet thrust, there was a lot of interest in the control of jets by means of periodic perturbation. A combination of water tunnel and high-speed airflow facilities is used to assess the near-field jet behaviour. Solid tabs, steady fluid tabs (i.e. discrete radially discharged control jets located close to the core jet exit), and pulsed fluid tabs are compared. The effect of fluid tab velocity amplitude, pulse rate, and pulse phase are studied using open loop control. The measurements indicate that fluid tabs generate a similar streamwise vortex formation process (and hence display increased mixing) as previously observed in solid-tabbed nozzle flows. In incompressible testing the mixing effectiveness with a pair of pulsed fluid tabs 180° out-of-phase was as good as a twin solid tab nozzle for a control jet flow rate of only 0.5 percent of the primary (core) jet flow (Jahanmiri, 2010).

2.4.2. Contributing factors to flow field on vehicles

The major factors, which affect the flow field around the vehicle, are the boundary layers, separation of flow field, friction drag and lastly the pressure drag.

2.5. Boundary layer

The equations of fluid flow by dividing the flow field into two areas: one inside the boundary layer and the one outside the boundary layer. In this boundary layer around the vehicle, the viscosity is dominant and it plays a major role in drag of the vehicle. The viscosity is neglected in the fluid regions outside this boundary layer since it does not have significant effect on the solution. In the design of the body shape, the boundary layer is given high attention to reduce drag There are two reasons why designers consider the boundary layer as a major factor in aerodynamic drag. The first is that the boundary layer adds to the effective thickness of the body, through the displacement thickness, hence increasing the pressure drag (Pranav et al. 2017).

2.6. Flow separation

In Figure 2.3 the flow over the surface of the vehicle, there are some points when the change in velocity comes to stall and the fluid starts flowing in reverse direction. This phenomenon is called ‘Separation’ of the fluid flow. This usually occurs at the rear part of the vehicle. This separation is mostly dependent on the pressure distribution, which is imposed by the outer layer of the flow. This separation causes the flow to change its behavior behind the vehicle and thereby affects the flow field around the vehicle. This phenomenon is the major factor to be considered while studying the wake of the vehicle. Flow separation is bad because it leads to a larger wake and less pressure on the rear surface which reducing pressure recovery. To avoid bad flow separation, the transitions of the airflows from roof to the rear window need to be smoothed. The bad separation also can create more drag. The aerodynamic will be more effective if the flows working in clean air (laminar flow). By improving the aerodynamic of the car can reduce the boundary layer thickness thus avoids worst flow separations (Pranav et al. 2017).

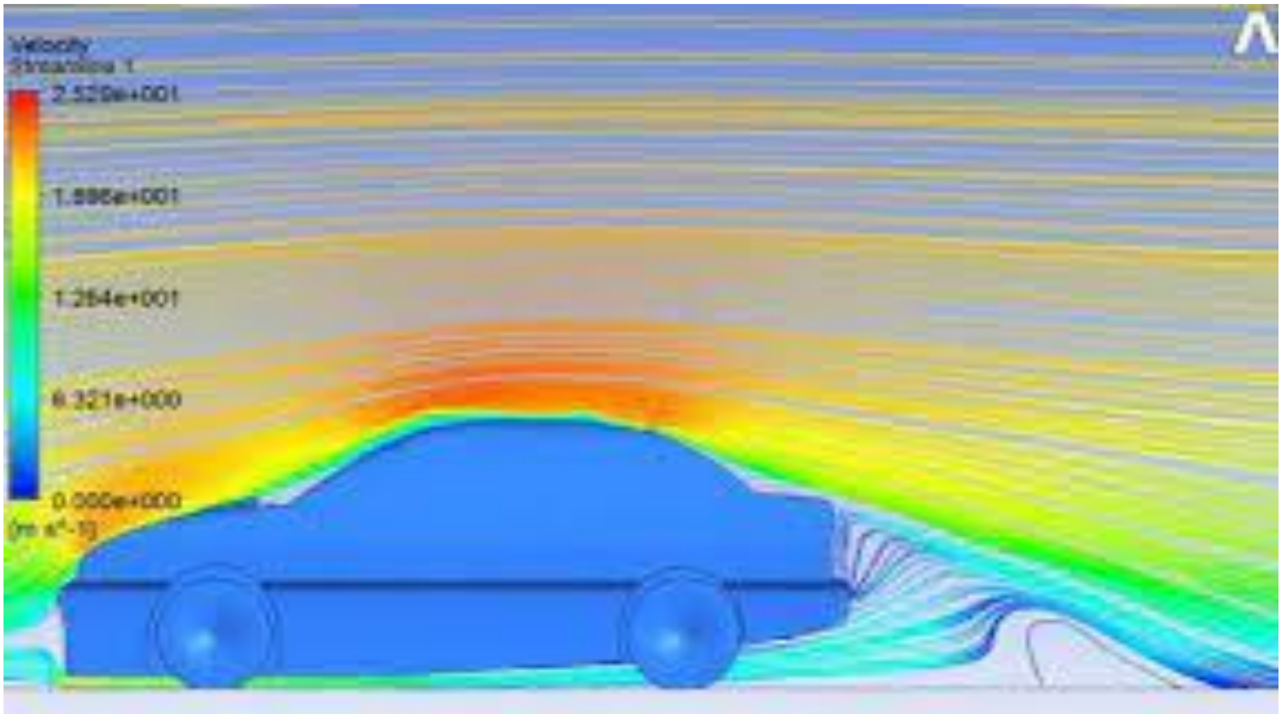

Figure 2.3. Flow separation at the rear of the vehicle

2.6.1. Friction drag

Every material or wall has a distinct friction, which resists the flow of fluids. Due to molecular friction, a stress acts on every surface of the vehicle. The integration of the corresponding force component in the free stream direction leads to a friction drag. If the separation does not occur, then friction drag is one of the main reasons to cause overall drag.

2.6.2. Pressure drag

Behind the vehicles, there is a steep pressure gradient, which leads to the separation of the flow separation in viscous flow. The front part of the flow field shows high-pressure value, whereas on the rear part flow separates leading to a high suction in the area. As we integrate the force component created by such high change in pressure, the resultant is called as ‘Pressure Drag’. This factor is affected by the height of the vehicle as well as the separation of the flow field.

2.7. Forces and moment on vehicle

When the vehicle is moving at a considerable speed, there are several forces are applied to vehicle in different directions. Figure 2.4 shows the details sketch view of the various forces acting on the vehicle body.

As shown in the free body diagram below, there are six forces acting on the vehicle:

- ♣ Rolling Resistance
- ♣ Drag
- ♣ Lift
- ♣ Gravity
- ♣ Normal
- ♣ Motor

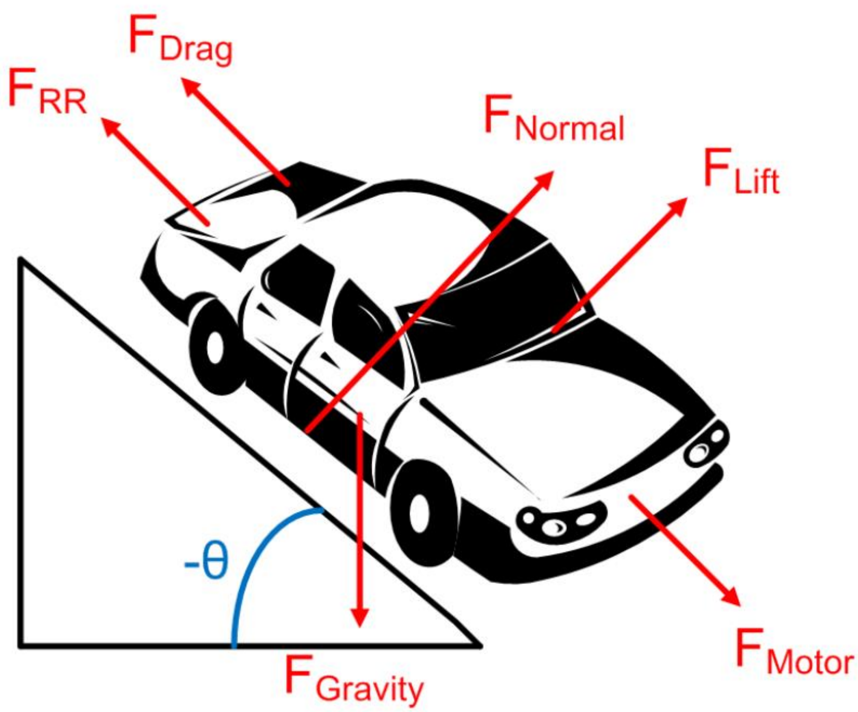

Figure 2.4. Forces on vehicles body

Rolling resistance force is due the tires deforming when contacting the surface of a road and varies depending on the surface being driven on. The normal force is the force exerted by the road on the vehicle's tires. Because the vehicle is not moving up or down (relative to the road), the magnitude of the normal forces equals the magnitude of the force due to gravity in the direction normal to the road.

Lift force acting on the vehicle body vertically. This force causes the vehicle to get lifted in air as applied in the positive direction, whereas it can result in excessive wheel down force if it is applied in negative direction. Engineers try to keep this value to a required limit to avoid excess down force or lift. The formula usually used to define this force is written as:

$$C_L = \frac{L}{1/2\rho V^2 A} \quad \ldots\ldots\ldots\ldots\ldots\ldots\ldots\ldots\ldots\ldots (2.1)$$

Where:

L: Lift force

C_L: Lift coefficient

A: Frontal area of the vehicle

ρ: Air density

V: Vehicle Velocity

Aerodynamic drag force is the force acting on the vehicle body resisting its forward motion. This force is an important force to be considered while designing the external body of the vehicle, since it covers about 65% of the total force acting on the complete body. The Aerodynamic drag force is calculated by the following formula:

$$C_D = \frac{D}{1/2\rho V^2 A} \quad \ldots\ldots\ldots\ldots\ldots\ldots\ldots\ldots\ldots\ldots (2.2)$$

Where:

D: Drag force

C_D: Drag coefficient

A: Frontal area of the vehicle

ρ: Air density

V: Vehicle Velocity

2.8. Passive flow control

The passive control systems consist on the use of more or less discrete obstacles, added around or on the roof of the vehicle. They can be declined in two groups according to their influence on the flow control. The first group consists on obstacles positioned on the surface of the geometry. The second group consists of the obstacles positioned upstream or downstream of the geometry to be controlled (Sudin et al. 2014).

2.8.1. Passive control: Effect of VG on aerodynamic drag

A VG is an aerodynamic surface which is basically a small vane that creates a vortex. VG widely used in the aerospace industry, mainly to control boundary layer transition and to delay flow separations. Figure 2.5 different type of VG is used figure on race cars for manipulating the flow over and under the vehicle, mainly to generate down force (which is needed for better performance). The airfoil shaped VGs were tested to demonstrate the incremental effect of the vortex wake and the effect of rake (vehicle's angle of attack), was investigated as well. The results of this study provide quantitative information on the expected loads and pressure distribution behind such large-scale VGs; data needed for the successful application of such devices to actual vehicles. In order to delay the flow separation at the rear, bump-shaped VGs at the roof end of a car were tested for two different types of car models Sedan and Hatchback. In separate study, the aerodynamic analysis was carried out using GAMBIT and FLUENT for Sedan and Hatchback models. CFD analysis confirms that the use of VGs reduces both the drag and lift coefficient (Sudin et al. 2014).

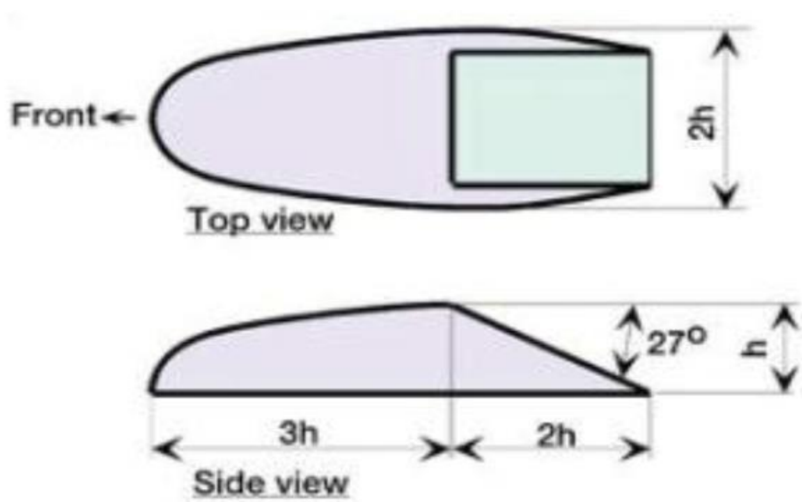

Figure 2.5. Position of VG at the rear end of the roof (above) dimensions of a bump shaped VG

2.8.2. Passive control: Effect of spoiler on aerodynamic drag

The spoiler is used as a tool to minimize unfavorable air movement around the vehicle and can be divided into the front spoilers and the rear spoilers. A front spoiler, connected with the bumper, is mainly used to direct air flow away from the tires to the underbody. A rear spoiler is commonly installed upon the trunk lid of a passenger vehicle (Sudin et al. 2014). The added spoiler can diffuse the airflow passing a vehicle, which minimizes the turbulence at the rear of the vehicle, adds more downward pressure to the back end and reduces lift acted on the rear trunk. The rear spoiler is no longer just a decoration and they do have measurable effect on aerodynamic drag reduction and vehicle stability. The simulation of external aerodynamics is one of the most challenging and important automotive CFD applications. With the rapid developments of digital computers, CFD is used as a practical tool in modern fluid dynamics research. It integrates fluid mechanics disciplines, mathematics and computer science. With high-speed automobiles much more common nowadays, reducing the lift coefficient to enhance stability on the road is no longer just a concern for race cars. Spoilers are one of the well-known devices for producing down force on a moving vehicle. Studied the flow around a simplified high speed passenger car with a rear-spoiler and without a rear-spoiler. The standard k-ε model was selected to numerically simulate the external flow field of the simplified Camry model with or without a rear-spoiler. Through an analysis of the simulation results, a new rear spoiler was designed and it shows a mild reduction of the vehicle aerodynamics drag. This leads to less vehicle fuel consumption on the road. Studied the three-dimensional turbulent flow over both a simple car model and a real road vehicle. They found that flow pattern and the results for aerodynamic forces were in good agreement with experimental results. In addition, the same method was used to investigate the effect of numerous rear-spoilers on lift and drag coefficients of the models. They found a significant reduction in lift and drag on the models. The popular k-ω SST turbulence model was used to assess aerodynamic forces, as well as pressure and velocity distribution.

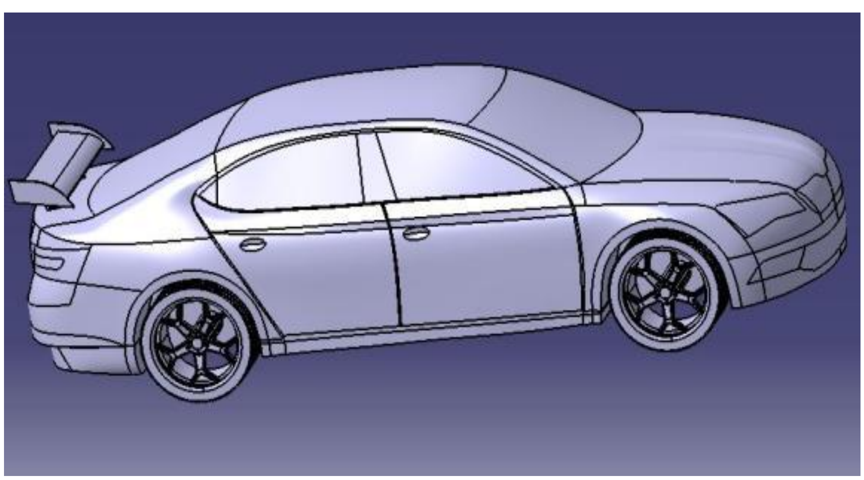

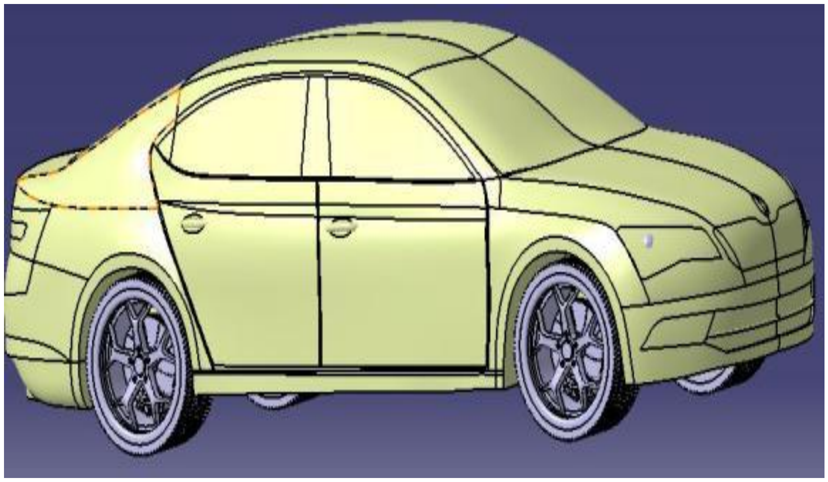

Figure 2.6. Automobile without and with Spoiler effect (S. Socrates, 2018)

2.8.3. Passive control: Underbody diffuser

Analyzing the effect of applying drag reducing devices on a sedan, sports utility vehicle (SUV) and a tractor trailer model to improve the fuel consumption of the vehicle. Both RANS (Reynolds-averaged Navier–Stokes equations) and LES are used to analyze the percent drag reduction due to the use of different drag reducing devices. The numerical procedure is first validated against the experimental data for the tractor-trailer model with no drag reducing devices installed. Following the validation, simulations are carried out to investigate the percent drag reduction by installing a modified front head to help the flow transition from the tractor to the trailer, and inventive rear wings that direct the air flow towards the rear of the vehicle where low pressure exists. The tractor trailer results showed a total drag reduction of around 21% when the front and rear drag reducing devices was installed. Reducing resistance forces all over the vehicle is the most sustainable way to reduce fuel consumption. Aerodynamic drag is the dominating resistance force at highway speeds, and the power required to overcome this force increases by the power three of speed. The exterior body and especially the under-body and rear-end geometry of a passenger car are significant contributors to the overall aerodynamic drag. To reduce the aerodynamic drag it is of great importance to have a good pressure recovery at the rear. Since pressure drag is the dominating aerodynamic drag force for a passenger vehicle, the drag force will be a measure of the difference between the pressure in front and at the rear. There is high stagnation pressure at the front which requires a base pressure as high as possible. The pressure will recover from the sides by a taper angle, from the top by the rear wind screen, and from the bottom, by a diffuser. It is not necessarily the case that an optimized lower part of the rear end for a wagon-type car has the same performance as for a sedan or hatch-back car (Sudin et al., 2014).

2.8.4. Passive control: Others add-on devices

Numerically investigated the use of lateral guide vanes as a drag reducing device for ground vehicles. Two types of ground vehicles were considered, a simplified bus model and a simplified sport utility vehicle (SUV) model. The guide vanes were used to direct air into the low-pressure wake region in order to enhance pressure recovery, which in turn would reduce form drag and hence the overall aerodynamic drag. CFD simulations were used to assess the efficiency of the drag reducing device. The steady-state simulations were based on the RANS equations, with turbulence closure provided through two-equation eddy-viscosity models. Guide vane cross-section, chord length and angle of attack were varied in order to obtain the optimal configuration for improved aerodynamic performance. Results of simulations indicated that an overall reduction in the aerodynamic drag coefficient is up to 18% for the bus and SUV models with lateral guide vanes. Comparison with available data in the literature was carried out for validation (Sudin et al., 2014).

2.9. Impact of aerodynamic drag on fuel consumption

Sudden spike in fuel prices and concern of greenhouse gas emissions, automotive design engineers are facing a new challenge for introducing more aerodynamic design vehicles. The ineffective aerodynamic shape results in excessive drag which leads to increased fuel consumption rates. The main cause of vehicle aerodynamic drag is due to pressure drag or form drag. Pressure drag on vehicles due to flow separation constitutes more than 80% of the total aerodynamic drag, while frictional drag constitutes for the remaining 20%. Thus, reducing aerodynamic drag is significant for the fuel consumption efficiency. In United States, the ground vehicles consumed about 77% of all (domestic and imported) petroleum; 34% is consumed by automobiles, 25% by light trucks and 18% by large heavy-duty trucks and trailers. It has been estimated that 1% increase in fuel economy can save 245 million gallons of fuel per year. Additionally, the fuel consumption by ground vehicles accounts for over 30% of CO_2 and other greenhouse gas (GHG) emissions. Moreover, most of the usable energy from the engine goes into overcoming the aerodynamic drag (53%) and rolling resistance (32%); only 9% is required for auxiliary equipment and 6% is used by the drive-train. 15% reduction in aerodynamic drag at highway speed of 55mph can result in about 5–7% in fuel saving (Sudin et al., 2014).

2.10. CFD (computational fluid dynamics)

2.10.1. What is CFD?

CFD can be defined as: "CFD (Computational fluid dynamics) is a set of numerical methods applied to obtain approximate solution of problems of fluid dynamics and heat transfer (Sivakumar et al., 2019).

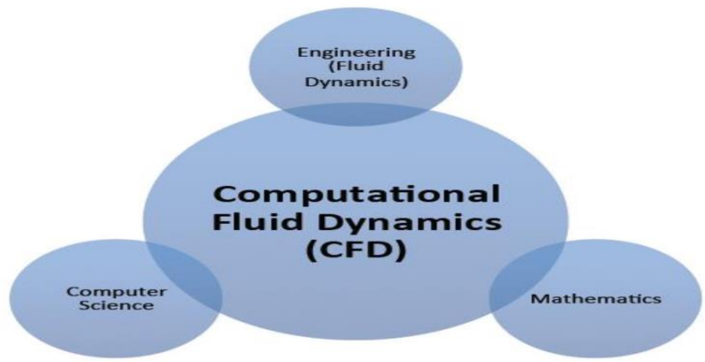

Figure 2.7. The different disciplines contained within CFD

According to this definition, CFD is not a science by itself but a way to apply methods of one discipline (numerical analysis) to another (heat and mass transfer). In retrospect, it is integrating not only the disciplines of fluid mechanics with mathematics but also with computer science as illustrated in Figure 2.7.

The physical characteristics of the fluid motion can usually be described through fundamental mathematical equations, usually in partial differential form, which govern a process of interest and are often called governing equations in CFD (Sivakumar et al., 2019).

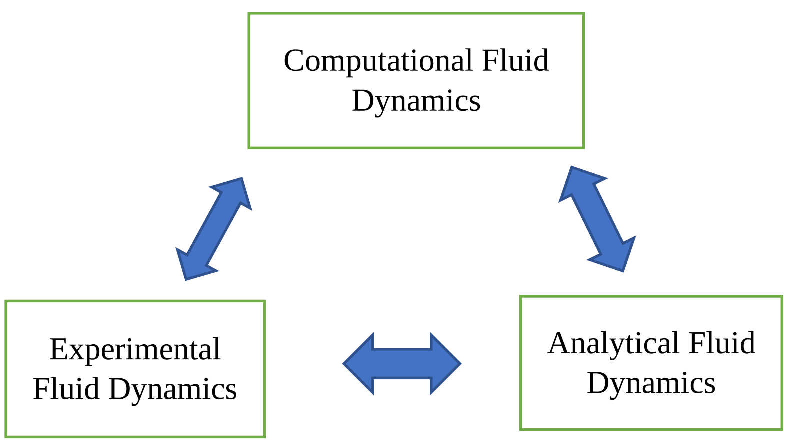

Figure 2.8. The three basic approaches to solve problems in fluid dynamics and heat transfer

CFD has also become one of the three basic methods or approaches that can be employed to solve problems in fluid dynamics and heat transfer. As demonstrated in Figure2.8, each approach is strongly interlinked and does not lie in isolation.

2.10.2. How does CFD code work?

CFD codes are structured around the numerical algorithms that can be engaged in fluid problems. In order to provide easy access to their solving power, all commercial CFD packages include difficult user interfaces, input problem parameters and to examine the results.

Hence all codes contain three main elements:

- Pre-Processor
- Solver
- post-processor

Pre-Processor

A pre-processor is used to define the geometry for the computational domain of interest and generate the mesh of control volumes (for calculations). Generally, the finer the mesh in the areas of large changes is the more accurate solution. Fineness of the grid also determines the computer hardware and calculation time needed (Taha, 2005).

Solver

The solver makes the calculations using a numerical solution technique, which can use finite difference, finite element, or spectral methods. Most CFD codes use finite volumes, which is a special finite difference method. First the fluid flow equations are integrated over the control volumes (resulting in the exact conservation of relevant properties for each finite volume), then these integral equations are discretized (producing algebraic equations through converting of the integral fluid flow equations), and finally an iterative method is used to solve the algebraic equations (Taha, 2005).

Post Processor

The post-processor provides for visualization of the results, and includes the capability to display the geometry/mesh, create vector, contour, and 2D and 3D surface plots. Particles can be tracked throughout a simulation, and the model can be manipulated (i.e. changed by scaling, rotating, etc.), and all in full colour animated graphics (Taha, 2005).

Problem Solving with CFD

There are many decisions to be made before setting up the problem in the CFD code. Some of the decisions to be made can include: whether the problem should be 2D or 3D, which type of boundary conditions to use, whether or not to calculate pressure/temperature variations based on the air flow density, which turbulence model to use, etc. The assumptions made should be reduced to a level as simple as possible, yet still retaining the most important features of the problem to be solved in order to reach an accurate solution. After the above decisions are made, the geometry and mesh can be created. The grid should be made as fine as required to make the simulation grid independent.

2.11. Turbulence Modeling

Flow fields around bluff bodies, such as the buses can be considered to have extremely turbulent flow patterns. Separation bubbles, boundary layers, and wakes present on bluff bodies are examples of turbulence within a flow field. Reynolds-Averaged Navier–Stokes (RANS) equations combined with turbulence modeling provide an adequate model of turbulent flow effects. The choice of turbulence model will depend on considerations such as the physics encompassed in the flow, the established practice for a specific class of problem, the level of accuracy required, the available computational resources, and the amount of time available for the simulation There are mainly three categories of turbulence models such as Classical Turbulence Models (also known as Reynolds Averaged Navier-Stokes), Direct Numerical Simulation (DNS) and the Large Eddy Simulation (LES). Algebraic (Zero-Equation) Models, One-Equation Models (for example Spalart-Allmaras), Two-Equation Models (k-epsilon, k omega, SST, etc.) and Second-Order Closure Models all these four types of models are referred to as RANS turbulence models Each turbulence models have their own advantage and disadvantage. Understanding their strengths and weaknesses is of paramount importance in order to achieve accurate results from CFD simulations. In this study, the two-equation k-epsilon turbulence model has been chosen for reasons that are explained in the following section (Sodja, 2007).

2.11.1. Governing Equations

The flows being considered involve mechanically induced flow (air entering thought a vent) and buoyant forces that drive the air motion in the domain considered. An important factor in the flow calculations is taking into consideration the buoyant forces (natural convective flow) that arise due to differences in fluid density due to temperature difference. The air flow can be considered incompressible as the velocities are low (air flows can usually be considered incompressible if the Mach number is less than roughly 0.3 or about 100m/s). Also air being a Newtonian fluid displays a linear relationship between shear and strain rate. below are Navier Stokes equations in the x, y and z directions and the continuity equation which describes the flow (Cable, 2009).

Momentum in x-direction

$$\frac{\partial}{\partial t}(\rho u)+\frac{\partial}{\partial x}(\rho uu)+\frac{\partial}{\partial y}(\rho vu)+\frac{\partial}{\partial z}(\rho wu)=-\frac{\partial P}{\partial x}+\mu\left(\frac{\partial^2 u}{\partial x^2}+\frac{\partial^2 u}{\partial y^2}+\frac{\partial^2 u}{\partial z^2}\right) \quad \text{………………} (2.3)$$

Momentum in y-direction

$$\frac{\partial}{\partial t}(\rho v)+\frac{\partial}{\partial x}(\rho uv)+\frac{\partial}{\partial y}(\rho vv)+\frac{\partial}{\partial z}(\rho wv)=$$

$$-\frac{\partial P}{\partial y}+\mu\left(\frac{\partial^2 v}{\partial x^2}+\frac{\partial^2 v}{\partial y^2}+\frac{\partial^2 v}{\partial z^2}\right)-\rho g\beta(T_\infty - T) \quad \text{…………..} (2.3)$$

Momentum in z-direction

$$\frac{\partial}{\partial t}(\rho w)+\frac{\partial}{\partial x}(\rho uw)+\frac{\partial}{\partial y}(\rho vw)+\frac{\partial}{\partial z}(\rho ww)=-\frac{\partial P}{\partial z}+\mu\left(\frac{\partial^2 w}{\partial x^2}+\frac{\partial^2 w}{\partial y^2}+\frac{\partial^2 w}{\partial z^2}\right) \quad \text{……………..} (2.4)$$

Continuity

$$\frac{\partial}{\partial x}(\rho u)+\frac{\partial}{\partial y}(\rho v)+\frac{\partial}{\partial z}(\rho w)=0 \quad \text{…………………………………………………..}(2.5)$$

u, *v* and *w* are the velocity components in the *x*, *y* and *z* directions respectively, ρ ρ is the mass density, μ is the viscosity and β is the thermal expansion coefficient of air. *t* is time, *T* is the temperature, *P* is the pressure, and *g* is the gravitational acceleration. The Boussinesq approximation was used and therefore fluid properties were assumed constant except for the density change with temperature which leads to the buoyancy forces. The density change is assumed to be proportional to the temperature difference.

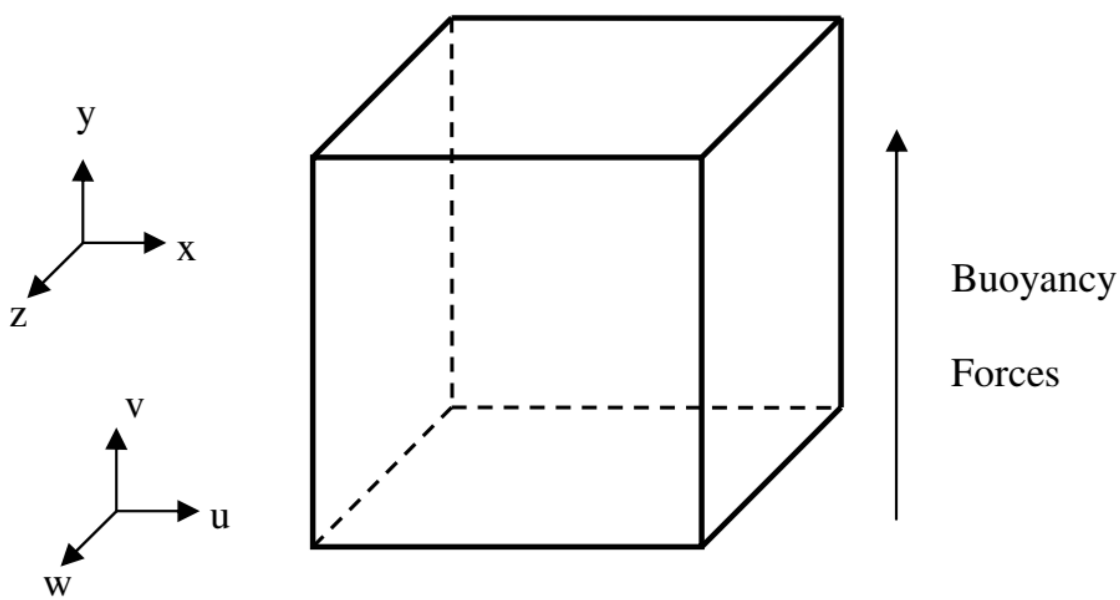

Figure 2.9. Coordinate system and control volume used in present study

The equation of continuity simply states that mass is conserved or that the net accumulation of mass in the control volume is zero in steady flow. Each term in the continuity equation represents the net mass flow through a face perpendicular to one of the respective axis.

Because the y direction equation contains a temperature dependent term, a necessary addition to the Navier Stokes equations is the energy equation. Because of the assumptions being used, the conservation of energy equation is:

$$\frac{\partial}{\partial t}(\rho c_p T) + \frac{\partial}{\partial x}(\rho u c_p T) + \frac{\partial}{\partial y}(\rho v c_p T) + \frac{\partial}{\partial z}(\rho w c_p T) = K\left(\frac{\partial^2 T}{\partial x^2} + \frac{\partial^2 T}{\partial y^2} + \frac{\partial^2 T}{\partial z^2}\right) + q''' \qquad \text{……………….(2.6)}$$

where:

cp is the specific heat (J/kgK), and *K* is the conductivity (W/m K) of the fluid and q''' is the rate of internal heat generation.

2.11.2. K-Epsilon Turbulence Model

The K-Epsilon model has become one of the most widely used turbulence models as it provides robustness, economy and reasonable accuracy for a wide range of turbulent flows. Improvements have been made to the standard model which improves its performance and two variants are available in Fluent; the RNG (renormalization group) model and the realizable model. Three versions of the K-Epsilon model will be investigated here. The standard, RNG, and realizable models have similar form with transport equations for *k* and Ɛ . The two transport equations independently solve for the turbulent velocity and length scales (Cable, 2009). The main differences between the three models are as follows;

- The turbulent Prandtl Numbers governing the turbulent diffusion of *k* and Ɛ
- The generation and destruction terms in the equation for Ɛ
- The method of calculating turbulent viscosity

Standard K-Epsilon Turbulence Model

For this model the transport equation for *k* is derived from the exact equation, but the transport for Ɛ was obtained using physical reasoning and is therefore similar to the mathematically derived transport equation of *k* , but is not exact (Cable, 2009). The turbulent kinetic energy *k* , and its rate of dissipation Ɛ , for this model are obtained by the following equations.

$$\frac{\partial}{\partial t}(\rho k)+\frac{\partial}{\partial x_i}(\rho k u_i)=\frac{\partial}{\partial x_j}\left[\left(\mu+\frac{\mu_t}{\sigma_k}\right)\frac{\partial k}{\partial x_j}\right]+G_k+G_b-\rho\varepsilon-Y_M+S_K \quad \text{.......................(2.7)}$$

$$\frac{\partial}{\partial t}(\rho\varepsilon)+\frac{\partial}{\partial x_i}(\rho\varepsilon u_i)=\frac{\partial}{\partial x_j}\left[\left(\mu+\frac{\mu_t}{\sigma_\varepsilon}\right)\frac{\partial \varepsilon}{\partial x_j}\right]+C_{1\varepsilon}\frac{\varepsilon}{k}\left(G_k+C_{3\varepsilon}G_b\right)-C_{2\varepsilon}\rho\frac{\varepsilon^2}{k}+S_\varepsilon \quad \text{.........................(2.8)}$$

where Gk represents the generation of turbulent kinetic energy the arises due to mean velocity gradients, Gb is the generation of turbulent kinetic energy that arises due to buoyancy, and *YM* represents the fluctuating dilation in compressible turbulence that contributes to the overall dissipation rate. *S*ε and *Sk* are source terms defined by the user. *C*1ε , *C* 2ε and *C* μ are constants that have been determined experimentally and are taken to have the following values;

$$C_{1\varepsilon}=1.44, \quad C_{2\varepsilon}=1.92, \quad C_\mu=0.09$$

σ_k and σ_ε are turbulent Prandtl numbers for the turbulent kinetic energy and its dissipation rate. These have also been derived experimentally and are defined as follows.

$$\sigma_k=1.0, \quad \sigma_\varepsilon=1.3$$

The turbulent (or eddy) viscosity at each point is related to the local values of turbulent kinetic energy and its dissipation rate by;

$$\mu_t = \rho C_\mu \frac{k^2}{\varepsilon} \quad \text{.....(2.9)}$$

Where C_μ is constant and defined above.

The term for the production of turbulent kinetic energy G_k is common in many of the turbulence models studied and is defined as

$$G_k = -\rho \overline{u_i' u_j'} \frac{\partial u_j}{\partial x_i} \quad \text{.....(2.10)}$$

The modulus of mean rate-of-strain tensor, *S* is defined as

$$S = \sqrt{2 S_{ij} S_{ij}} \quad \text{.....(2.11)}$$

The generation of turbulent kinetic energy that arises due to buoyancy, Gb is defined as follows

$$G_b = \beta g_i \frac{\mu_t}{\mathrm{Pr}_t} \frac{\partial T}{\partial x_i} \quad \text{.....(2.12)}$$

As the present study uses relatively low velocities, the dilation dissipation term, *YM* which accounts for turbulence from compressibility effects is defined as

$$Y_M = 2 \rho \varepsilon M_t^2 \quad \text{.....(2.13)}$$

RNG K-Epsilon Turbulence Model

Similar to the standard k-epsilon model, the RNG model was derived from the instantaneous Navier Stokes equations, except it uses a technique called renormalization group theory. This derivation produces a model with different constants to those used in the standard k-epsilon model and also adds new terms to the transport equations for the turbulent kinetic energy and its dissipation. The effect of swirl is also accounted for in the RNG model enhancing the accuracy of swirling flows. An analytical formula for turbulent Prandtl numbers is provided in this model while the standard model relies on user-specific constant values. Finally, assuming appropriate treatment of the near wall region, the RNG model uses an analytically derived differential formula for the effective turbulent viscosity which accounts for low Reynolds number flows. The RNG K-Epsilon model is therefore more accurate and more reliable than the standard K-Epsilon model for a wider range of flows (Cable, 2009).

As a result, from these differences, the transport equations appear as follows.

$$\frac{\partial}{\partial t}(\rho k)+\frac{\partial}{\partial x_i}(\rho k u_i)=\frac{\partial}{\partial x_j}\left[\alpha_k \mu_{eff}\frac{\partial k}{\partial x_j}\right]+G_k+G_b-\rho\varepsilon-Y_M+S_K \qquad \text{……………………....(2.14)}$$

$$\frac{\partial}{\partial t}(\rho \varepsilon)+\frac{\partial}{\partial x_i}(\rho \varepsilon u_i)=\frac{\partial}{\partial x_j}\left[\alpha_\varepsilon \mu_{eff}\frac{\partial \varepsilon}{\partial x_j}\right]+C_{1\varepsilon}\frac{\varepsilon}{k}(G_k+C_{3\varepsilon}G_b)-C_{2\varepsilon}\rho\frac{\varepsilon^2}{k}-R_\varepsilon+S_\varepsilon \qquad \text{……………….......(2.15)}$$

where Gk represents the generation of turbulent kinetic energy that arises due to mean velocity gradients, Gb is generation of turbulent kinetic energy the arises due to buoyancy, and *YM* represents the fluctuating dilation in compressible turbulence that contributes to the overall dissipation rate. *S*ε and *Sk* are source terms defined by the user. α*k* and αε are inverse effective Prandtl numbers for the turbulent kinetic energy and its dissipation.

The RNG theory uses a scale elimination procedure that defines the effective viscosity given in the following equation.

$$d\left(\frac{\rho^2 k}{\sqrt{\varepsilon\mu}}\right)=1.72\frac{\hat{v}}{\sqrt{\hat{v}^3-1+C_v}}d\hat{v} \qquad \text{…………………………………………(2.16)}$$

Where $\hat{v}=\mu_{eff}/\mu$ and C_v is a constant equal approximately to 100. This equation incorporates the ability to accurately define how the effective turbulent transport varies with effective Reynolds number to obtain more accurate results for low-Re flows and near-wall flows. For high Reynolds numbers, the effective viscosity is defined by the following ratio;

$$\mu_t = \rho C_\mu \frac{k^2}{\varepsilon}$$ ………………………………………………………………….(2.17)

Although this is similar to the turbulent viscosity of the standard model, the constant C_μ is derived using the RNG theory and found to be 0.0845 which is very close to the value used in the standard model (i.e., 0.09).

$C_{1\varepsilon}$ and $C_{2\varepsilon}$ are constants that have been derived analytically by the RNG theory and are defined as follows.

$$C_{1\varepsilon} = 1.42, \quad C_{2\varepsilon} = 1.68$$ ……………………………………………………………….(2.18)

Realizable K-Epsilon Turbulence Model

The Realizable model is the most recently developed of the three K-Epsilon variations and features two main differences from the standard K-Epsilon model. It uses a new equation for the turbulent viscosity and the dissipation rate transport equation has been derived from the equation for the transport of the mean-square vorticity fluctuation. The form of the eddy viscosity (turbulent) equations is based on the realizability constraints; the positivity of normal Reynolds stresses and Schwarz' inequality for turbulent shear stresses (i.e., certain mathematical constraints on the normal stresses are satisfied). This is not satisfied by either the standard or the RNG K-Epsilon models which makes the realizable model more precise than both models at predicting flows such as separated flows and flows with complex secondary flow features (Cable, 2009).

In terms of the improved changes by Shih (1995), the transport equations become:

$$\frac{\partial}{\partial t}(\rho k) + \frac{\partial}{\partial x_j}(\rho k u_j) = \frac{\partial}{\partial x_j}\left[\left(\mu + \frac{\mu_t}{\sigma_k}\right)\frac{\partial k}{\partial x_j}\right] + G_k + G_b - \rho\varepsilon - Y_M + S_K$$ ………………….(2.19)

$$\frac{\partial}{\partial t}(\rho\varepsilon) + \frac{\partial}{\partial x_j}(\rho\varepsilon u_j)$$

$$= \frac{\partial}{\partial x_j}\left[\left(\mu + \frac{\mu_t}{\sigma_\varepsilon}\right)\frac{\partial \varepsilon}{\partial x_j}\right] + \rho C_1 S\varepsilon - \rho C_2 \frac{\varepsilon^2}{k + \sqrt{v\varepsilon}} + C_{1\varepsilon}\frac{\varepsilon}{k}C_{3\varepsilon}G_b + S_\varepsilon \qquad \text{……………..(2.20)}$$

where Gk represents the generation of turbulent kinetic energy the arises due to mean velocity gradients, Gb is generation of turbulent kinetic energy the arises due to buoyancy, and *YM* represents the fluctuating dilation in compressible turbulence that contributes to the overall dissipation rate. $S\varepsilon$ and Sk are source terms defined by the user. αk and $\alpha\varepsilon$ are the turbulent Prandtl numbers for the turbulent kinetic energy and its dissipation.

Similar to the previous variations of the K-Epsilon models, the turbulent viscosity is determined by the formula given below; however it produces different results as $C\mu$is not constant.

$$\mu_t = \rho C_\mu \frac{k^2}{\varepsilon} \qquad \text{…………………………………………………………........(2.21)}$$

Where $C\mu$ is computed from

$$C_\mu = \frac{1}{A_0 + A_S \frac{kU^*}{\varepsilon}} \qquad \text{……………………………………………………………..(2.22)}$$

Where:

$$U^* = \sqrt{S_{ij}S_{ij} + \tilde{\Omega}_{ij}\tilde{\Omega}_{ij}} \qquad \text{and} \qquad \tilde{\Omega}_{ij} = \overline{\Omega_{ij}} - \varepsilon_{ijk}\omega_k - 2\varepsilon_{ijk}\omega_k$$

In the above equation, Ωij is the mean rate of rotation tensor viewed in a rotating reference frame with angular velocity ωk . The constants $A0$ and AS are defined as;

$$A_0 = 4.04, \quad A_S = \sqrt{6}\cos\phi \qquad \text{………………………………………………….(2.23)}$$

Where:

$$\phi = \frac{1}{3}\cos^{-1}\left(\sqrt{6}\,\frac{S_{ij}S_{jk}S_{ki}}{\tilde{S}^{3}}\right), \quad \tilde{S} = \sqrt{S_{ij}S_{ij}}\ , \quad S_{ij} = \frac{1}{2}\left(\frac{\partial u_j}{\partial x_i} + \frac{\partial u_i}{\partial x_j}\right)$$

……………(2.24)

It has been shown that $C\mu$ is a function of the mean strain and rotational rates, the angular velocity of the rotating system, and the turbulent kinetic energy and its dissipation rate. The standard value of 09.0 = $C\mu$ is found to be the solution of equation 2.32 for an inertial sub layer in the equilibrium boundary layer.

The constants $C1\varepsilon$, $C2$, σk and $\sigma\varepsilon$ have been determined by Shih (1995) and are defined as follows.

$$C_{1\varepsilon} = 1.44, \quad C_2 = 1.9, \quad \sigma_k = 1.0, \quad \sigma_\varepsilon = 1.2$$

………………………...(2.25)

K-Omega Turbulence Model

The second turbulence model to be investigated is the K-Omega turbulence model. The K-Omega model has two variations that will both be described in this section; the standard K-Omega model, and the shear stress transport (SST) model (Cable, 2009). Both of these models use similar transport equations for k and ω but the SST model differs from the standard model as follows:

- There is a gradual change from the standard k-omega model in the inner region of the boundary layer to the k-epsilon model in the outer part of the boundary layer.
- In order to account for the transport effects of the principal turbulent shear stresses the SST model incorporates a modified turbulent viscosity equation

Standard K-Omega Turbulence Model

FLUENT uses a standard K-Omega model developed was formulated to better compute low-Reynolds number effects, compressibility, and shear flow spreading. The standard model is an empirical based model with transport equations for turbulent kinetic energy (k) and its specific dissipation rate (ω) (Cable, 2009). This model has been modified numerous times in an attempt to improve its accuracy and as a result the transport equations used in FLUENT for Wilcox's model are as follows.

$$\frac{\partial}{\partial t}(\rho k)+\frac{\partial}{\partial x_i}(\rho k u_i)=\frac{\partial}{\partial x_i}\left[\left(\mu+\frac{\mu_t}{\sigma_k}\right)\frac{\partial k}{\partial x_j}\right]+G_k-Y_k+S_K$$
…………………………..(2.26)

$$\frac{\partial}{\partial t}(\rho\omega)+\frac{\partial}{\partial x_i}(\rho\omega u_i)=\frac{\partial}{\partial x_j}\left[\left(\mu+\frac{\mu_t}{\sigma_\omega}\right)\frac{\partial\omega}{\partial x_j}\right]+G_\omega-Y_\omega+S_\omega$$
……………………(2.27)

where Gk represents the generation of turbulent kinetic energy the arises due to mean velocity gradients and *G*ω is generation of ω which are defined in the exact manor as the K-Epsilon model. *Yk* and *Y*ω represent the dissipation of *k* and ω due to turbulence. α*k* and αω are the turbulent Prandtl numbers (constants in this case; equal to 2) for *k* and ω respectively and *S*ε and *Sk* are source terms defined by the user.

The turbulent viscosity is defined using a damping coefficient (α^*);

$$\mu_t=\alpha^*\frac{\rho k}{\omega}$$
……………………………………………………….(2.28)

The low-Reynolds number correlation is obtained from this coefficient α^* which damps the turbulent viscosity. This coefficient is given by,

$$\alpha^*=\alpha_\infty^*\left(\frac{\alpha_0^*+\mathrm{Re}_t/R_k}{1+\mathrm{Re}_t/R_k}\right)$$
…………………………………………………...(2.29)

Where $\mathrm{Re}_t=\frac{\rho k}{\mu\omega}$, $R_k=6$, $\alpha_0^*=\beta_i/3$ and $\beta_i=0.072$. For the high-Re form of the standard k-omega model, $\alpha^*=\alpha_\infty^*=1$

The term for the dissipation of *k* due to turbulence, *Yk* is defined as

$$Y_k = \rho \beta^* f_{\beta^*} k\omega$$ ……………………………………………………..(2.30)

and the term for the dissipation of ω due to turbulence, $Y\omega$ is defined as

$$Y_\omega = \rho \beta f_\beta \omega^2$$ ………………………………..………………………(2.31)

This k-omega model was developed has shown comparable results for far wakes, mixing layers and various jet types which make it applicable to wall bounded flows and free shear flows. It incorporates modifications for compressibility, shear flow spreading, and low-Re number effects which are applicable in the present study (Wilcox, 2006).

SST K-Omega Turbulence Model

The shear stress transport K-Omega model is the only variation of the standard komega model available in FLUENT. It was developed using the standard k-omega model and a transformed k-epsilon model. The main difference is the way in which the model calculates the turbulent viscosity to account for the transport of the principal turbulent shear stress. This model also incorporates a cross-diffusion term in the ω equation and a blending function to allow proper calculation of the near-wall and far-field areas. The blending function triggers the standard K-Omega model in near wall regions, and triggers the K-Epsilon-like model in areas away from the surface. These differences make the SST model more precise for a larger variety of flows than the standard model (Cable, 2009).

Similar to the standard K-Omega model, the transport equations for *k* and are slightly modified and are given by;

$$\frac{\partial}{\partial t}(\rho k) + \frac{\partial}{\partial x_i}(\rho k u_i) = \frac{\partial}{\partial x_j}\left[\left(\mu + \frac{\mu_t}{\sigma_k}\right)\frac{\partial k}{\partial x_j}\right] + \tilde{G}_k - Y_k + S_K$$ ……………(2.32)

$$\frac{\partial}{\partial t}(\rho \omega) + \frac{\partial}{\partial x_i}(\rho \omega u_i) = \frac{\partial}{\partial x_j}\left[\left(\mu + \frac{\mu_t}{\sigma_\omega}\right)\frac{\partial \omega}{\partial x_j}\right] + G_\omega - Y_\omega + D_\omega + S_\omega$$ ……………….(2.33)

Where $\tilde{G}_k$ represents the generation of turbulent kinetic energy the arises due to mean velocity gradients, $G\omega$ is generation of ω , and Yk and $Y\omega$ represent the dissipation of k and ω due to turbulence. αk and $\alpha\omega$are the turbulent Prandtl numbers for k and ω respectively and $S\varepsilon$ and Sk are source terms defined by the user. $D\omega$ is the crossdiffusion term which will be described below.

The term for production of turbulent kinetic energy, $\tilde{G}_k$ is determined slightly differently from the other models and is defined as

$$\tilde{G}_k = \min\left(G_k, 10\rho\beta^* k\omega\right) \quad \text{……….(2.34)}$$

Where Gk is defined the same way as described in the previous models. The term for the production of ω , $G\omega$ is defined as

$$G_\omega = \frac{\alpha}{v_t} G_k \quad \text{……….(2.35)}$$

The terms for the dissipation of k and ω due to turbulence, Yk and $Y\omega$, are defined in a similar manner to that used in the standard model with the main difference being that $* f\beta$and $f\beta$ are both considered constants with a value of 1.

The turbulent viscosity is computed in a different way from that used in the standard model and is given by;

$$\mu_t = \frac{\rho k}{\omega} \frac{1}{\max\left[\frac{1}{\alpha^*}, \frac{SF_2}{a_1\omega}\right]} \quad \text{……….(2.36)}$$

The turbulent Prandtl numbers which were constant in the standard model are equated below and incorporate the blending functions F1 and F2. Blending functions have been added to the SST model to ensure that the model equations behave appropriately in both near wall and far field zones.

$$\sigma_k = \frac{1}{F_1/\sigma_{k,1} + (1 - F_1)/\sigma_{k,2}} \quad \text{...(2.37)}$$

$$\sigma_\omega = \frac{1}{F_1/\sigma_{\omega,1} + (1 - F_1)/\sigma_{\omega,2}} \quad \text{...(2.38)}$$

where;

$$F_1 = \tanh(\Phi_1^4) \qquad F_2 = \tanh(\Phi_2^2)$$

The cross-diffusion term, D_ω blends the standard k-epsilon model and the standard k-omega model and is defined as

$$D_\omega = 2(1 - F_1)\rho\sigma_{\omega,2}\frac{1}{\omega}\frac{\partial k}{\partial x_j}\frac{\partial \omega}{\partial x_j} \quad \text{...(2.39)}$$

The constants specific to the SST k-omega model are defined as

$$\sigma_{\omega,1} = 2.0, \ \ \sigma_{\omega,2} = 1.168, \ \ \sigma_{k,1} = 1.176, \ \ \sigma_{k,2} = 1.0, \ \ a_1 = 0.31$$

2.12. Reference Models in Automotive

There are different reference models in the Automotive industry to study the airflow around a vehicle. All of them are considered as Bluff bodies. Every vehicle reference model has particular geometric shapes to study the fluid flow behavior around the models, under some defined conditions. The comprehension of that behavior on simple shapes helps to understand what will happen with more complex shapes. The most important reference model is the Ahmed model.

2.12.1. Bluff body

In aerodynamics, a bluff body is one which has a length in the flow direction close or equal to that perpendicular to the flow direction. This spawns the characteristic that the contribution of skin friction is much lower than that of pressure to the integrated force acting on the body. Even a streamlined body such as an airfoil behaves much like a bluff body at large angles of incidence.

A circular cylinder is a paradigm often employed for studying bluff body flows. Bluff body flows are characterized by flow separation which produces a region of disturbed flow behind, i.e. the wake. Within the near-wake various forms of flow instabilities, both convective and absolute, may be triggered and amplified (Konstantinidis & Bouris, 2012).

2.12.2. Ahmed Body

The generic Ahmed Body reference model has been chosen as the benchmark for carrying out computations for studying of the aerodynamic parameters. The Ahmed body is a very simple bluff body which has its shape simple enough to allow for accurate flow simulation but retains some important practical features relevant to automobile bodies. As shown on Figure 2.10 below it has a slant on its rear end, whose angle can be manipulated and the corresponding drag and lift coefficients calculated. This is done to exhibit the air flow over the different geometry sections of an automobile and in its vicinity, at different slant angles. This model portrays how to calculate the turbulent flow field around a simple car-like geometry using the turbulent flow, k-epsilon interface.

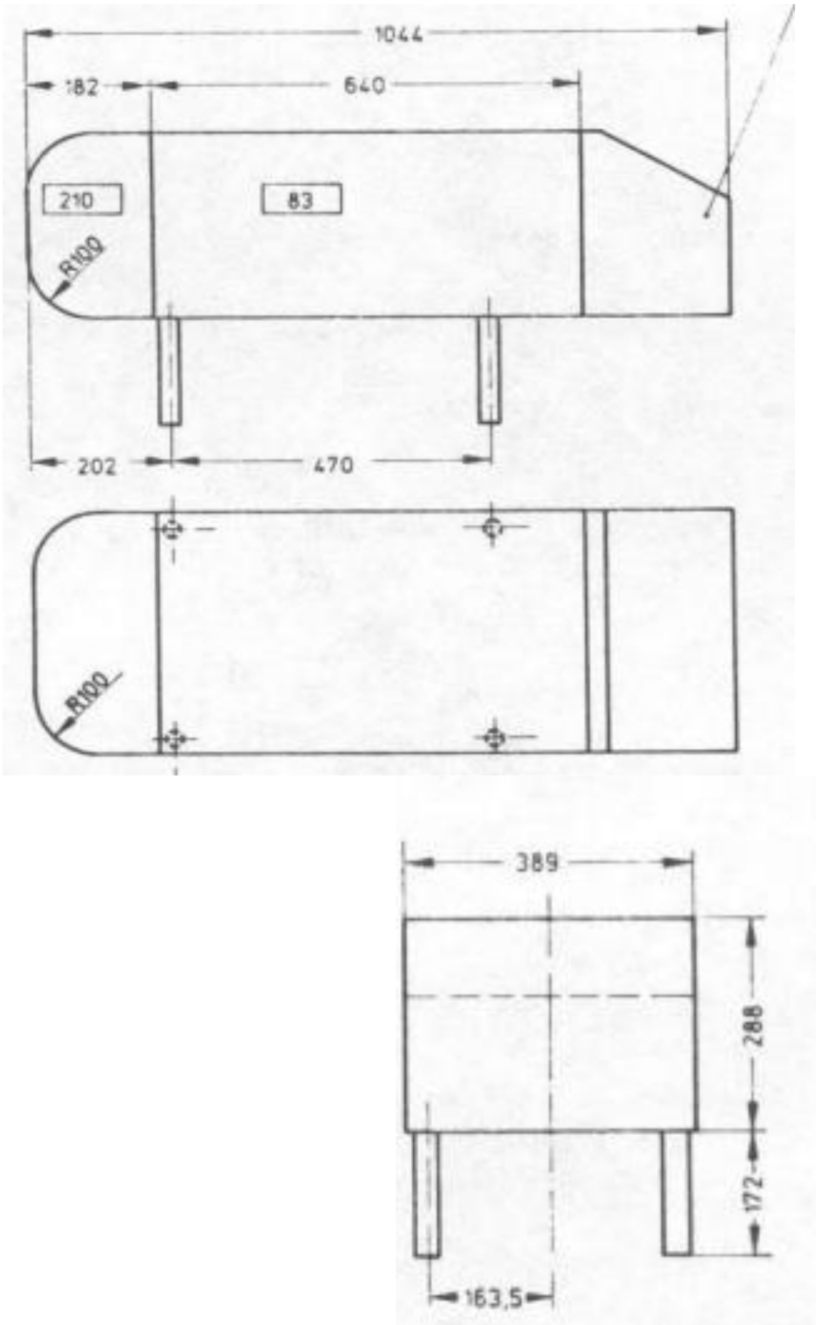

Figure 2.10. Ahmed body schematic figure

This study vortex generator and spoiler used on minibus vehicle by using NACA2415 in fluent. The drag coefficient of base minibus model was 0.415. The CD coefficient of the model minibus was decreased 10.94 % with original designed NACA 2415 airfoil structured vortex generator in model 1. In total of 22.59 % drag reduction was obtained by designed front spoiler. The effect of this drag reduction on fuel consumption about 6 ~ 12 % at high vehicle speeds (LEE, 2012).

Basic Model and Assumptions

Assumptions

The numerical model is based on the following assumptions:

- the flow is steady, turbulent and three-dimensional;
- the flow is single phase, i.e., the effects of dust particles and/or water vapor have been neglected;
- the velocity is uniform over the vent inlet
- the air properties are constant, except for the density change with temperature**.**

Improvement in drag coefficient were obtained in models with spoilers adjusted at zero degree and – 15 degree but this resulted in an increase in lift coefficient than the baseline model. A drag reduction of 1.2% and 4.8% was achieved in model one and model three respectively and a maximum of 0.78% and 2.8% reduction in fuel consumption was achieved but the lift coefficient increases than the baseline model by 102.36% and 164% respectively. Model two with a spoiler having a gap of 5 cm adjusted at zero degree was used and it resulted in an increase in aerodynamic drag by 3% which resulted in increase in fuel economy by 1.8% but it resulted decrement in aerodynamic lift by 120% than the baseline model (Dilu et al., 2020).

Improvements in drag coefficient and lift coefficient were obtained in models with spoiler when compared to the baseline model without any add-on device. A drag reduction of 6.50%, 6.12%, and 0.493% was achieved on model one, model three and model two respectively when compared to the baseline model. The decrease in the amount of drag was attributed to the decrease in wake region and swirling air inside the bed box of the pickup. Because of the reduction in drag a maximum of 3.90% reduction in fuel consumption was achieved. The lift coefficient of the baseline model was also reduced to 22.47% on model two, 14.55% on model three and 4.30% on model one at a vehicle speed of 120 kmph. This reduction in lift coefficient increases vehicle stability at high speed (Wolde, 2019).

Four models such as model I, model II, model III, and model IV were prepared. The coefficient of drag was later converted into quantifiable performance parameters such as fuel efficiency and CO_2 emissions. The aerodynamic shape improvement in model IV reduced the drag coefficient by 54.35% which has resulted in the percentage reduction in fuel consumption of 32.61% and exhaust gas emission 9.7%. This reduction of exhaust emission has a significant effect in the environment(Bekele, 2019).

Summary

In general, the different literature studied suggested that the importance of spoilers on the aerodynamic drag reduction and reduction of coefficient of lift for the better fuel efficiency, stability of the vehicle on high speed, on cornering, tire capability on grasping the road and for better environment. And also, CFD/ANSYS has shown better and dependable results. Analysis in Improving drag and lift coefficients for various vehicles with different types of add-on devices have been carried out using CFD/ANSYS Fluent.

Research gap

The effects of different aerodynamic add-on devices on flow and its structure over a generic passenger car may be analyzed using CFD approach. The objective is to analyze aerodynamic effect acting on the vehicle and thus improve the fuel efficiency of passenger car. Hence, the drag force can be reduced by using add-on devices on vehicle and fuel economy, and stability of a passenger car can be improved. Different researchers studied on aerodynamic on different vehicles and came up with different conclusion but there is a limited literature on the selected vehicle on how add-on device affects its aerodynamic with its versatility and importance by reducing drag and lift, which in return increases its performance. This study aims to fill this gap by exploring the effect of rear spoiler on aerodynamic drag and lift of the Toyota hiace midibus(dolphin).

CHAPTER THREE

MATERIALS AND METHODS

This chapter explains about the materials to be used and the methodology to be followed through this work.

3.1. Materials

The materials used in this study are:

SOLIDWORKS: Used to construct model of vehicle with and without rear spoiler.

ANSYS Fluent: Used to simulate the flow on rear of the vehicle as well as analyze drag and lift coefficients.

Microsoft Excel: Used to draw the ANSYS calibration corresponding to the input value.

3.2. Methods

3.2.1. Baseline Model

Toyota HIACE LWB vehicle model was used for the present work. The model represents a 1:12 scale of the full-scale passenger (Dolphin) vehicle. The model was designed with a smooth underbody, enclosed wheel wells, with no side view mirrors and without openings for cooling airflow. The model used has been modified to resemble the generic passenger (Dolphin) vehicle.

3.2.2. Bench marking the baseline model

The baseline model of Toyota HIACE LWB 1/12 scaled down vehicle model was generated using SOLIDWORKS. The dimensions of the body which are almost considered for aerodynamic analysis were bench marked for the study. These dimensions give the basic geometry of the vehicle. The modeled vehicle shown in Figure 3.1 below was selected as the baseline for studying the aerodynamic performances.

Figure 3.1. Selected Passenger (Dolphin) vehicle

Table 3.1. Shows the basic dimension of the selected vehicle

Table 3.1. Basic Dimension of Toyota HIACE LWB

Parameters	Actual Dimension (mm)	Scaled-down 1/12th Dimension (mm)
Length	5160	430
Width	1800	156.6
Height	1995	166.25
Wheelbase	3430	285.8

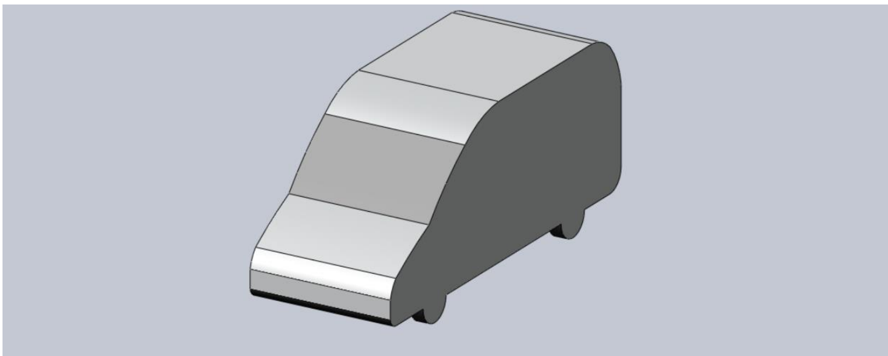

Figure 3.2. 1/12 Scaled Toyota Hiace lwb(Dolphin)

Criteria for selecting generic Toyota HIACE LWB(Dolphin) vehicle (baseline model)

- It’s one of the basic transportations in our country
- To reduce lift and drag of vehicle when driving at high speed

- The other criteria for selecting generic Toyota HIACE LWB(Dolphin) vehicle is for validation purpose.

3.2.4. Turbulence Modeling

In this study Realizable k-ε Turbulence Model (RKE) described in the turbulence modelling section was used. The solver used for the analysis is ANSYS 19.2 and it uses a control-volume method to solve the governing equations that can be solved numerically. The solver selected was the pressure based implicit solver. In this type the equations of continuity and momentum are solved sequentially. The flow is considered to be incompressible and steady in nature and the equations are solved using both first and second order upwind method.

Reasons for selecting Realizable k-ε Turbulence Model (RKE)

The realizable k-ε model is a relatively recent development and differs from the standard k-ε model in two important ways:

- The realizable k-ε model contains a new formulation for the turbulent viscosity.
- A new transport equation for the dissipation rate, ε, has been derived from an exact equation for the transport of the mean-square vorticity fluctuation.

The term "realizable" means that the model satisfies certain mathematical constraints on the Reynolds stresses, consistent with the physics of turbulent flows. Neither the standard k-ε model nor the RNG k-ε model is realizable. An immediate benefit of the realizable k- ε model is that it more accurately predicts the spreading rate of both planar and round jets. It is also likely to provide superior performance for flows involving rotation, boundary layers under strong adverse pressure gradients, separation, and recirculation. Both the realizable and RNG k-ε models have shown substantial improvements over the standard k- ε model where the flow features include strong streamline curvature, vortices, and rotation. Since the model is still relatively new, it is not clear in exactly which instances the realizable k- ε model consistently outperforms the RNG model. However, initial studies have shown that the realizable model provides the best performance of all the k- ε model versions for several validations of separated flows and flows with complex secondary flow features.

3.2.3. Aerodynamic drag reducing device

In this study one drag reducing device with different arrangement is employed and each arrangement are simulated using Ansys Fluent, and their values are compared with each other and to the baseline. Rear spoiler which is externally attached to the rear end of the roof, is meant to push the flow separation a bit rearward and reduce the amount of drag by minimizing the wake region, and by throwing the turbulent air behind the truck. The spoiler minimizes the amount of swirling air in the back of the vehicle. The arrangements are such that, for model one (Figure3.3) the spoiler with 22 mm slant length is attached to the rear end of the cab at an angle of zero-degree inclination. In the second model (Figure 3.4), the spoiler with 22 mm slant length is inclined upward at 8 degree and in the third model the spoiler with 22 mm slant length is inclined upward at 12-degree.

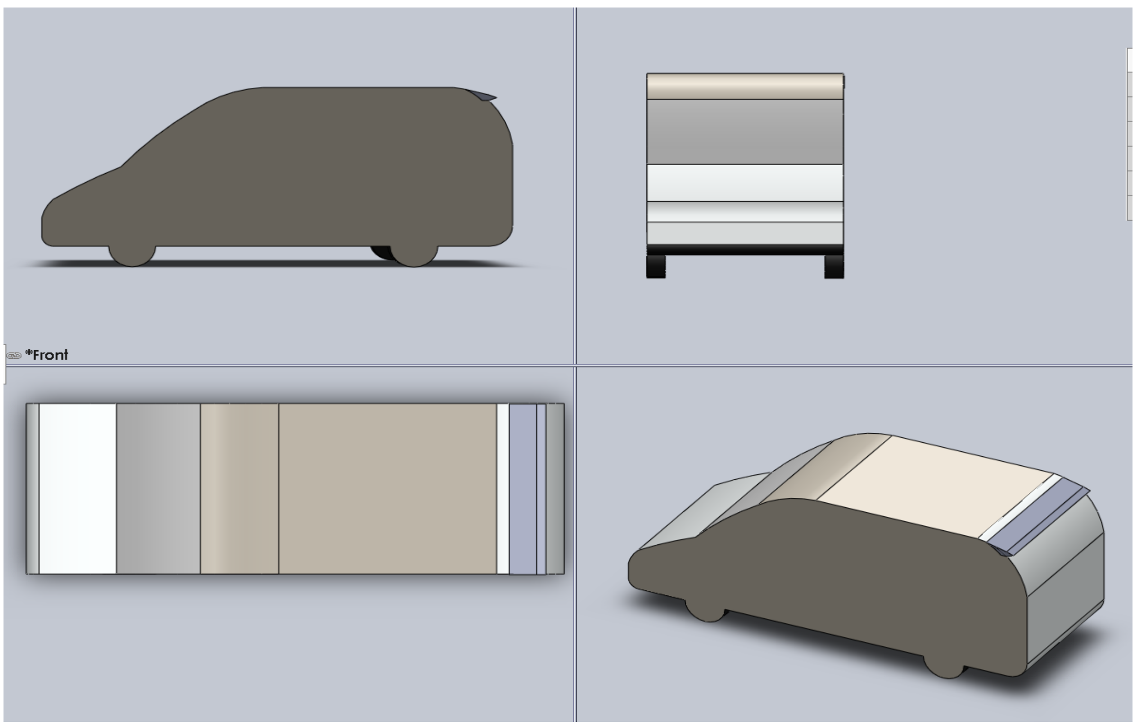

Figure 3.3. Model 1(slant angle of 0^0)

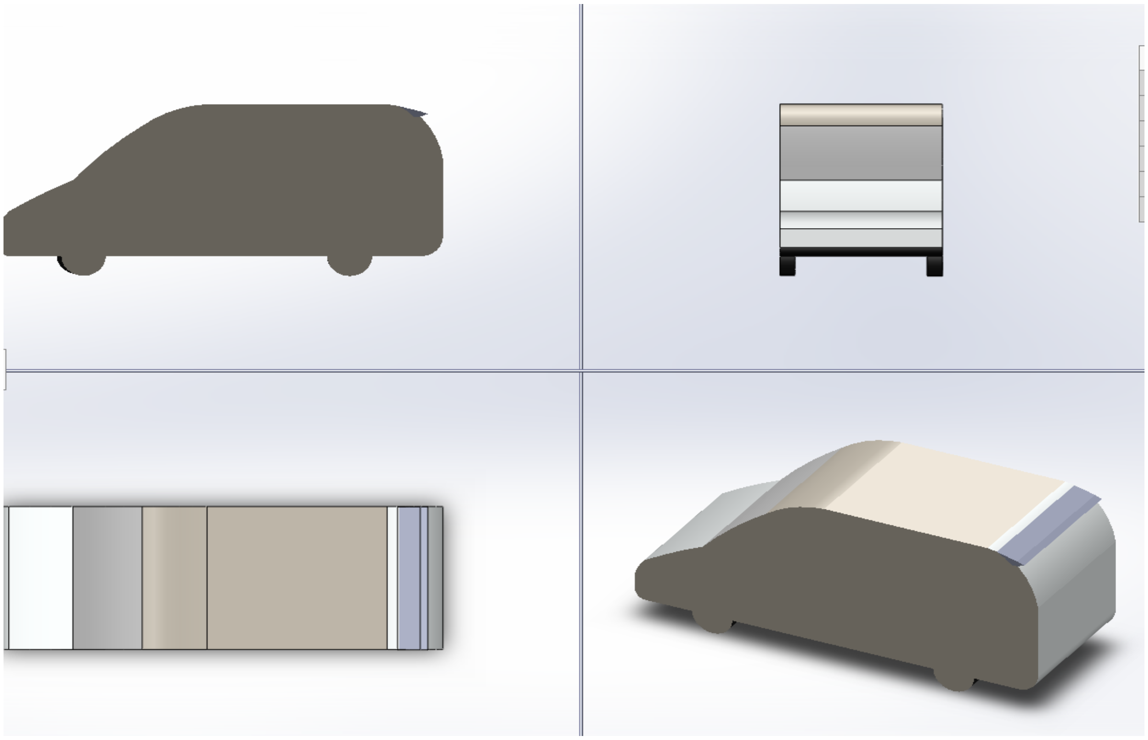

Figure 3.4. Model 2 (slant angle of 8^0)

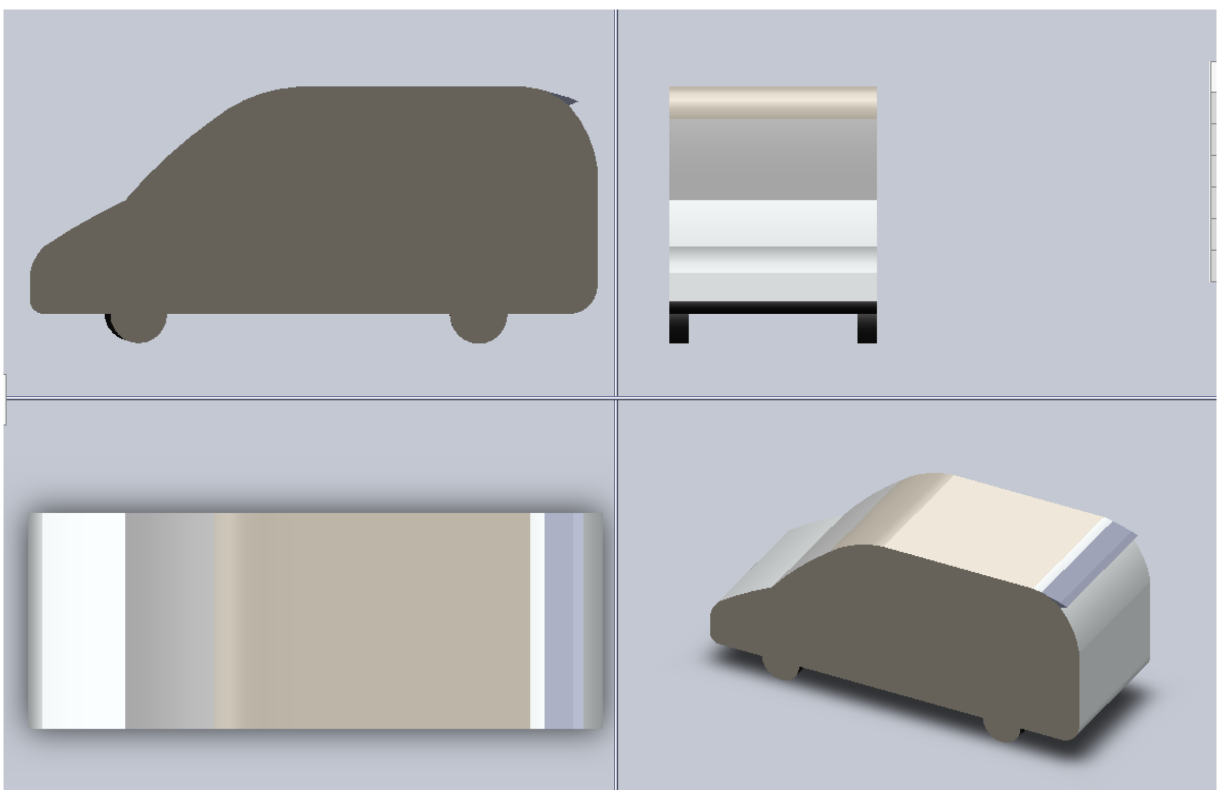

Figure 3.5. Model 3 (slant angle of 12^0)

Considerations taken in the design of a rear spoiler and selection of angle of inclination is that of it has to give a minimum drag, maximum stability and control that helps the vehicle tire in contact with the ground. Airfoil shapes are the basics in the design of car spoilers since it helps the air flowing on the surface of the spoiler being attached that is flow separation before the trailing edge of the airfoil will not happen. Airfoil should be designed to have a minimum drag and for that there is a catalogue for the design of airfoil that is commonly known as NACA (National Advisory Committee for Aeronautics) airfoil.

NACA airfoils one of the most reliable resources and widely used data base is the airfoils that have been developed by NACA (predecessor of NASA) in 1930s and 1940s. For the design of the car spoiler NACA four - digit airfoil shapes are commonly used. In this series the first digit represents the maximum camber as percentage of the chord of the airfoil and the second digit represents the maximum camber position as in tenths of the airfoil chord length and the last two digit represents the maximum thickness of the airfoil as in percentage of the airfoil chord length.

The spoiler airfoil shape was selected from NACA catalogue. NACA4412 airfoil was selected and the coordinates are imported to SolidWorks for modelling. For the model spoiler with 22 mm length. The model are configured with 0,8,12 degrees of inclinations.

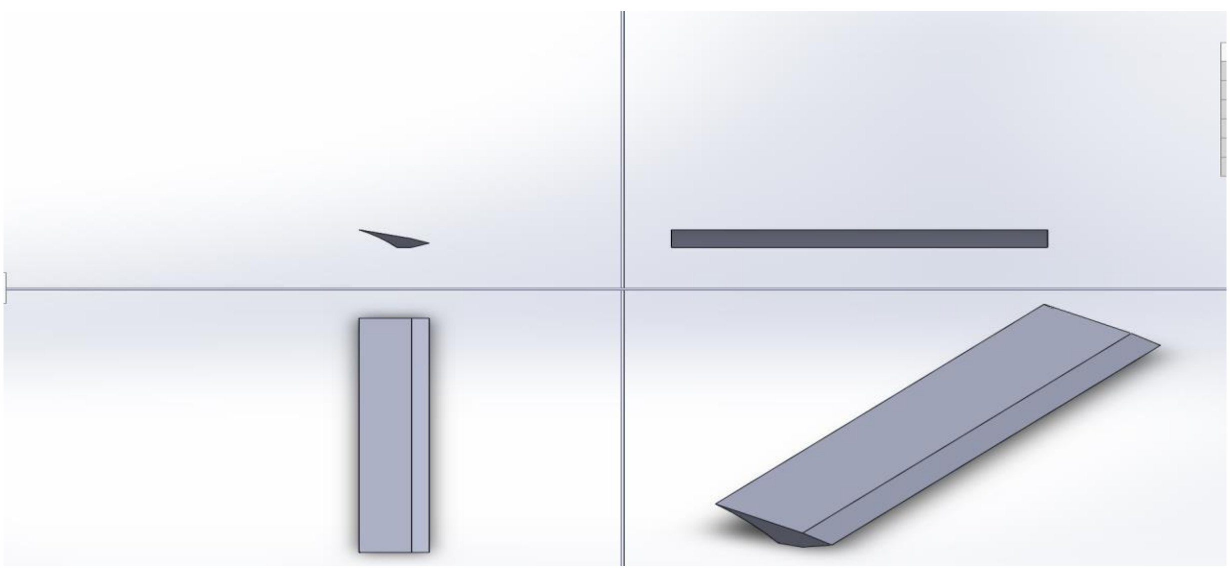

Figure 3.6. Spoiler

CHAPTER FOUR

NUMERICAL MODELING

4.1. CFD/ANSYS Fluent set up and procedure

ANSYS Fluent was used as the CFD software and it simulated the fluid flow around the CAD models which were generated using SolidWorks. The simulation process was divided into four separate sections such Geometry generation, Meshing, Setup, and Solution. For all simulations, for models with and without the drag reducing devices, the process was the same. The first Step on the fluent setup was to define the geometry that would be modeled by CAD software to represent the air neighboring the vehicle. After the vehicle model was uploaded an enclosure was generated surrounding it. For experimental study the enclosure was designed based on recommendation from Fluent for accurate results.

CFD codes are structured around the numerical algorithms that can be engaged in fluid problems. In order to provide easy access to their solving power, all commercial CFD packages include difficult user interfaces, input problem parameters and to examine the results.

Hence all codes contain three main elements:

- Pre-Processor
- Solver
- post-processor

4.1.1. Pre-Processor

A pre-processor is used to define the geometry for the computational domain of interest and generate the mesh of control volumes (for calculations). Generally, the finer the mesh in the areas of large changes is the more accurate solution. Fineness of the grid also determines the computer hardware and calculation time needed. At this stage, quite a lot of activities are carried out before the problem is being solved. In this stage, CFD users are needed to provide sufficient input to the computer in order to obtain the desired output. The pre-processing stage is divided into several steps such as Geometry generation, Boundary condition input, Mesh generation, Selecting flow type (Steady/Unsteady), Turbulence and near wall model input. The accuracy of the CFD solution is governed by the number of cells in the grid and is dependent on the fineness of the grid. The solution of the flow problem such as temperature, velocity, pressure etc. is defined at the node’s insides each cell.

4.1.1.1. Geometry Generation

The first Step on the fluent setup was to define the geometry that would be modeled by CAD software to represent the air neighboring the Toyota HIACE vehicle. After the vehicle model was uploaded an enclosure was generated surrounding it. For experimental study the enclosure was designed based on recommendation from Fluent for accurate results.

The dimensions of the computational domain should be at least 3 car lengths in front of the car, and 5 lengths behind. Dimensions used for the enclosure are given in Table 3.2 below. The wind tunnel and computational domain around the vehicle is shown in figure 3.7.

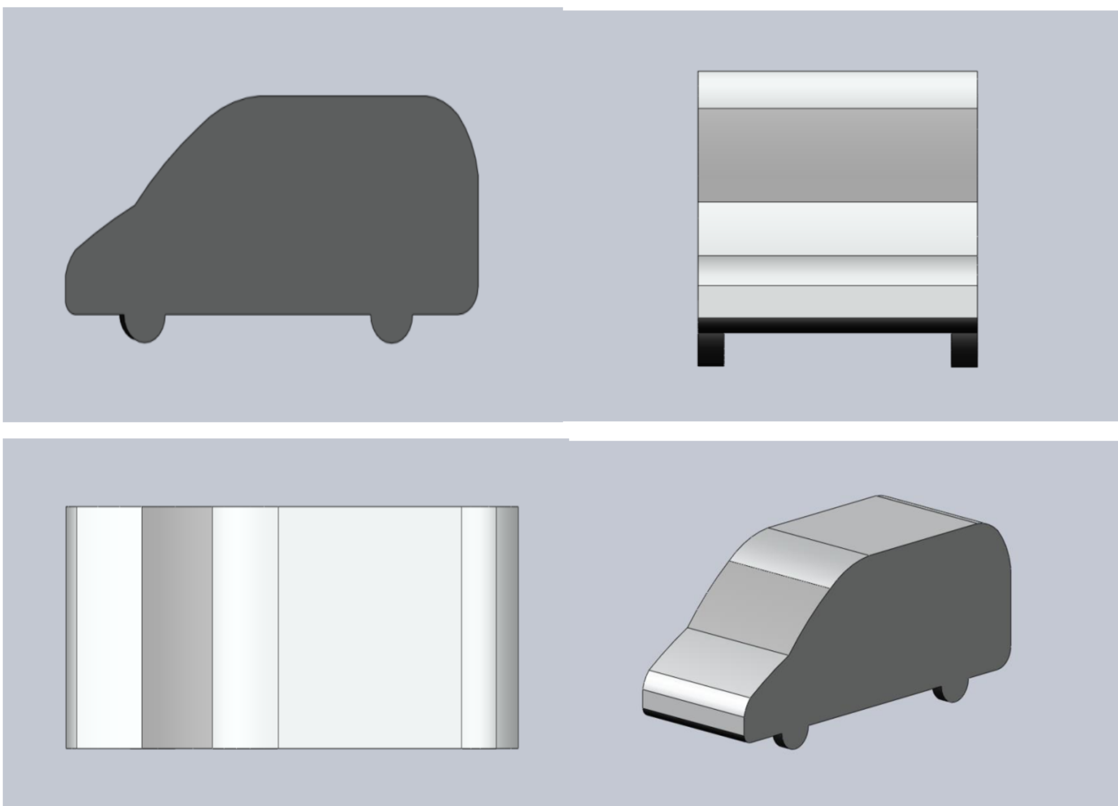

Figure 4.1. An Existing model with simplification

4.1.1.2. Design of Virtual Wind Tunnel

After the vehicle model has been uploaded into the ANSYS environment an enclosure was generated surrounding it. For the experimental study, the enclosure was designed based on recommendation from Fluent for accurate results. A virtual air-box (Figure 3.7) has been created around the 3D CAD model which represents the wind tunnel in real life. The measurements of the tunnel are relational to the bus. A virtual wind tunnel contains an inlet, an outlet, wall, and a ground surface. The flow inlet plane was located three car lengths away from the front of the car body, whereas the outlet plane five car lengths from the rear.

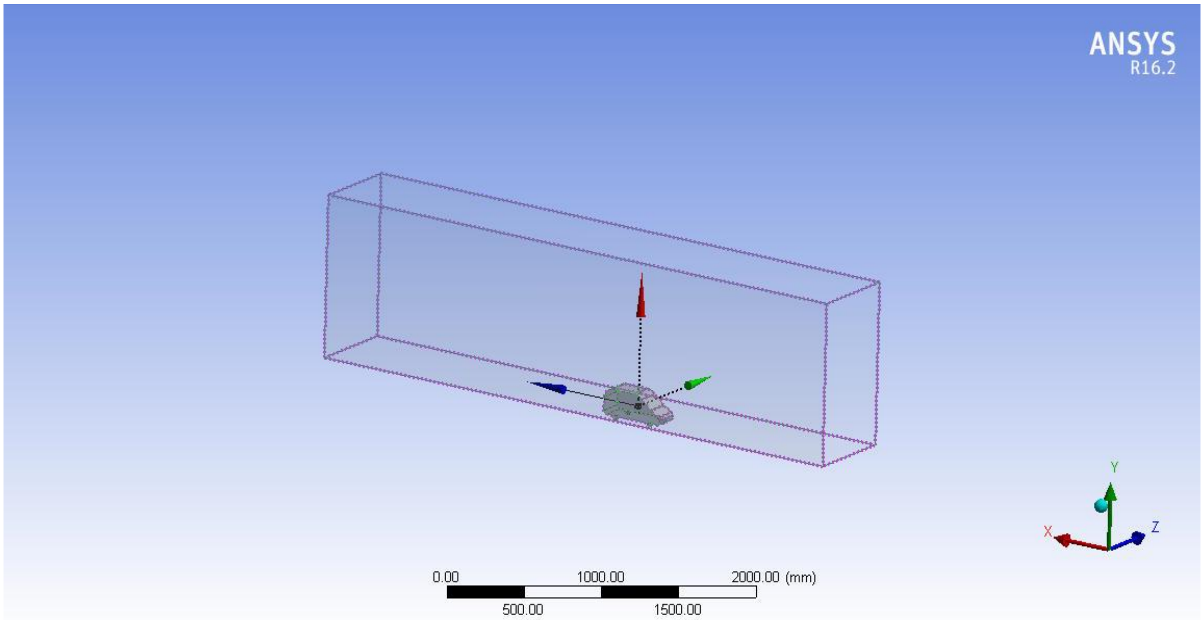

Figure 4.2. Virtual wind tunnel targeted for CFD simulation

The side plane was located sufficiently far from the car body side surface (about two car lengths), providing a vast simulation domain. The height of the domain was set to two times the length of the car body. Dimensions used for the enclosure are given in Table 3.2. The ground was located at the distance 1mm from the car body bottom surface. The rear side of vehicle is more interested because, which is the place where the “wake of vehicle” phenomenon occurs, more space has been left in the rear side of the vehicle model to capture the flow behavior mostly behind the vehicle. Due to the complexity of the simulation with limited computer resources and time, the complete domain was divided into half using a symmetry plane (YZ plane), which means, the simulation would be calculated for just the one side of the vehicle model. Since the other side is symmetric and the YZ plane has been defined as symmetric boundary in the solver to make the boundary condition as “a slip wall with zero shear forces”; the simulation results would be valid for full model as well. The assumptions made in the present simulation have the airflow steady state with constant velocity at inlet and with zero-degree yaw angle, constant pressure outlet, no-slip wall boundary conditions at the vehicle surfaces, and inviscid flow wall boundary condition on the top, sidewalls, and ground face of the virtual wind tunnel. And also, table 3.2 shows the dimension of the wind tunnel enclosure.

Table 4.1. Dimension for wind tunnel enclosure

Upstream length (mm)	Downstream length (mm)	Width (mm)	Height (mm)
1290	2150	430	860

After the wind tunnel enclosure was constructed the Boolean feature was employed to subtract the volume of the bus from the volume of an enclosure to create a new volume that represented only the air that surrounded the bus.

4.1.1.3. Mesh Generation

Mesh generation constitutes one of the most important steps during the preprocessing stage after the definition of the domain geometry. The mesh is produced on the design of the Toyota HIACE and on the surface of the domain.

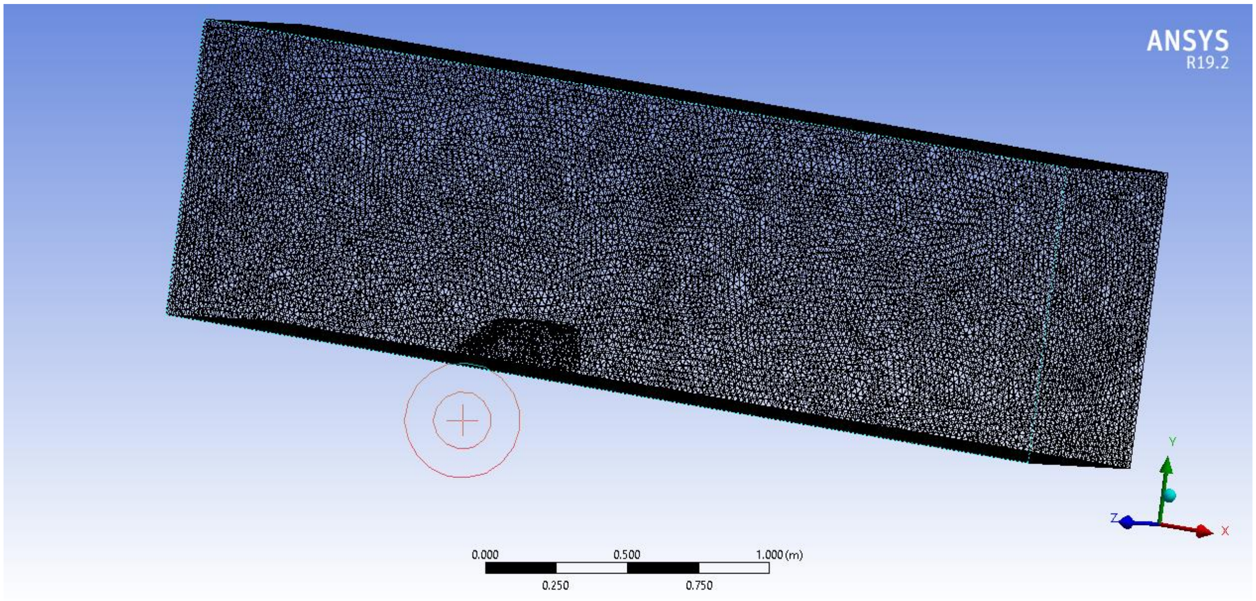

Figure 4.3. Mesh after surface sizing (Baseline model)

A fine mesh is necessary in order to have a converging simulation. The fineness of the entire mesh is described by relevance used. The relevance of 100 means high accuracy and low speed of processing, while a relevance of -100 means low accuracy and higher speed of processing. For this study zero relevance with fine relevance, the center was used. The advanced size function is proximity and curvature, used for the progression from minimum size elements, near and around the curvature of the vehicle to maximum size elements far away from the vehicle toward the walls of the wind tunnel box. High Smoothing which increases the number of smoothing iterations and improving element quality by moving nodes and elements in the vicinity was used.

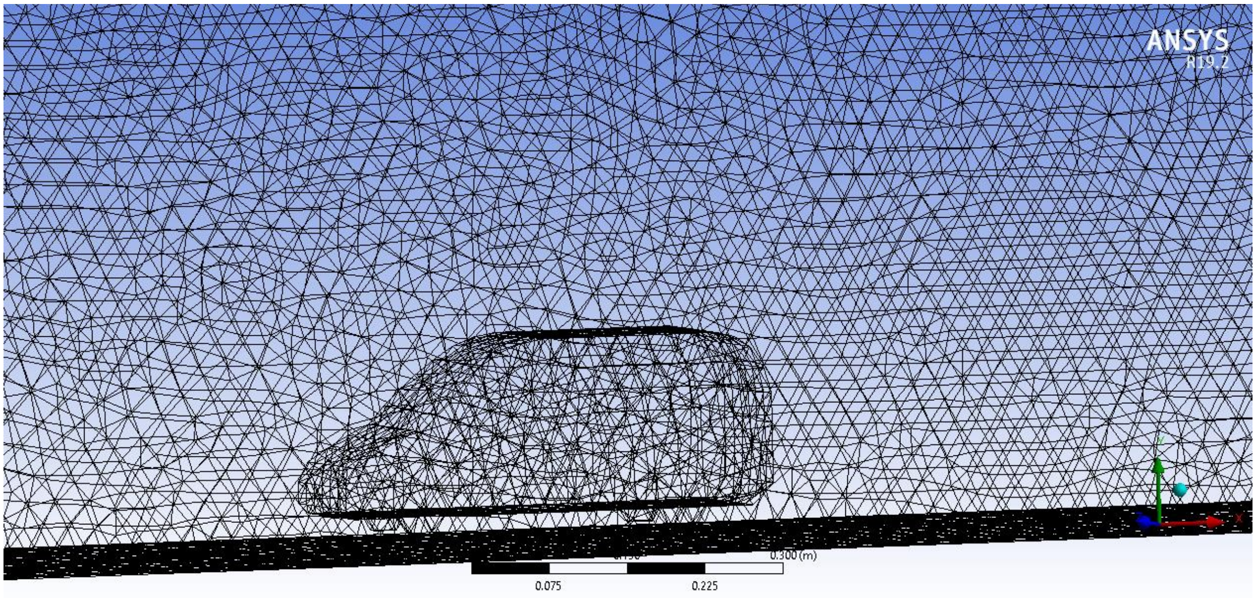

Figure 4.4. Mesh zoom after surface sizing

Lastly, named sections were created to differentiate among the faces, which is also used to establish the properties of each face. The plane in front of the vehicle was the velocity inlet while the plane behind was the pressure outlet. And the sides attached to the vehicles is named wall.

Grid independence test

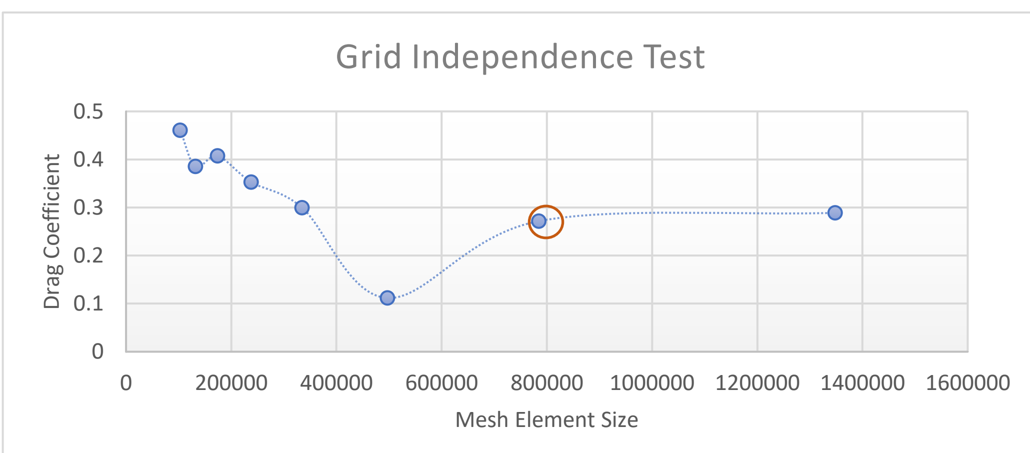

Figure 4.5. Grid Independence Test

Grid independence test graph which shows a constant line will not give any indication about the better mesh element size, so a comparison was done with another output parameters. The drag coefficient variation is significant with respect to the mesh. Result variation are not significant after the marked cell zone; hence this can be considered as the better mesh for calculation. This mesh size will give better result with less time as compared to finer mesh. Mesh element size higher than 1,200,000 can be used as a substitute for finer mesh, thus the selected element size for this study is 25 mm which is a mesh element size of 1,347,942 and it's acceptable as per the grid independence test. Models mesh element size higher than 1,200,000 can be acceptable as far as this work.

Boundary condition

The distribution of all flow variables needs to be specified. Inlet boundary conditions are mainly for flow velocity and this type of boundary condition is common and specified mostly where inlet velocities as known. In outlet boundary condition the flow tends to fully develop state where no change occurs in the flow direction when the outlet is selected far away from the geometrical. Distributions in such region an outlet could be outlined in gradient all variable equated to zero in the flow direction except pressure. Wall boundary condition the most common boundary that comes upon in the confined fluid flow problems is the wall. This is also commonly known as no slip boundary condition. This is appropriate for the velocity condition of the wall the normal component set to zero and the tangential component set to the velocity of the wall and all boundary condition used here are explained on table 3.3.

Table 4.2. Boundary conditions

Boundary conditions		
Inlet boundary condition	Speed of car (22.22,27.87,33.33) m/s	
Outlet boundary conditions	Standard pressure(1atm=101.325kpa)	
wall boundary condition	Top wall	Speed of car (22.22,27.87,33.33) m/s
	Left side wall	Speed of car (22.22,27.87,33.33) m/s
	Right side wall	Speed of car (22.22,27.87,33.33) m/s
	Road	Speed of car (22.22,27.87,33.33) m/s
Car boundary condition	Stationary car (zero velocity)	

4.1.2. Solver Stage

After the mesh has been imported in Ansys Fluent, a check has been performed to be sure that there are no negative volumes on the mesh then the solver settings to be completed before starting the simulations. The solver setting includes the type of solver (3D or 2D), the viscous model, boundary conditions and solution controls. The inlet of the wind tunnel was indicated by the term "velocity inlet", while the outlet of the wind tunnel was termed as "pressure-outlet". The realizable k-ε model was employed in the fluent simulations for all models. Realizable k-ε model was employed in the fluent simulations for all models. The simulations were run with a velocity of 80kmph, 100kmph and 120kmph. In the simulation the air flew from the velocity-inlet towards the pressure-outlet with a selected amount of velocity. The turbulence intensity for the velocity inlet was reduced to 1%. Turbulence intensity can be defined as the root-mean-square of the velocity fluctuations over the mean flow velocity. A turbulence intensity of 1% is relatively low meaning steady air flow and the velocity introduced to the simulation had very low fluctuations and therefore very little turbulence.

The area of each specific model was found using Fluent project area feature and was utilized in determining the drag coefficient of the vehicle model from the force that was calculated during the simulation. A coupled scheme was chosen for the pressure-velocity coupling. This scheme is more robust and efficient than other schemes for steady-state flows, such as the flow in this study. While employing a coupled scheme the flow Courant number was set to 50 while both the explicit relaxation factors for momentum and pressure was 0.25. The flow Courant number is the ratio between the computational distance step and the distance a disturbance travels in one-time step.

Reducing this value improves the accuracy and steadiness of the simulation. The reduction in the explicit relaxation factors allowed for a more skewed mesh to be converged easier. They represent the percent of the solution being used from iteration to iteration throughout the simulation. The turbulent viscosity relaxation factor was set to 0.8 during first upwind and changed to 0.95 for second upwind. In order to monitor the calculations and simulations a monitor was created for drag, lift, moment and scaled residuals on the vehicle.

Once the monitor was created it could be used to set the convergence criterion for the simulation. The convergence was set to none. The numerical computation was first started with the first order scheme to ensure numerical stability. After one hundred iterations, the numerical scheme was switched to the second order scheme for better numerical accuracy. This scheme was continued for another 600 iterations. Most of the scaled residuals and the global aerodynamic quantities such as the drag coefficient and the lift coefficient converged to 1e-3 long way before the 600th iteration. Once this convergence was met the simulation was complete and was stopped.

Once convergence was reached the solution could be analyzed to determine the effectiveness of the spoilers. After the simulations were completed the post-CFD part of Fluent and Excel were utilized to fully analyze the solution and the air flow around the vehicle and spoiler. Contours of the pressure, turbulence, velocity magnitudes, and graphs were created.

4.1.3. Post Processor

The post-processor provides for visualization of the results, and includes the capability to display the geometry/mesh, create vector, contour, and 2D and 3D surface plots. Particles can be tracked throughout a simulation, and the model can be manipulated (i.e. changed by scaling, rotating, etc.), and all in full colour animated graphics. Determining the convergence, whether the solution is consistent and stable for all range of flow variables, is important. Convergence is a property of a numerical method to produce a solution that approaches the exact solution by which the grid spacing and control volume size are reduced to a specific value or to zero value. Consistency is to produce the system of algebraic equations that can be equivalent to the original governing equation. Stability associates with the damping of errors as a numerical method proceeds. If a technique chosen is not stable, even the round-off error in the initial data can lead to wild oscillations or divergence.

CHAPTER FIVE

RESULT AND DISCUSSION

This chapter presents the results of the Computational Fluid Dynamics (CFD) analysis. The CFD analysis was performed using ANSYS FLUENT. The results and discussions of Computational analysis presented for the results of the baseline model, Model one, Model two and Model three simulations with the help of figures and tables are depicted. Each results are briefly discussed.

5.1. Baseline Model

Result of scaled residuals, drag and lift coefficient, pressure and velocity contour at speed of 80 kmph 100 kmph and 120 kmph of model one which is the baseline model is depicted below.

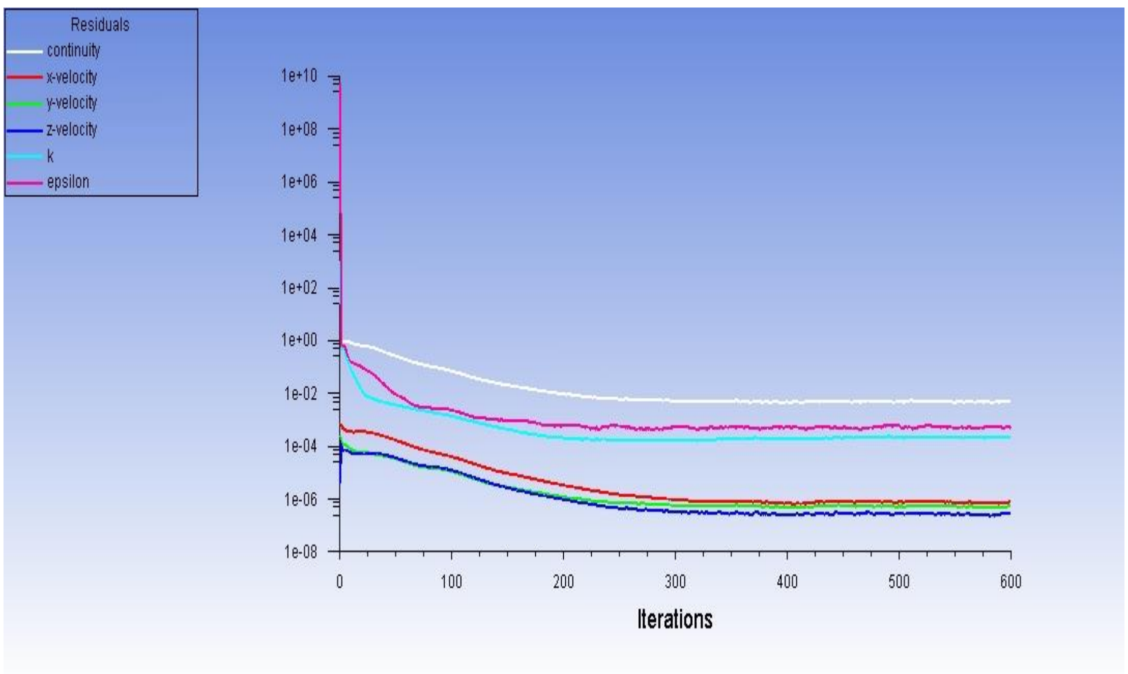

Figure 5.1. Scaled Residuals

The scaled residual for baseline model at 80 kmph, 100 kmph and 120 kmph shows how the parameters converge with each iteration. It can be seen on Figure 5.1 that how the graph changes after the 100th iteration. Here at the 100th iteration the scheme was changed from first order upwind to second order upwind.

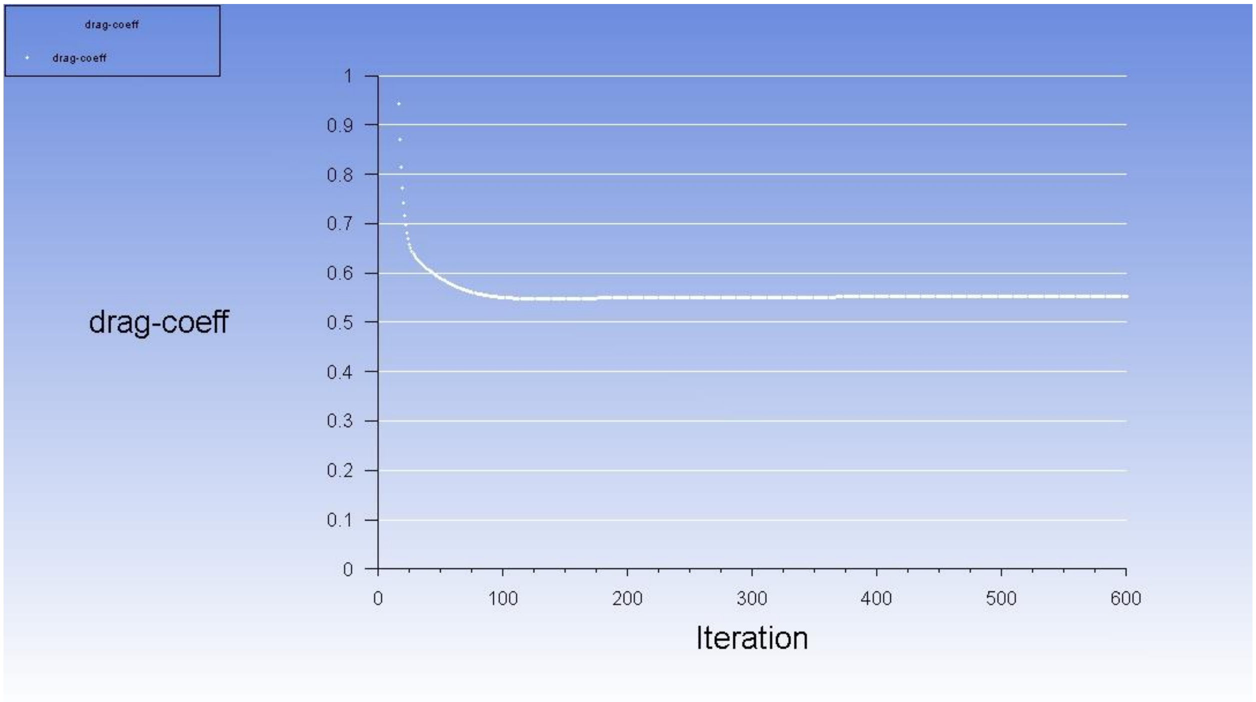

Figure 5.2. Drag coefficient of baseline model at 80 kmph

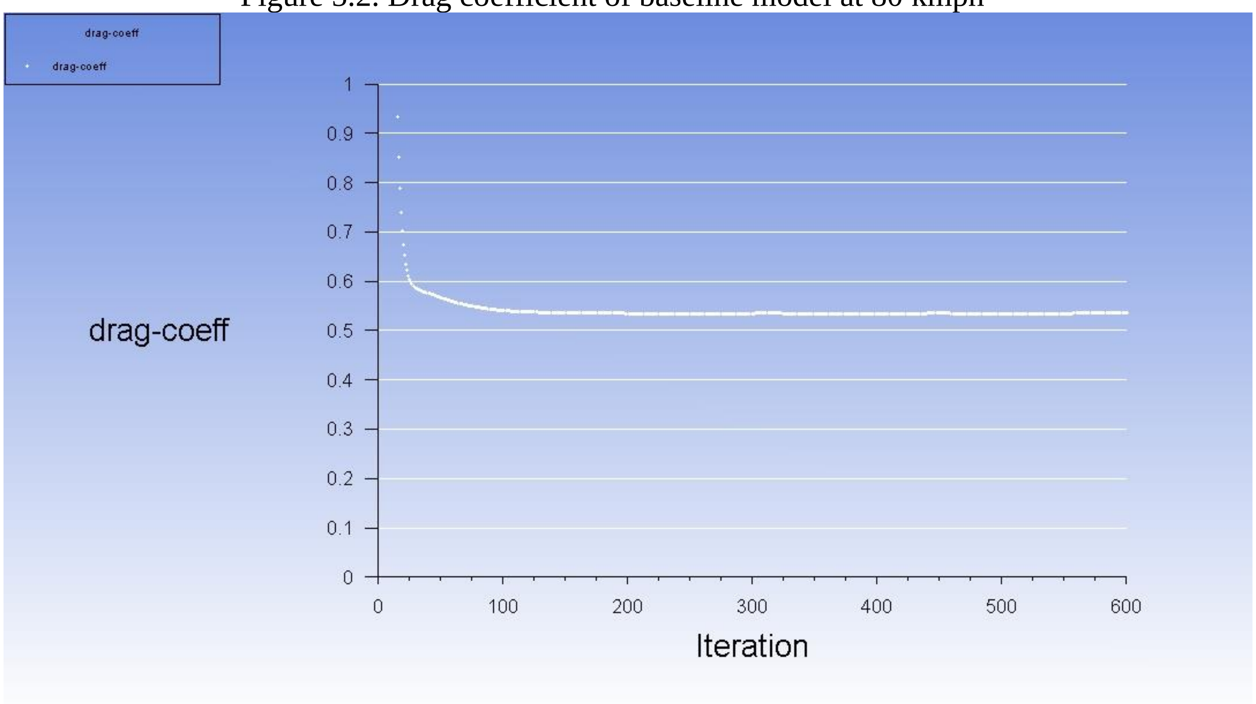

Figure 5.3. Drag coefficient of baseline model at 100 kmph

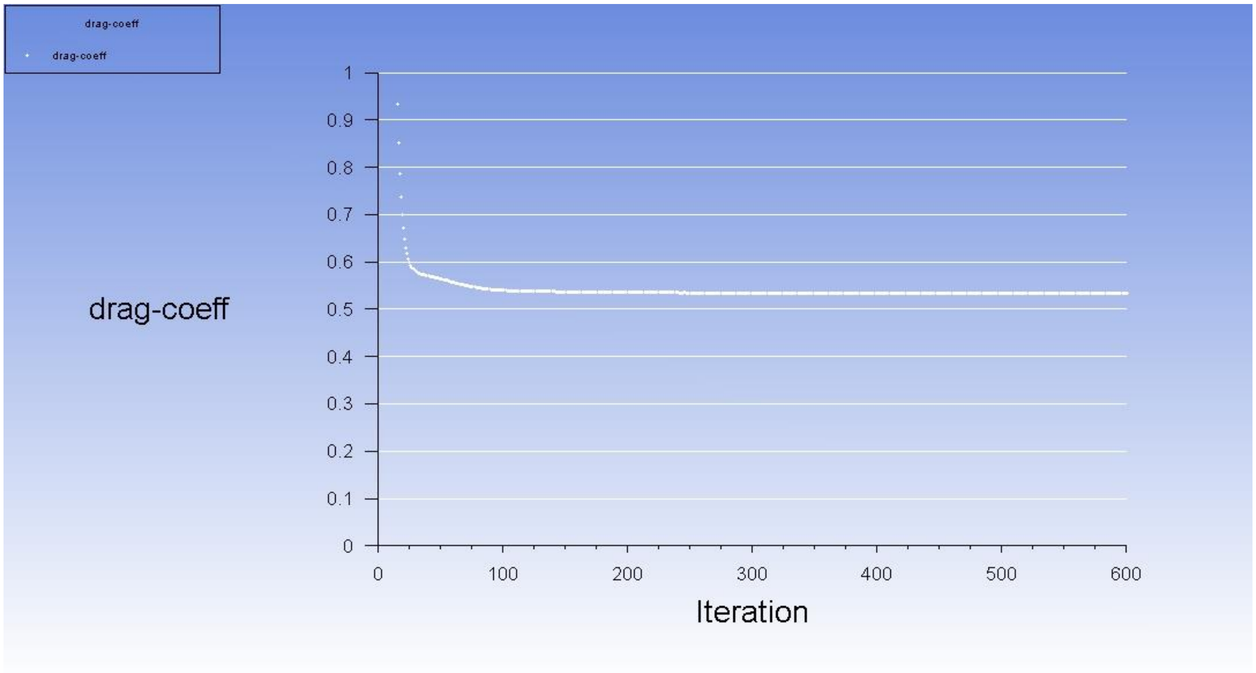

Figure 5.4. Drag coefficient of baseline model at 120 kmph

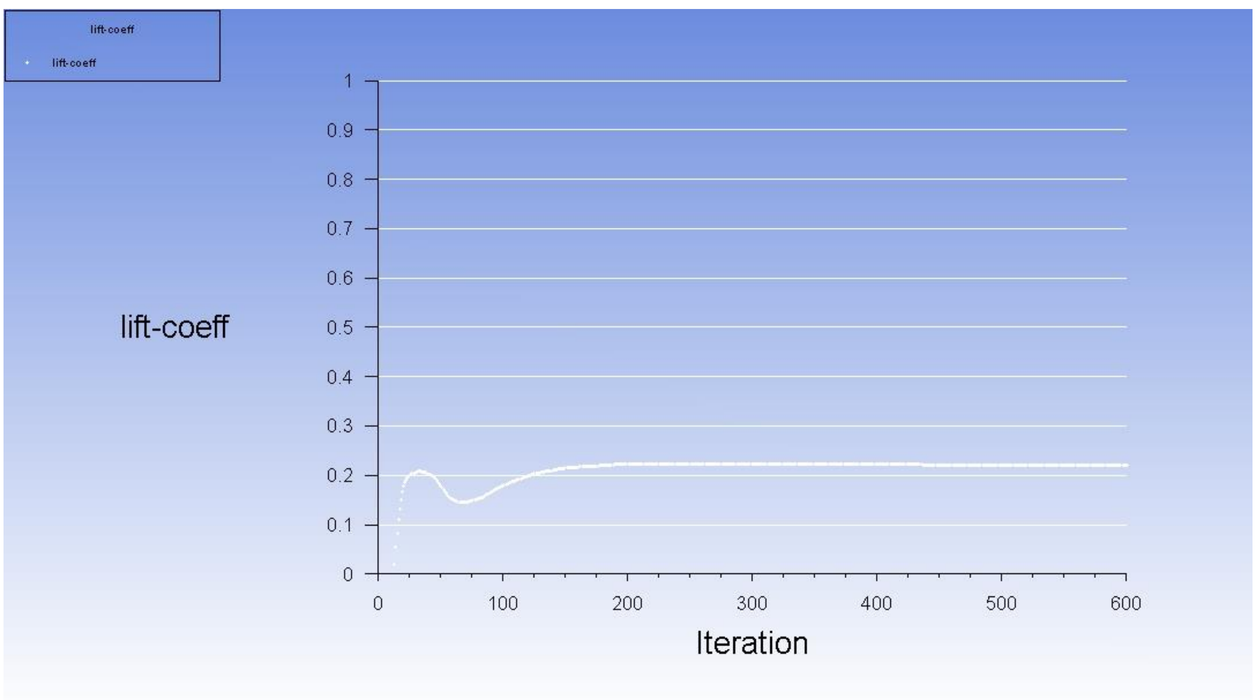

Figure 5.5. Lift coefficient of baseline model at 80 kmph

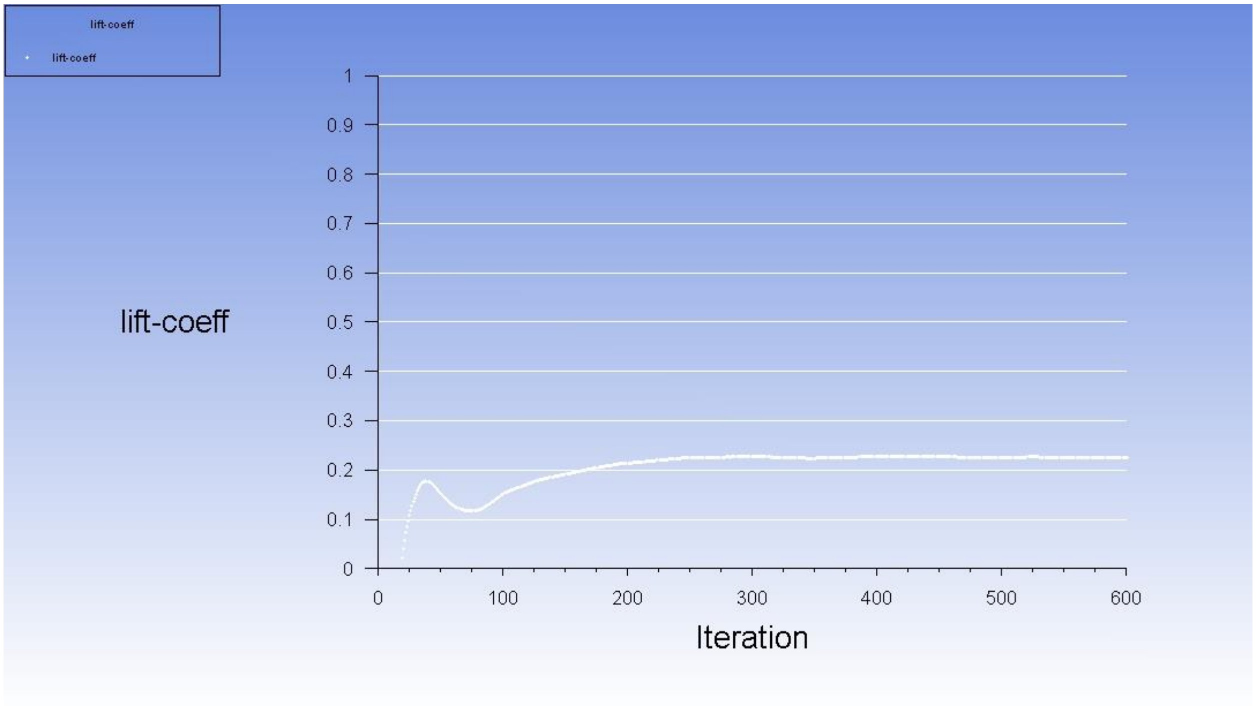

Figure 5.6. Lift coefficient of baseline model at 100 kmph

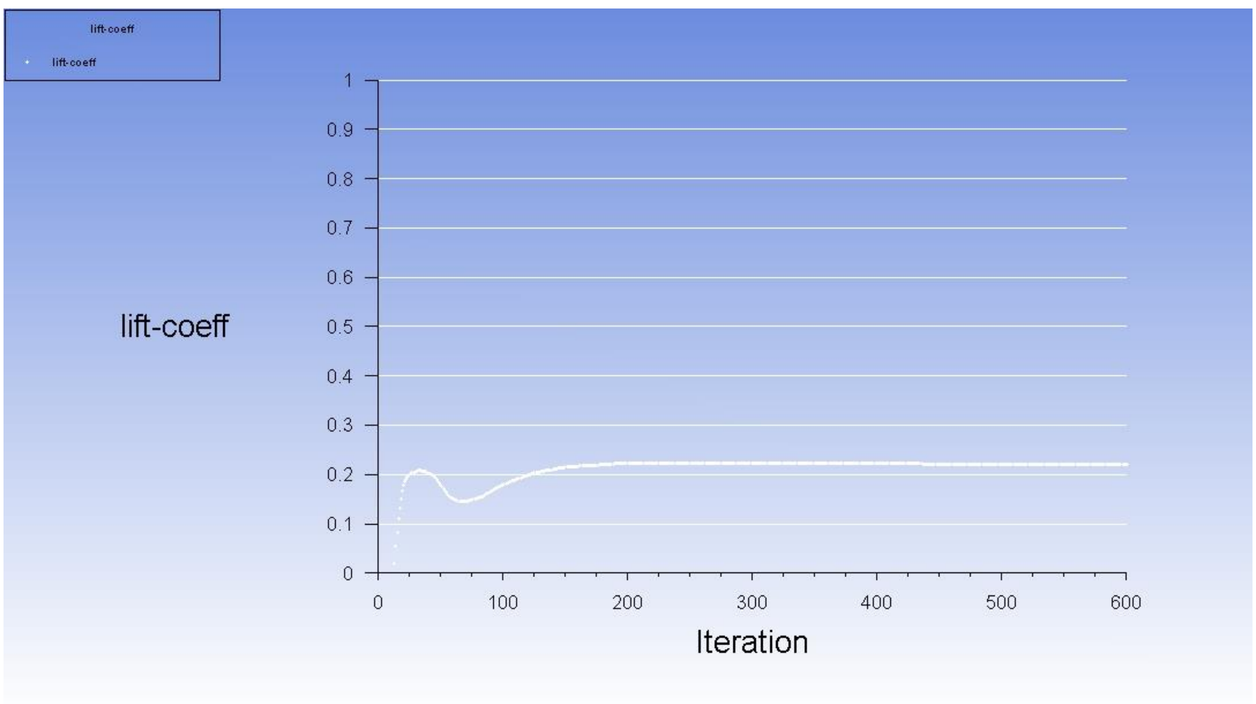

Figure 5.7. Lift coefficient of baseline model at 120 kmph

Table 5.1. Explains the drag and lift coefficient of baseline model at different speed of the vehicle.

Table 5.1. Drag and Lift coefficient of baseline at different speeds

Model	Speed (kmph)	Cd	Cl
Baseline Model	80	0.550895	0.220021
	100	0.544352	0.266892
	120	0.532913	0.243112

It can be noted from the above drag and lift coefficient figures (Figure 5.2-5.7) and/or table 5.1 that even if both parameters converge way before the 600th iteration, the lift coefficient converges much earlier. Another thing is that the drag coefficient (Figure 5.2-5.4) of the baseline model decreases with increasing speed, whereas the lift coefficient (Figure 5.5-5.7) decreases with speed. The decrease in lift coefficient at with speeds causes high downward force which is favorable that it increases vehicle stability at higher speed.

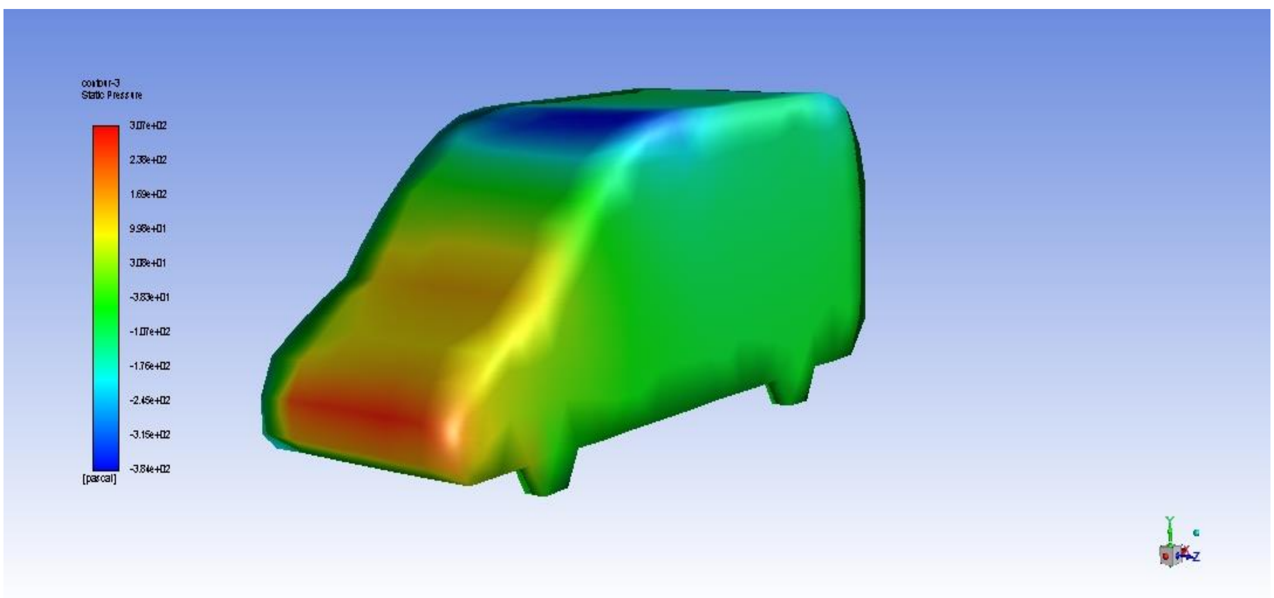

Figure 5.8. Pressure contour of baseline model at 80 kmph

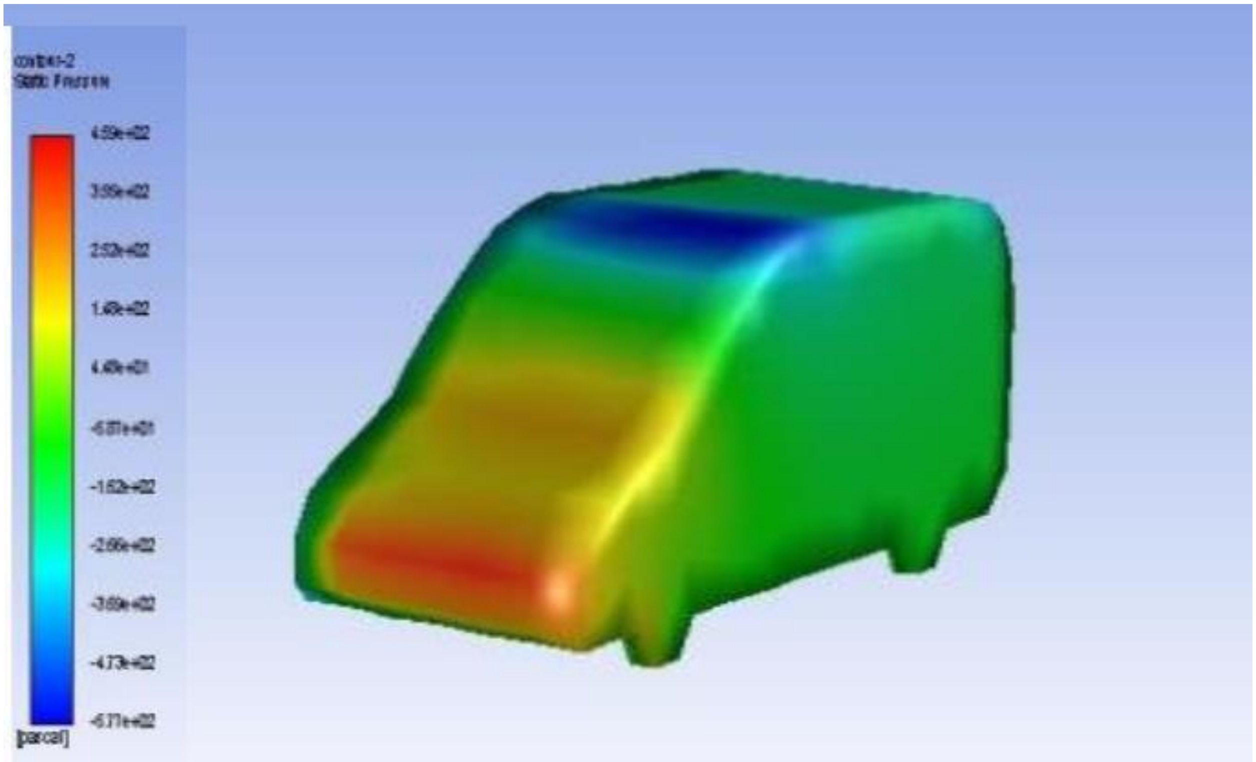

Figure 5.9. Pressure contour of baseline model at 100 kmph

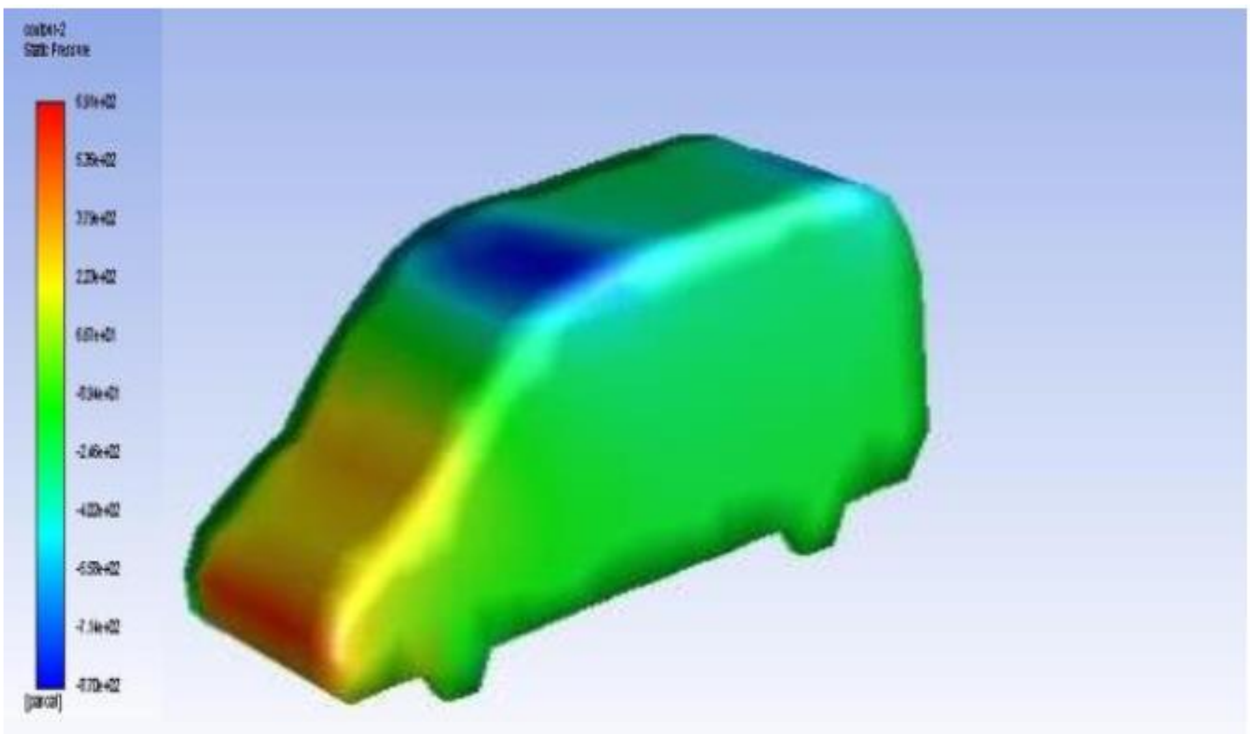

Figure 5.10. Pressure contour of baseline model at 120 kmph

The pressure distribution on the surface of the baseline model can be seen on Figure 5.8-5.10. From the figures we can see that the maximum pressure occurs on the grill and, at the junction between the engine hood and the windshield. We can also see that with increasing speed the maximum pressure increases which contributes to high amount of drag at higher speeds.

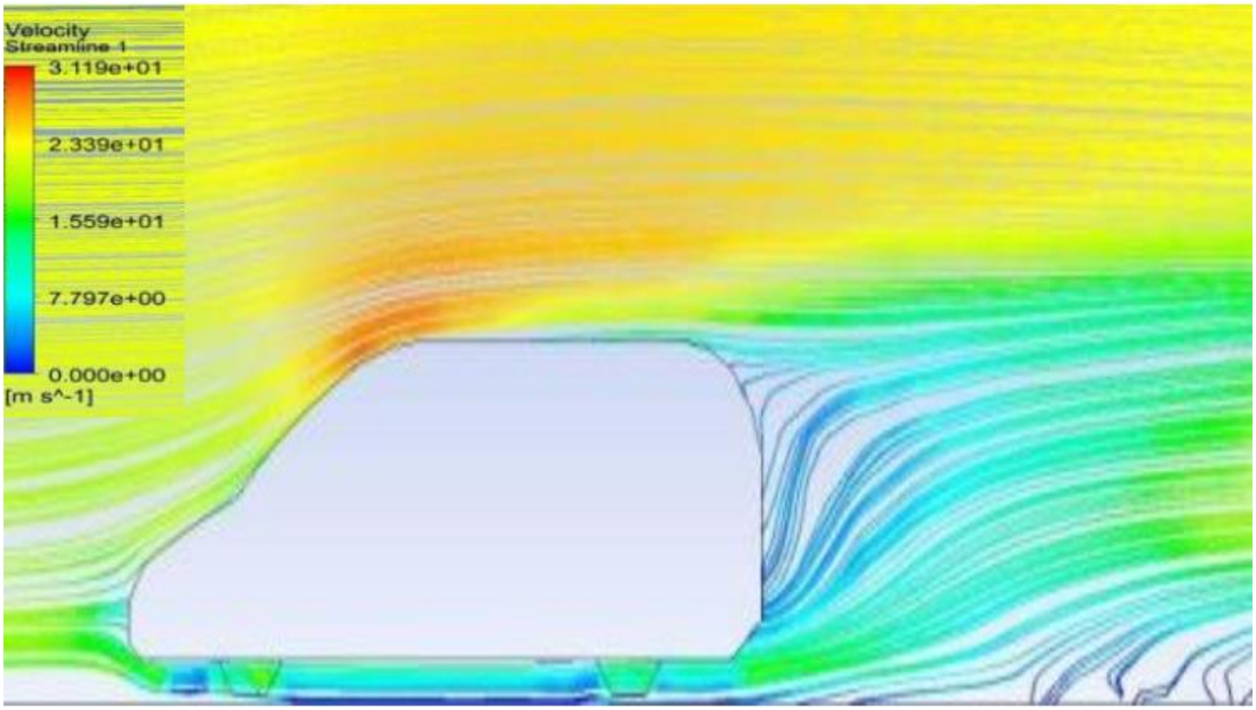

Figure 5.11. Velocity contour of baseline model at 80 kmph

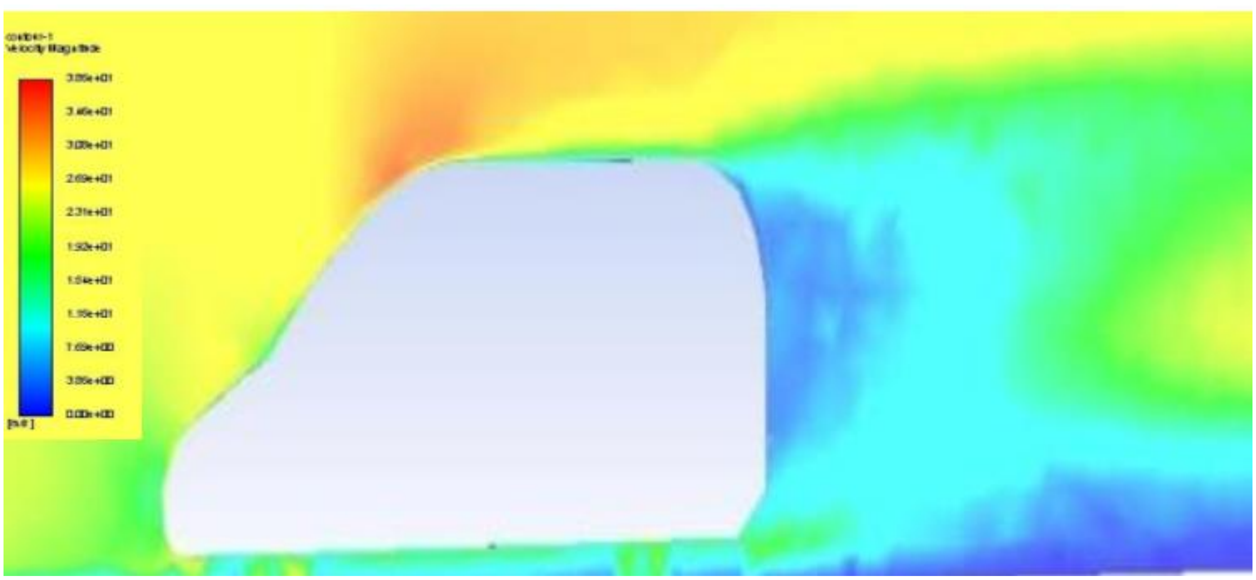

Figure 5.12. Velocity contour of baseline model at 100 kmph

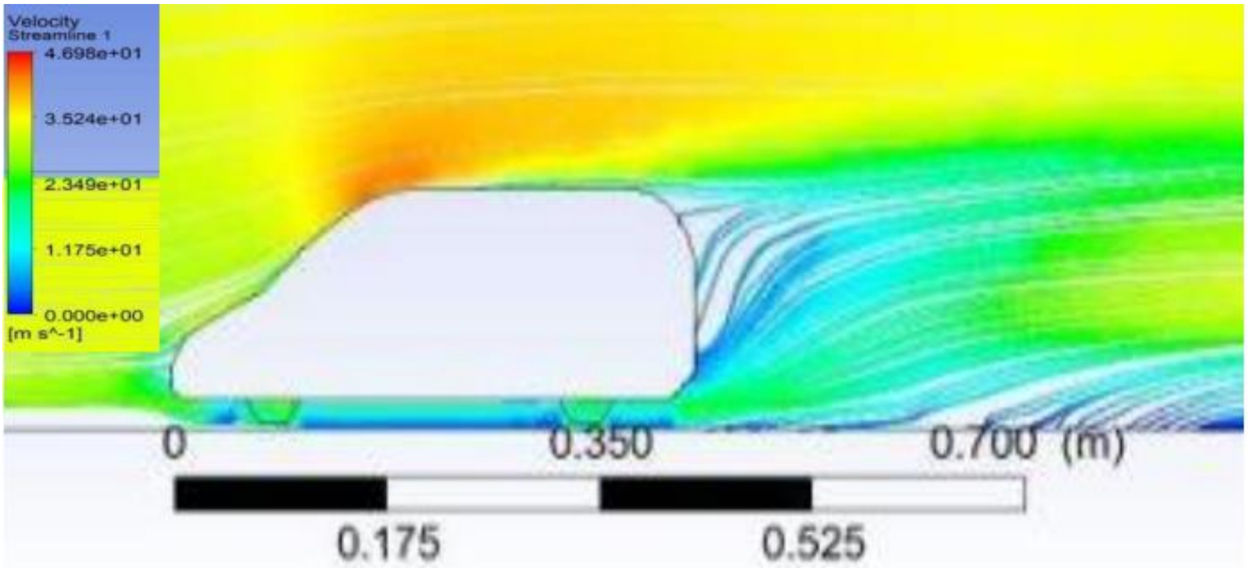

Figure 5.13. Velocity contour of baseline model at 120 kmph

To determine the reduction in the drag coefficient from the addition of spoiler on the rear end of the roof the drag coefficient, lift coefficient and flow field around the vehicle without any drag reduction device was examined first. These simulations give the base drag coefficient for the study. After simulating the baseline model, the modified models were simulated next. After simulation all models were compared to the flow field, drag and lift coefficient of the baseline vehicle. To determine the percent reduction of parameter due to the spoiler the drag coefficients were compared. To analyze the flow around the vehicle due to its motion it is important to look at the velocity field. This analysis was able to provide important information about the turbulence and air flow present around the vehicle. Figure (5.11-5.13) above illustrates the velocity contour obtained using Fluent for the midibus vehicle without any drag reducing device employed at three different speeds. A legend can be observed in Figure 5.11-5.13, representing the magnitude of the velocity of the air flow in m/s, with colors corresponding to the velocity contour shown. It should be noted that the velocities were 22.22 m/s, 27.78 m/s, and 33.33 m/s and the maximum velocity for each model in the flow field due to flow separation was nearly 31.58 m/s, 44.43 m/s and 47.51 m/s and the minimum velocity was 0.03205 m/s, 0.0678 m/s and 0.078 m/s respectively. The colors indicate the velocity magnitude. The green color in the contour represent the velocities close to the input velocity. Sudden changes in the geometry of the vehicle created sections of maximum velocities. Red color represents high velocity areas of the contour. These high velocities are surrounded by slowly decreasing velocities which are represented by orange through yellow colored sections in the contour. This was continued until, farther away from the vehicle, then the velocity evened out at the magnitude of the input velocity. Increase in the velocity from the input velocity to the maximum velocity causes flow to separate and makes the low velocity air to swirl at the back of the vehicle. From the velocity distribution shown in Figures 5.11, 5.12 and 5.13, it can be observed that flow separation occurs on the rear end of the vehicle due to sudden change in the shape. The flow separation produces a low-pressure zone and it is also seen that vortices are formed due to recirculation. It can also be inferred that the velocity of flow increases over the vehicle top surface. This can be attributed to the convergence of flow. The high-speed air will not follow the outer contour of the vehicle instead it gets separated on the rear end, forming a low-pressure zone and inducing pressure drag on the vehicle.

•

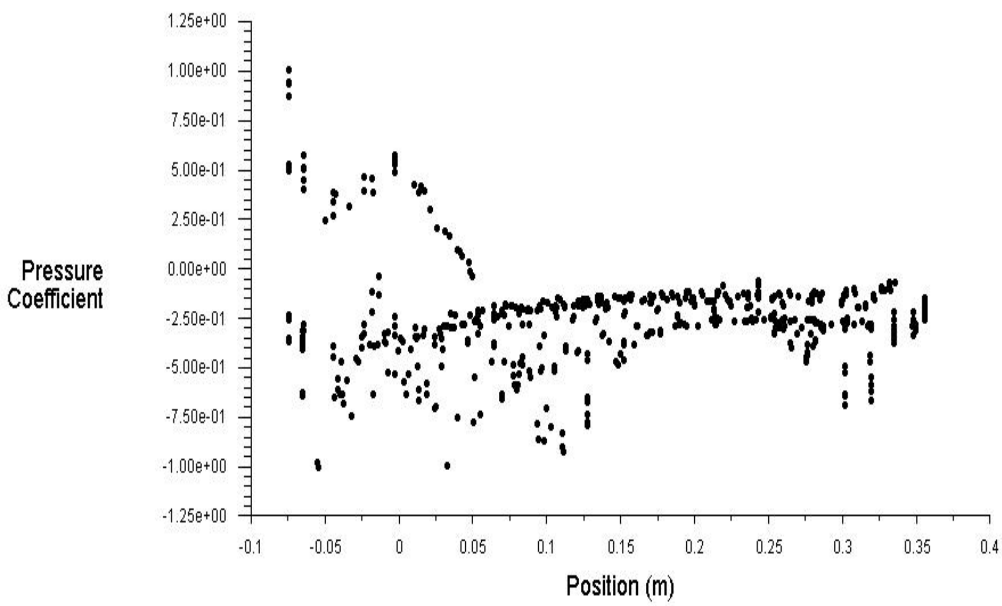

Figure 5.14. Surface pressure distribution along symmetry plane of baseline model

5.2. Validation of the result

This study was validated using results of previous studies conducted [39]. Comparison of streamlines, and Surface pressure distribution on the vehicle was made between the results from [39] and the present study as shown in figures (5.15-5.18) below.

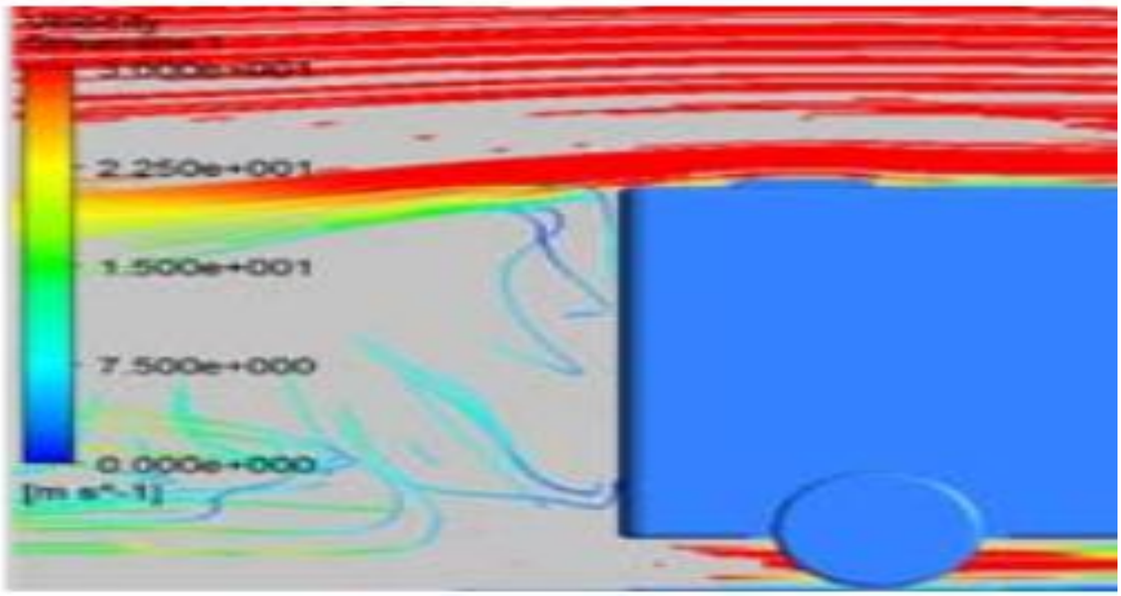

Figure 5.15. Streamline on symmetry plane [39]

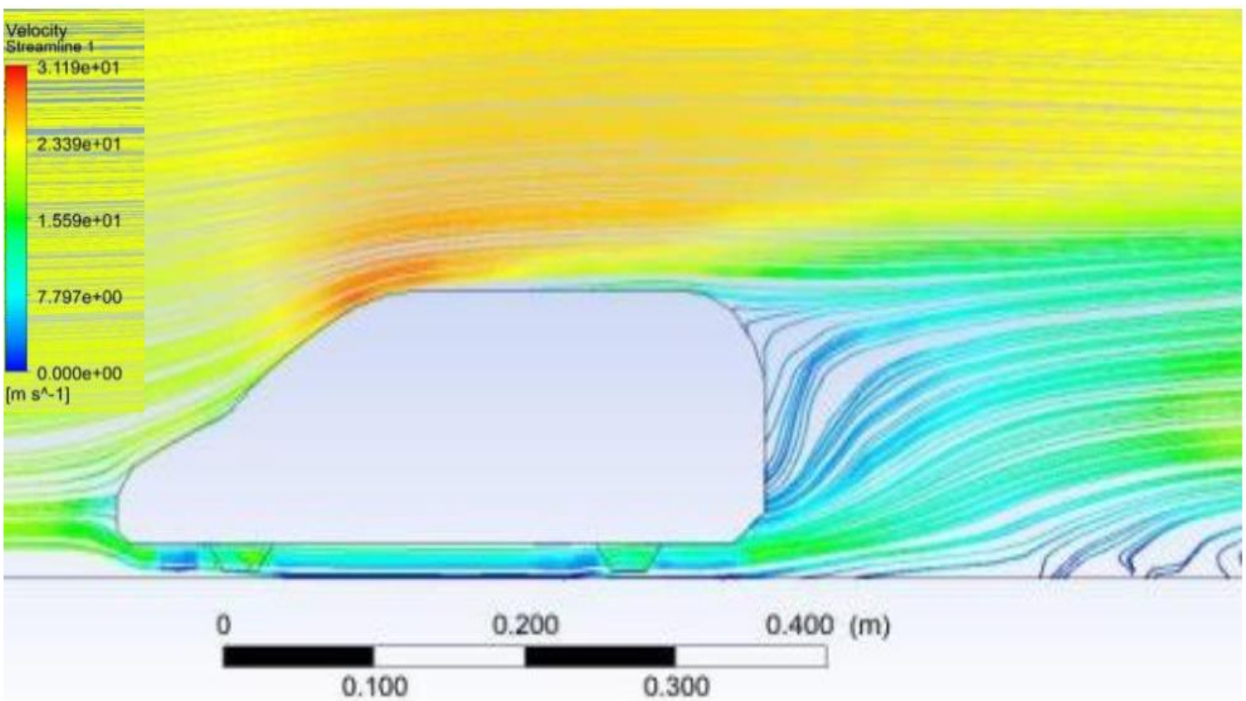

Figure 5.16. Streamline on symmetry plane

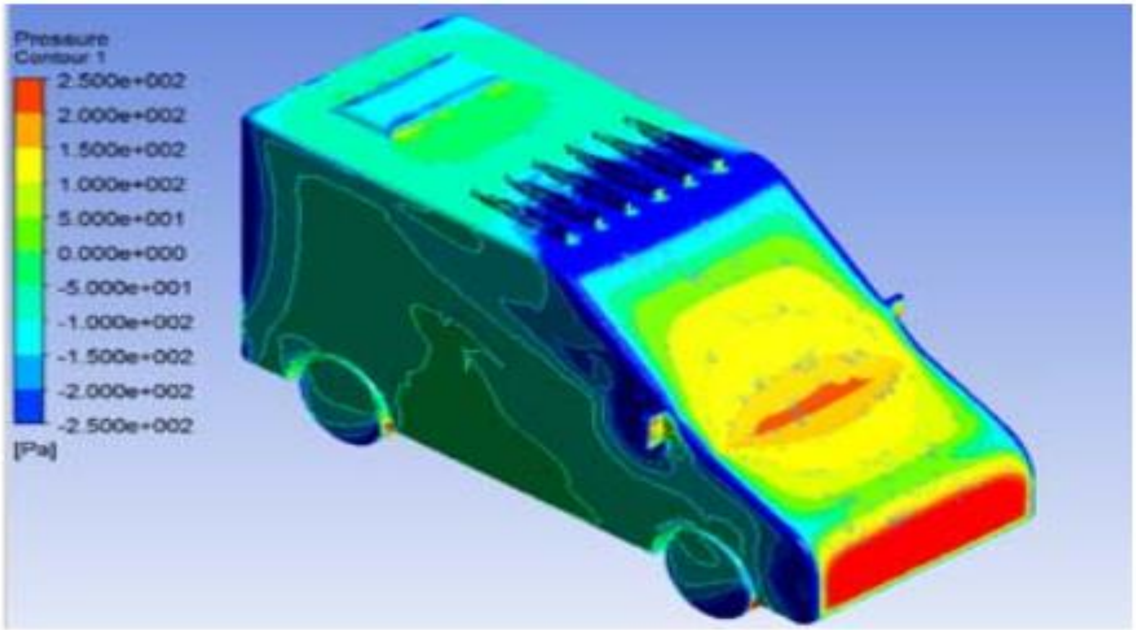

Figure 5.17. Pressure distribution [39]

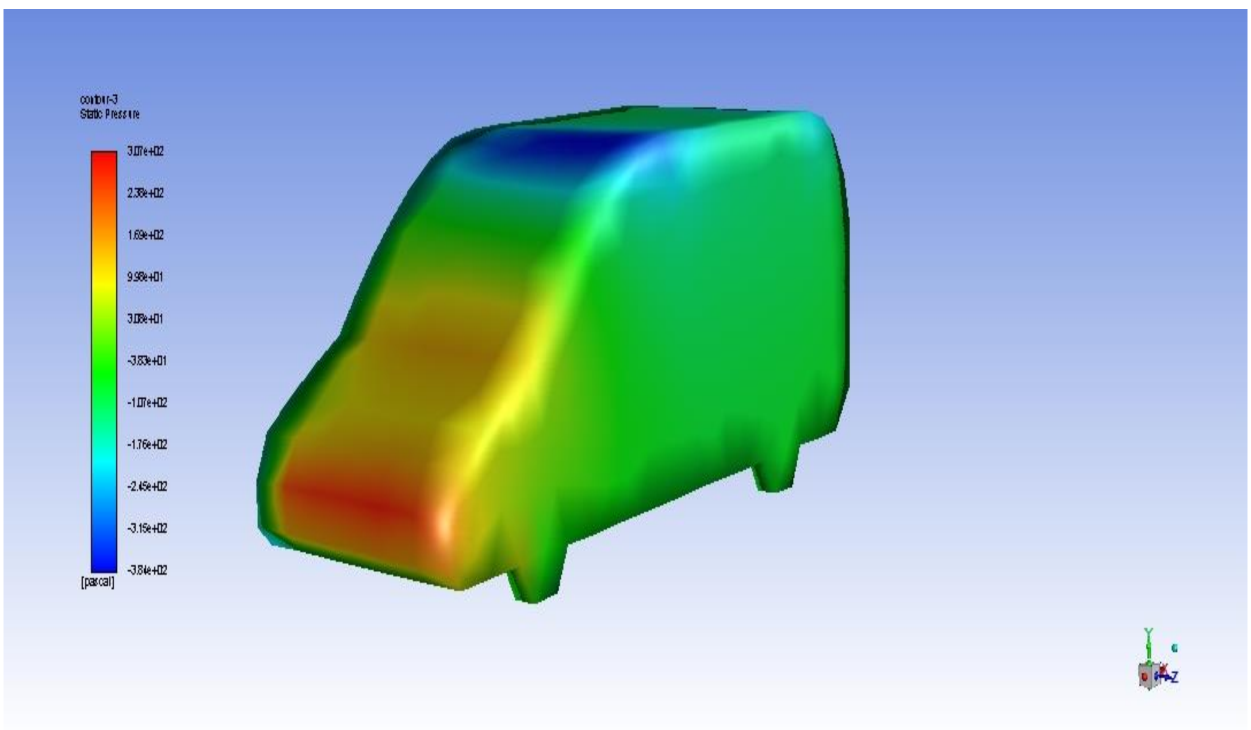

Figure 5.18. Pressure distribution

From above we can see that both the streamlines fashion, and pressure distribution on the minibus vehicle from Bayindirli Cihan[38] and present study are almost the same. On both studies how the air swirls at the back of minibus vehicle and the way the air flows in the wake region are similar. The surface pressure distribution on the vehicle surface in both cases changes between maximum and minimum values, whereas on the under body of the vehicle the surface pressure change is very small.

Additionally, as noted in the literature of different paper the drag coefficients of passenger vehicles range from $0.3 \leq C_d \leq 0.5$, therefore the drag coefficient found in this simulation is in range.

5.2.1. Model One

Results of scaled residuals, drag and lift coefficients, pressure and velocity contours at speed of 80 kmph 100 kmph and 120 kmph for model one are depicted here.

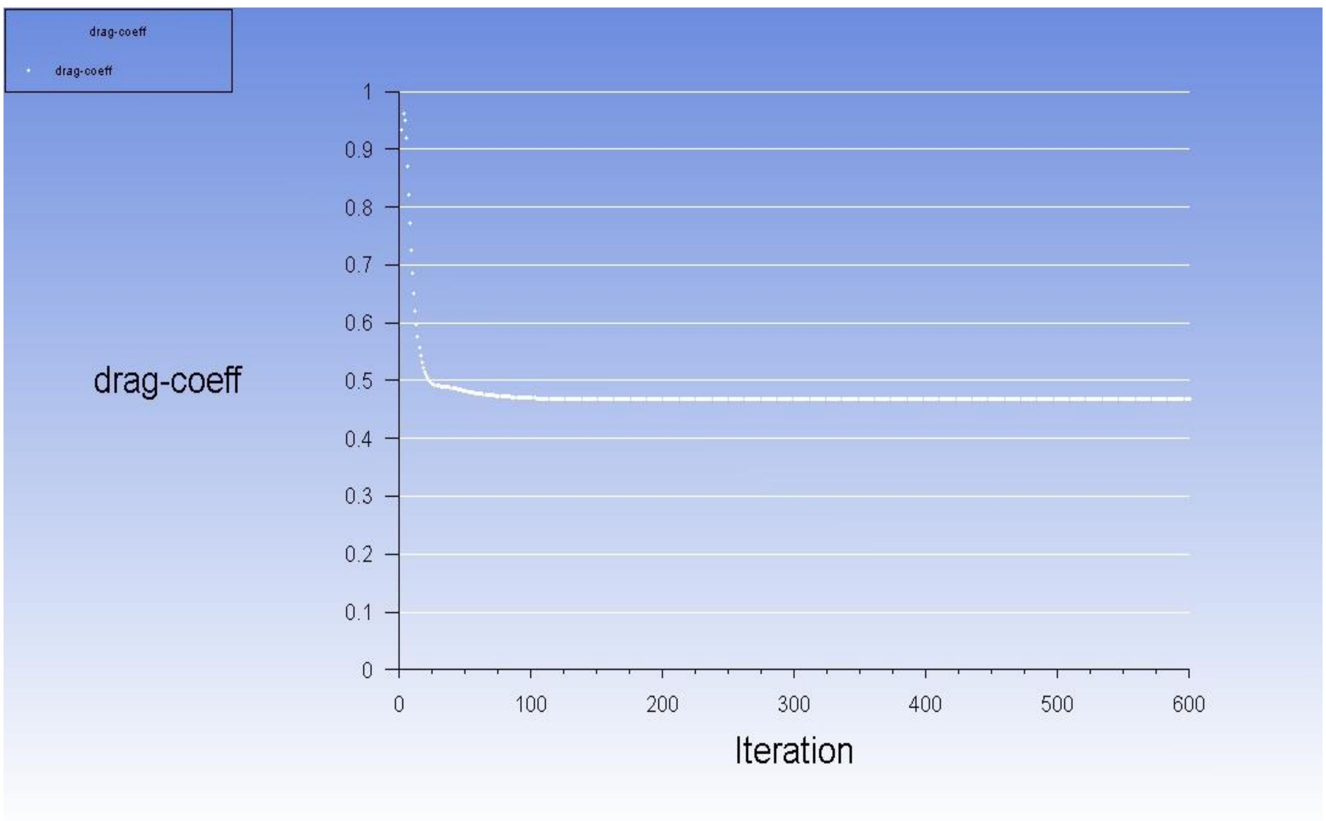

Figure 5.19. Drag coefficient of model one at 80 kmph

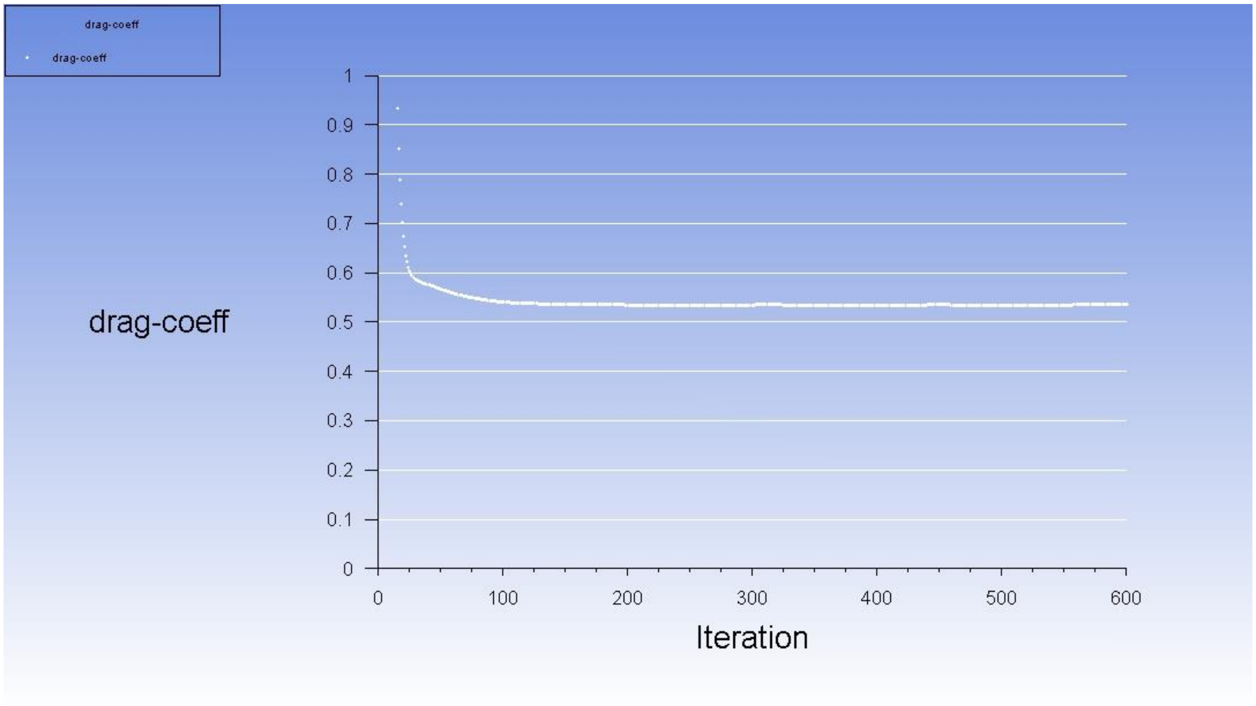

Figure 5.20. Drag coefficient of model one at 100 kmph

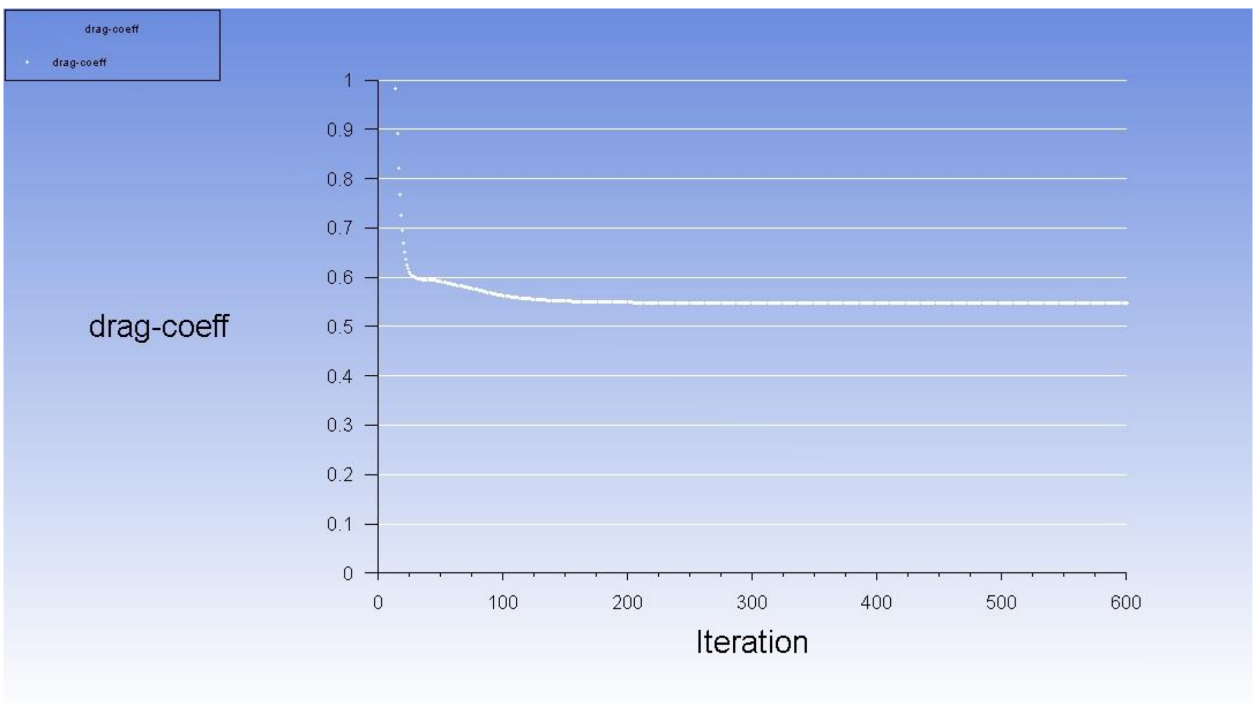

Figure 5.21. Drag coefficient of model one at 120 kmph

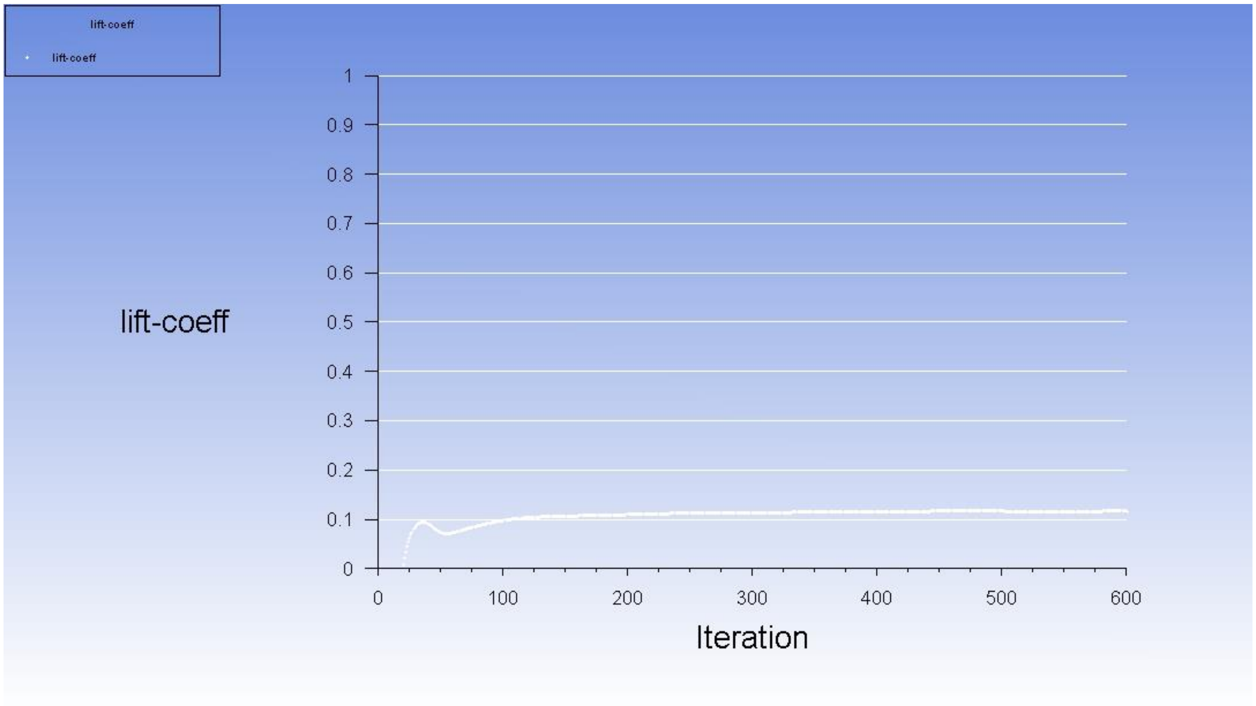

Figure 5.22. Lift coefficient of model one at 80 kmph

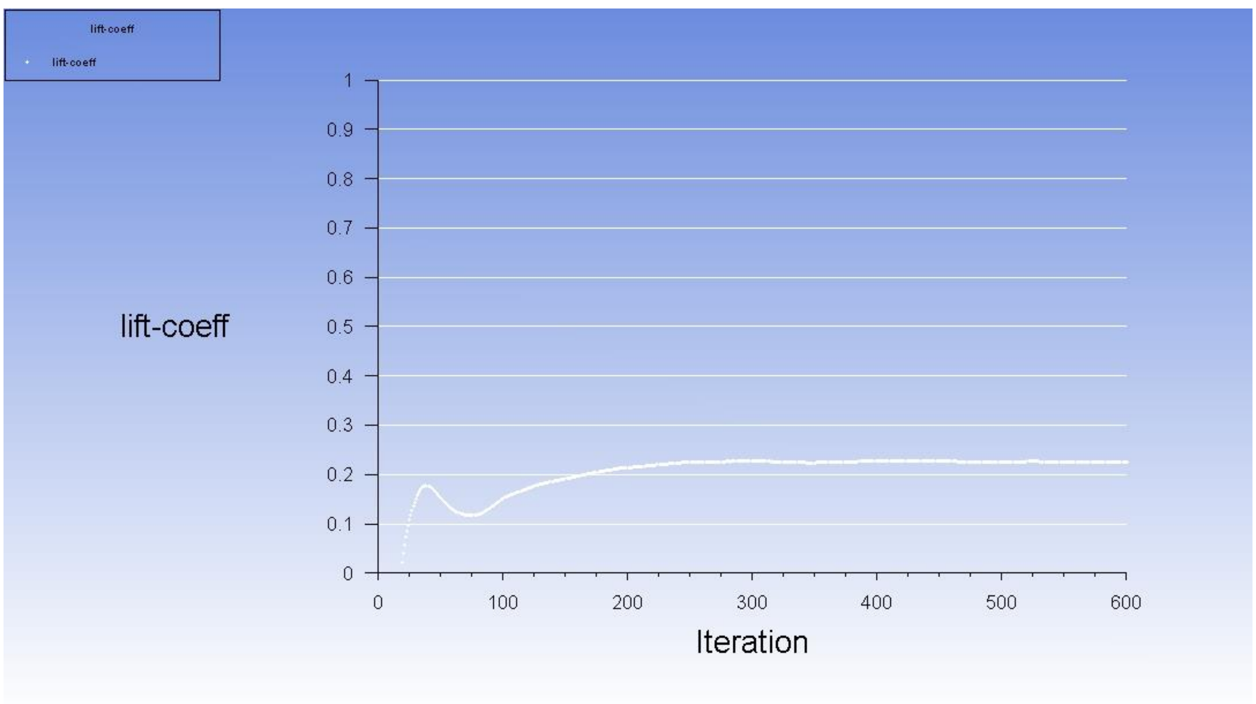

Figure 5.23. Lift coefficient of model one at 100 kmph

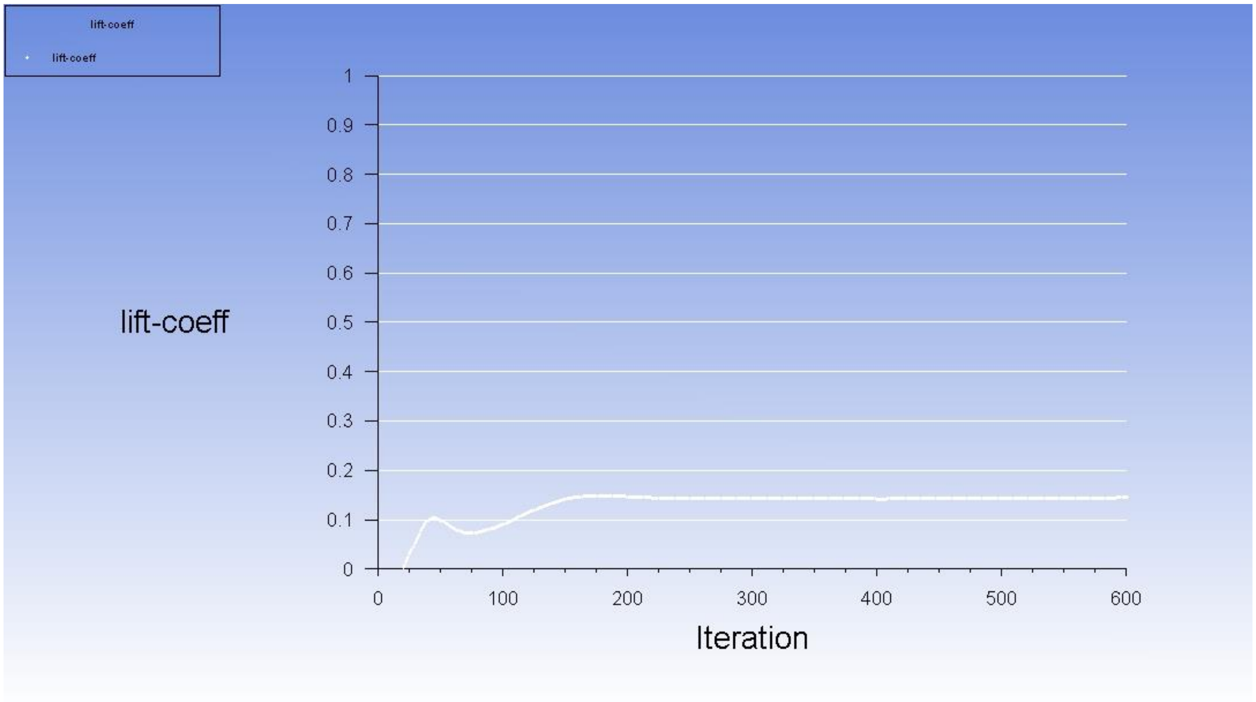

Figure 5.24. Lift coefficient of model one at 120 kmph

Table 5.2. Explains the drag and lift coefficient of model one at different speed of the vehicle.

Table 5. 2. Drag and lift coefficient of model one at different speeds

Model	Speed(kmph)	*Cd*	Cl
Model One	80	0.46708	0.11525
	100	0.53410	0.22325
	120	0.54728	0.14352

The drag coefficient Figures (5.19-5.21) given above for model one show that the drag coefficient increases with increasing speed, but the amount of drag is lower than that of the baseline model. And here also in model one the lift coefficient Figure 5.22-5.24 increases with increasing speed, but the amount of lift is lower than that of the baseline model. The Figures 5.22, 5.23 and 5.24 show how the lift coefficient converges with each iteration. The results of drag and lift coefficients are shown in Table 5.2. The increase in downward force is very necessary for stability of vehicle at high speed.

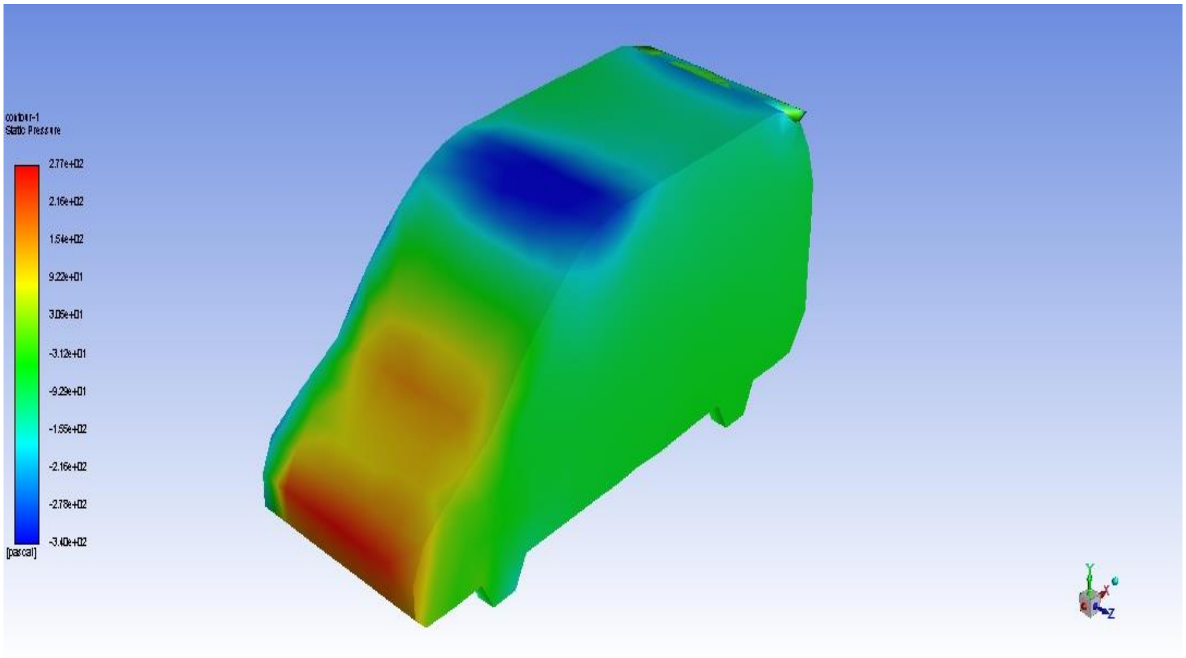

Figure 5.25. Pressure contour of model one at 80 kmph

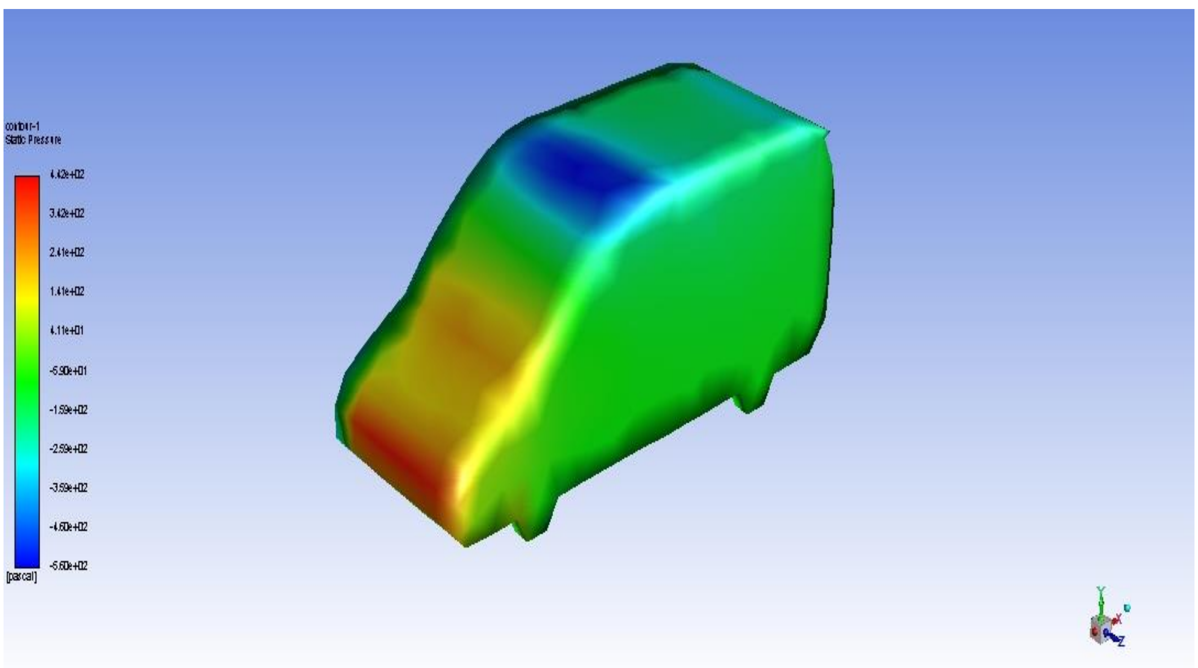

Figure 5.26. Pressure contour of model one at 100 kmph

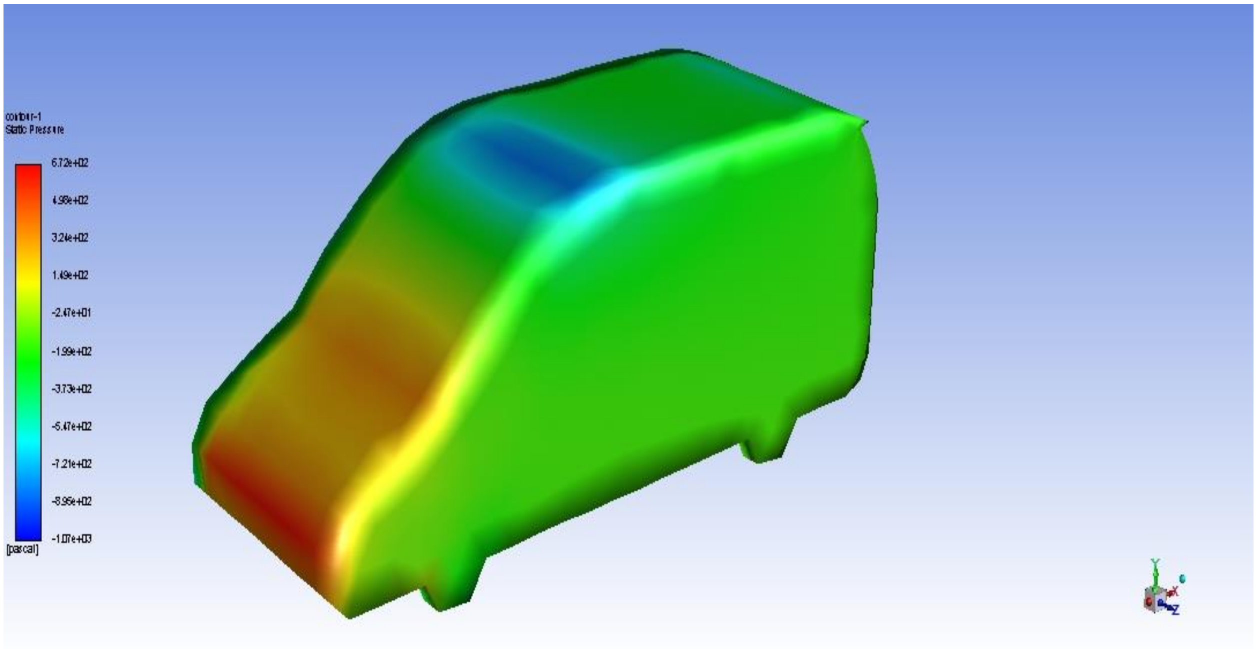

Figure 5.27. Pressure contour of model one at 120 kmph

From the pressure contour Figures 5.25-5.27 we can see how the maximum pressure varies with the increasing speed of the model. The stagnation pressure on the grill of the vehicle is the peak pressure. The second peak is on surface of the windshield and the engine hood. Due to the sudden change in the profile of the model on the cab pressure reduction occurs on the top(roof) of the vehicle and on the top of spoiler.

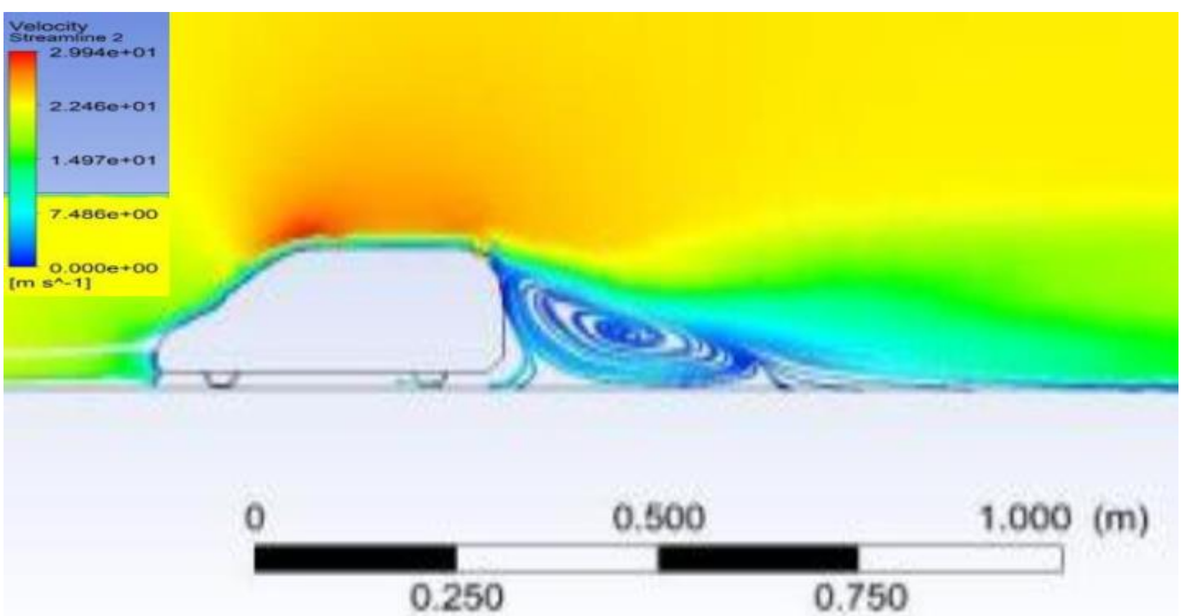

Figure 5.28. Velocity contour of model one at 80 kmph

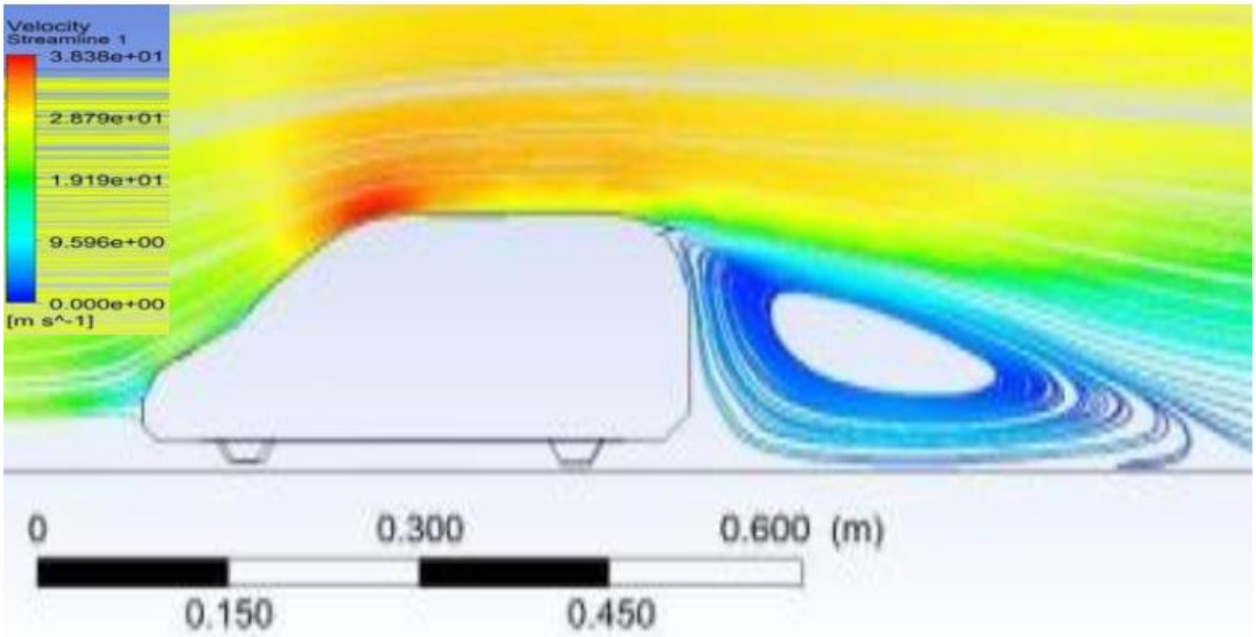

Figure 5.29. Velocity contour of model one at 100 kmph

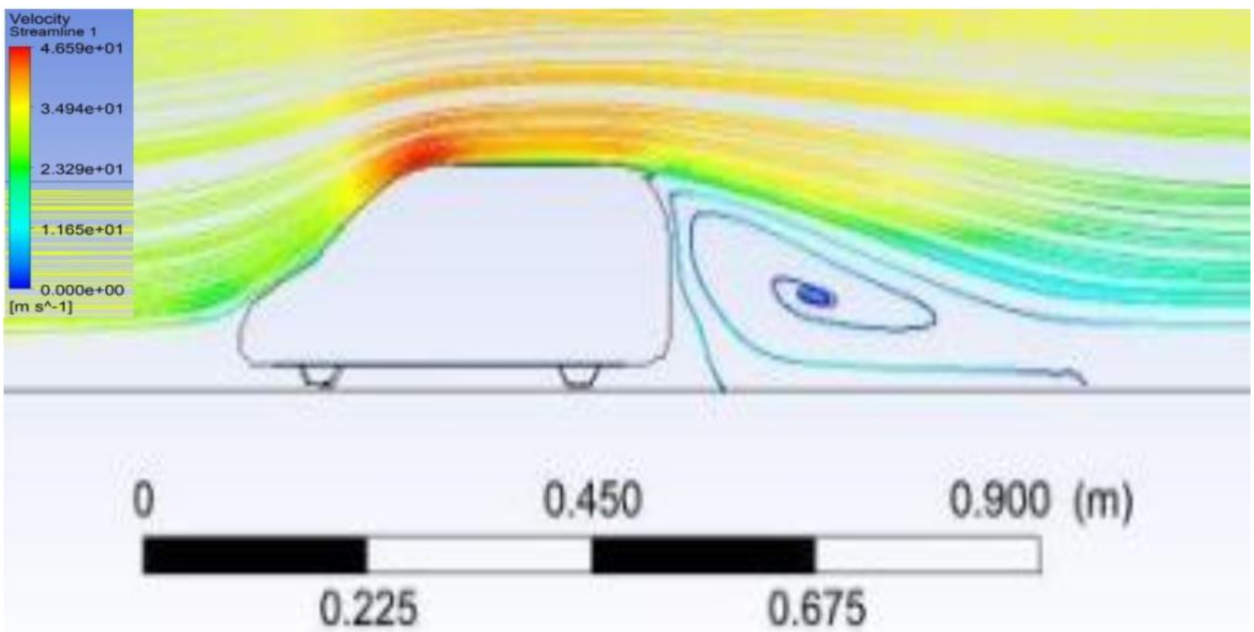

Figure 5.30. Velocity contour of model one at 120 kmph

On this model spoiler attached to the rear end of the roof of the baseline model roof at zero inclination angle. The simulation procedure was the same as model one. The scaled residuals were similar with the baseline model.

When examining the model the spoiler changes the air flow around the vehicle. From the baseline model and model one (Figure 5.28-5.30) the difference in contour can be clearly be seen. From the result the wake region behind the tail of the vehicle in model one has decreased than that of the baseline model. The decreament in wake region results in decreament the drag coefficient of the vehicle. Also the amount of air swirling at the back of the vehicle is reduced in model one. The reduction in the amount of the air at the back of the vehicle is because of the air being thrown and guided away from the back of the vehicle by the spoiler. The result can be seen from the drag and lift curves.

It can be noted from the pressure contour and the surface pressure distribution Figure 5.25-5.27, that there is a decrease in pressure on the upper surface of the spoiler. This shows that even if the lift coefficient decreases with increasing speed, the amount it decreases is not as much as the drag reduced from the baseline model due to the spoiler. In other way, it shows that the drag coefficient is reduced in model one sufficiently, but the spoiler does not decrease lift greatly. We can also see that the percent difference in lift coefficient between the baseline model and model one decreases as the speed increases. Whereas on the under body of the vehicle the surface pressure distribution is the same as that of the baseline model. The surface pressure distribution figure is the same in fashion and shape for all speeds.

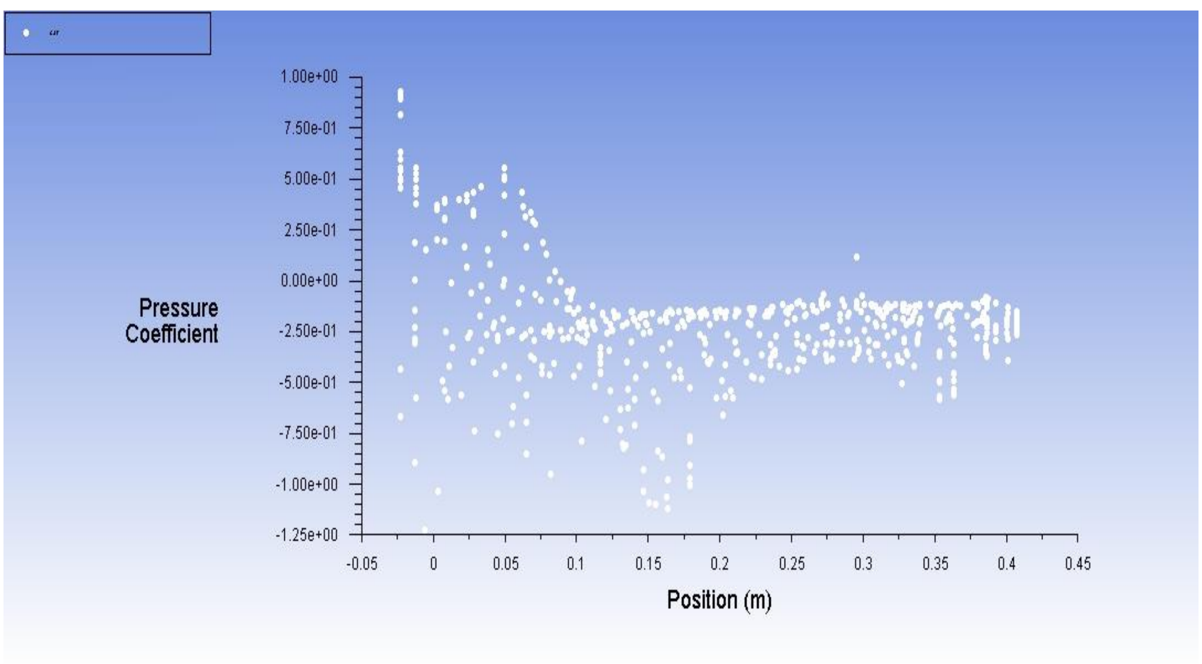

Figure 5.31. Surface pressure distribution along symmetry plane of model one

5.2.2. Model Two

Result of scaled residuals, drag and lift coefficient, pressure and velocity contour at speed of 80 kmph 100 kmph and 120 kmph for model two are depicted here.

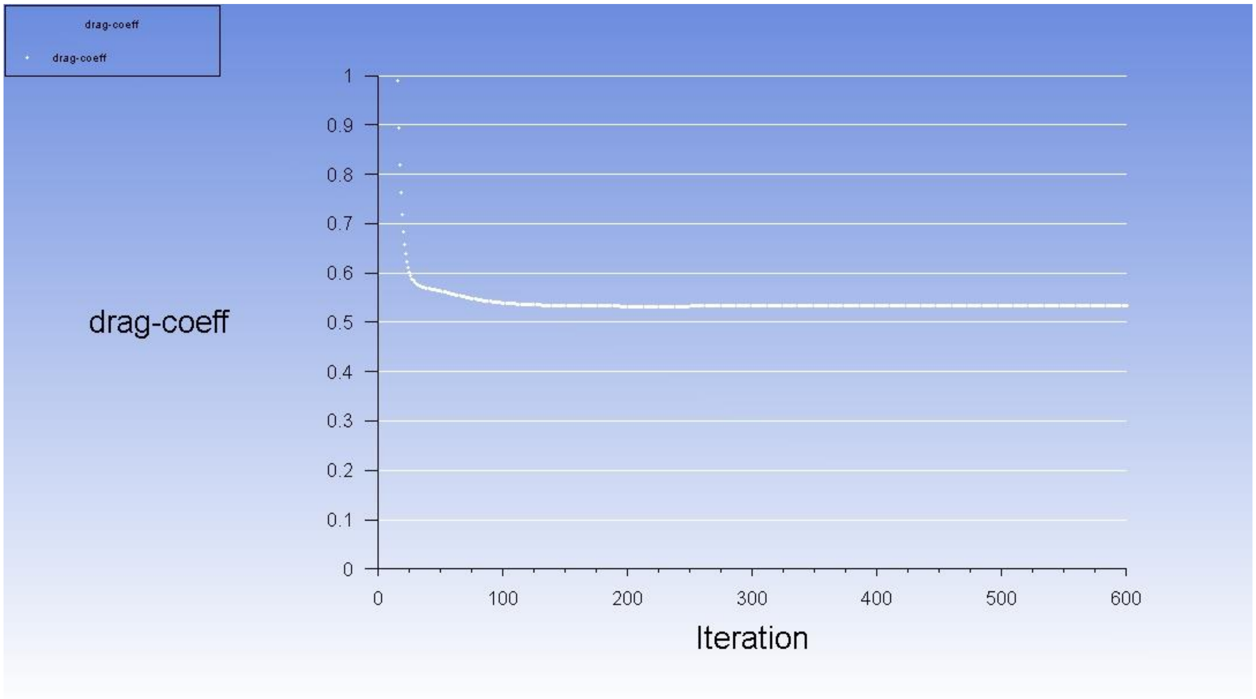

Figure 5.32. Drag coefficient of model two at 80 kmph

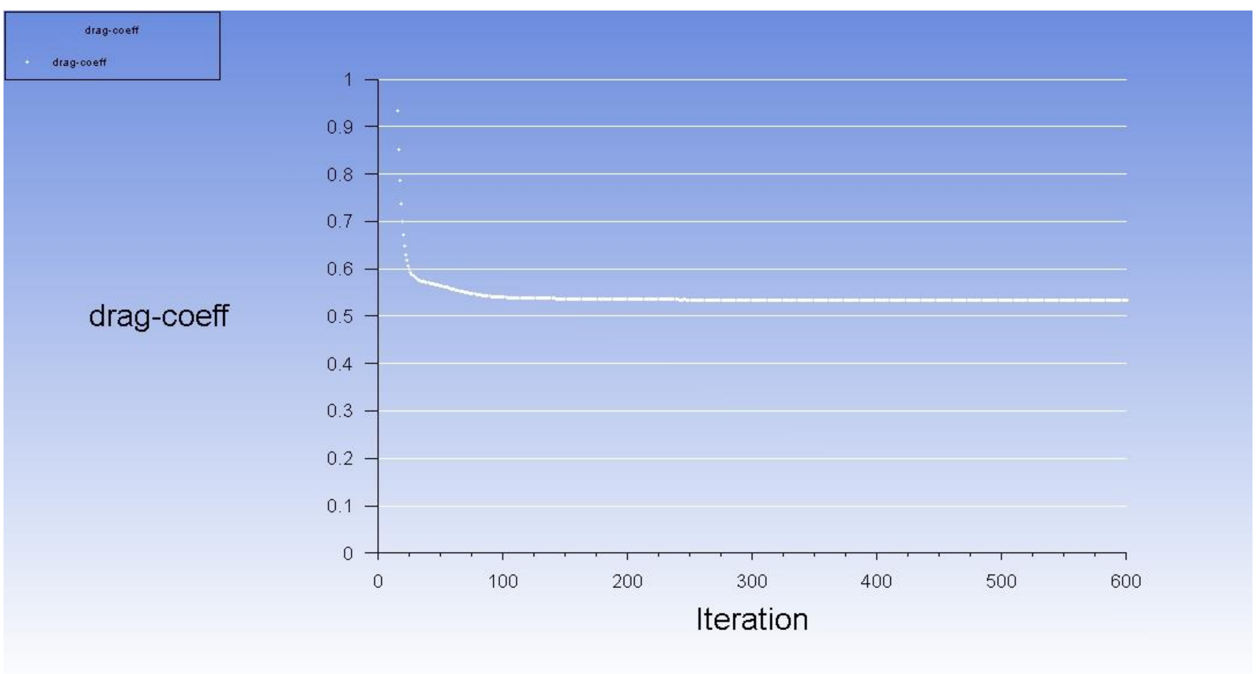

Figure 5.33. Drag coefficient of model two at 100 kmph

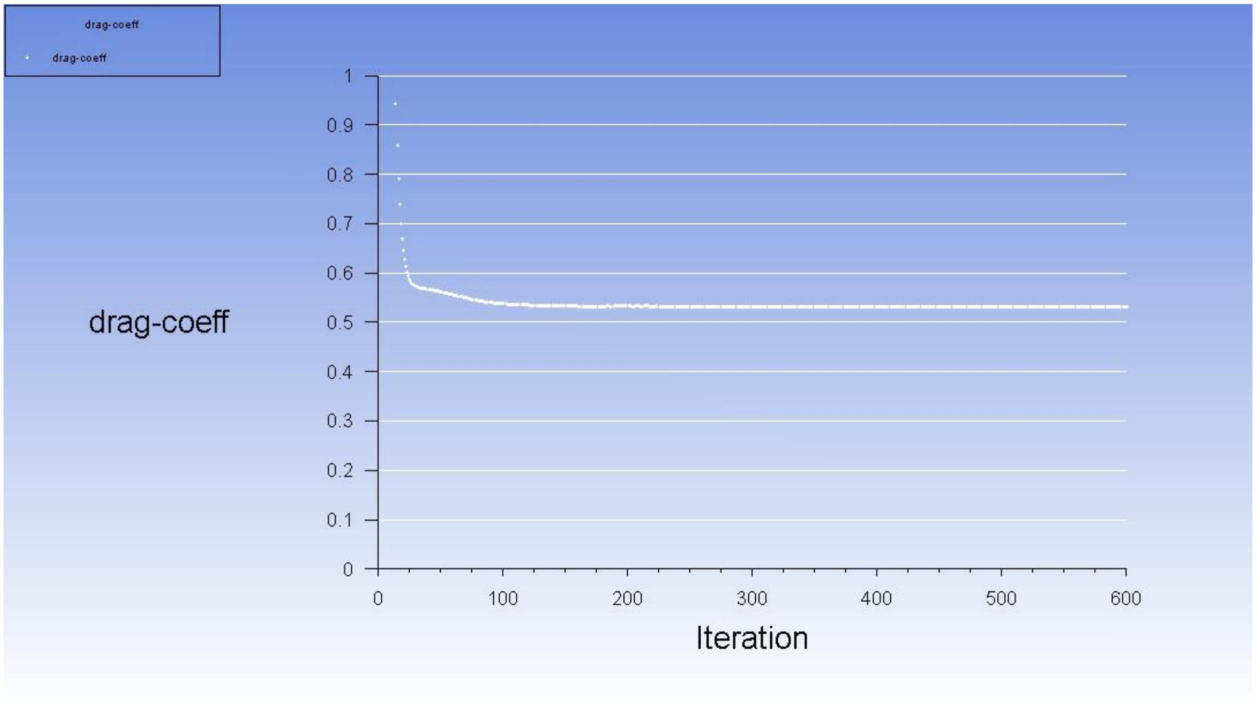

Figure 5.34. Drag coefficient of model two at 120 kmph

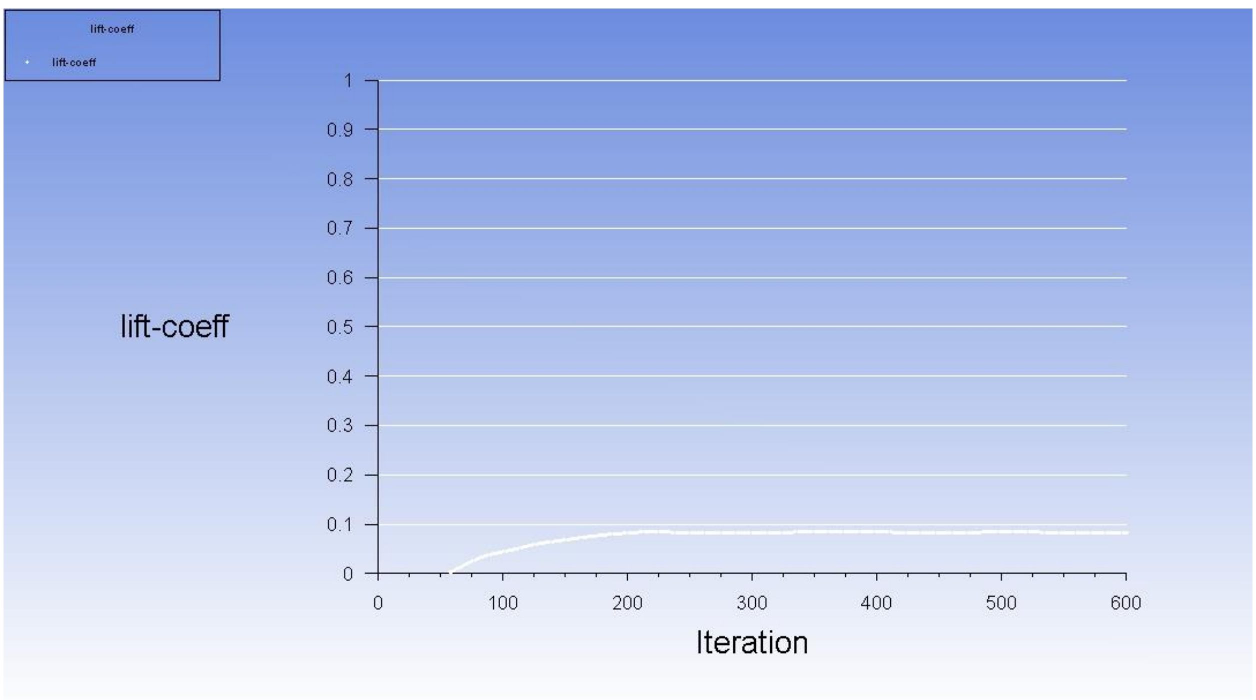

Figure 5.35. Lift coefficient of model two at 80 kmph

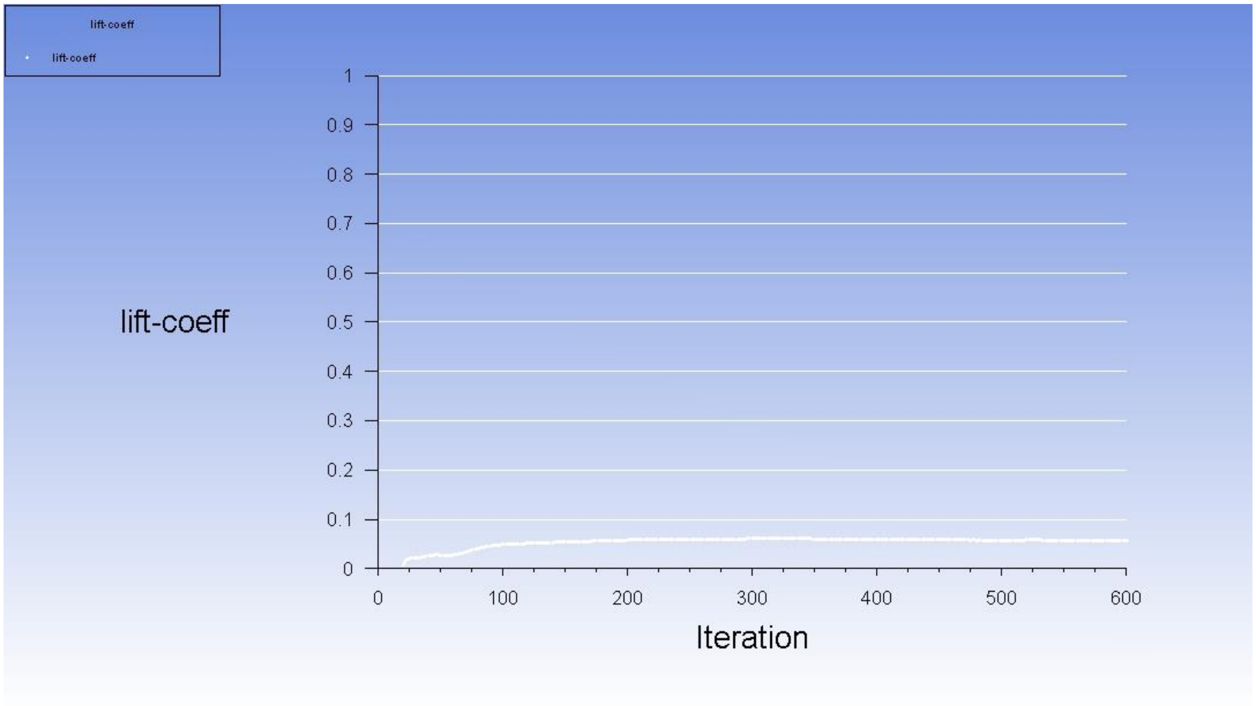

Figure 5.36. Lift coefficient of model two at 100 kmph

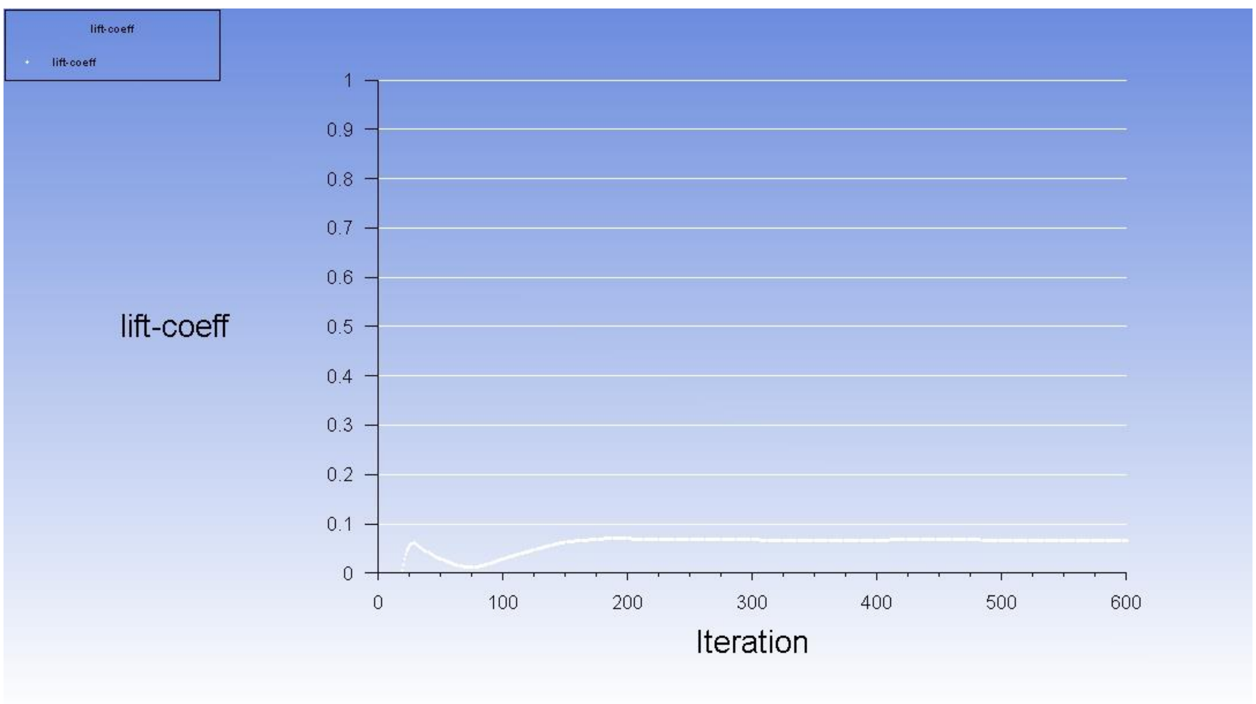

Figure 5.37. Lift coefficient of model two at 120 kmph

Table 5.3. Explains the drag and lift coefficient of model two at different speed of the vehicle.

Table 5.3. Drag and lift coefficient for model two at different speeds

Model	Speed(kmph)	*Cd*	Cl
Model Two	80	0.53193	0.08197
	100	0.53354	0.05648
	120	0.53122	0.06651

Here also the drag coefficient is reduced than the baseline model, and also lower than model one (Figure 5.32-5.34). And the drag decreases with increasing speed. The reduction in lift coefficient from the baseline model as the speed increases is greater than that of model one (Figure 5.35-5.37). The figures of lift coefficient show how the amount of lift converges with each iteration. The converged values are shown in Table 5.3. This means that the model two has higher stability at higher speed and reduced drag than model one and the baseline model.

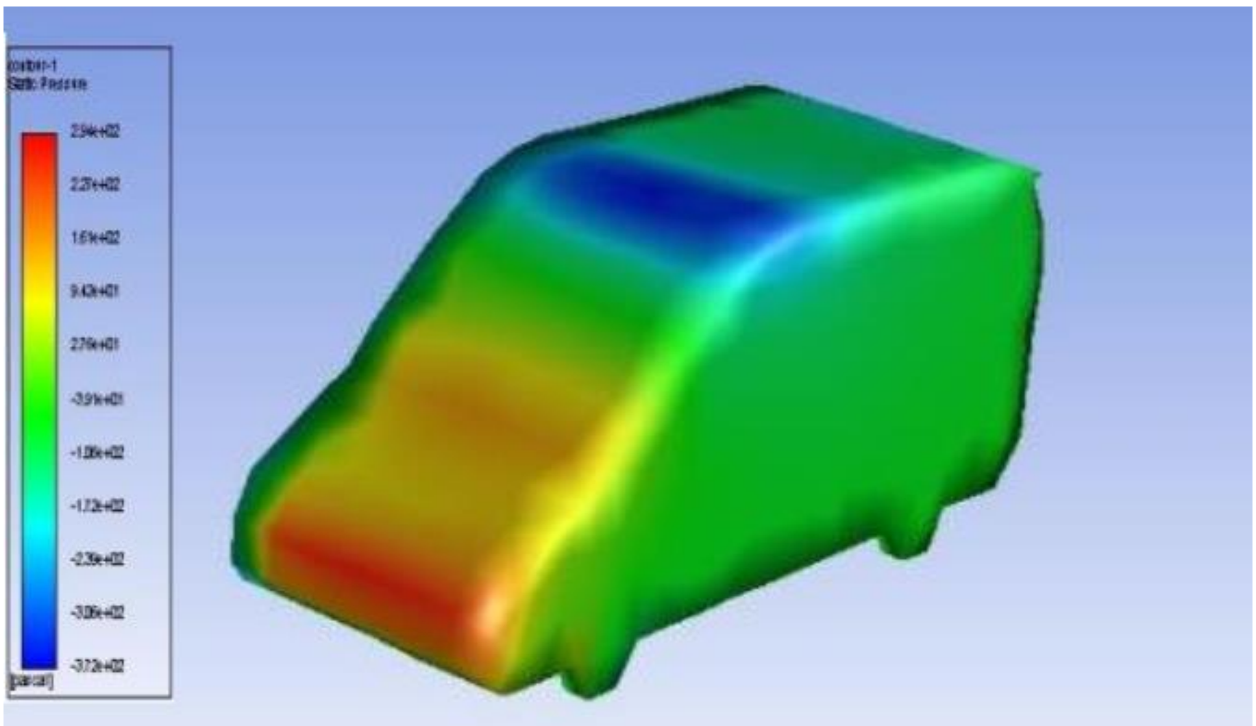

Figure 5.38. Pressure contour of model two at 80 kmph

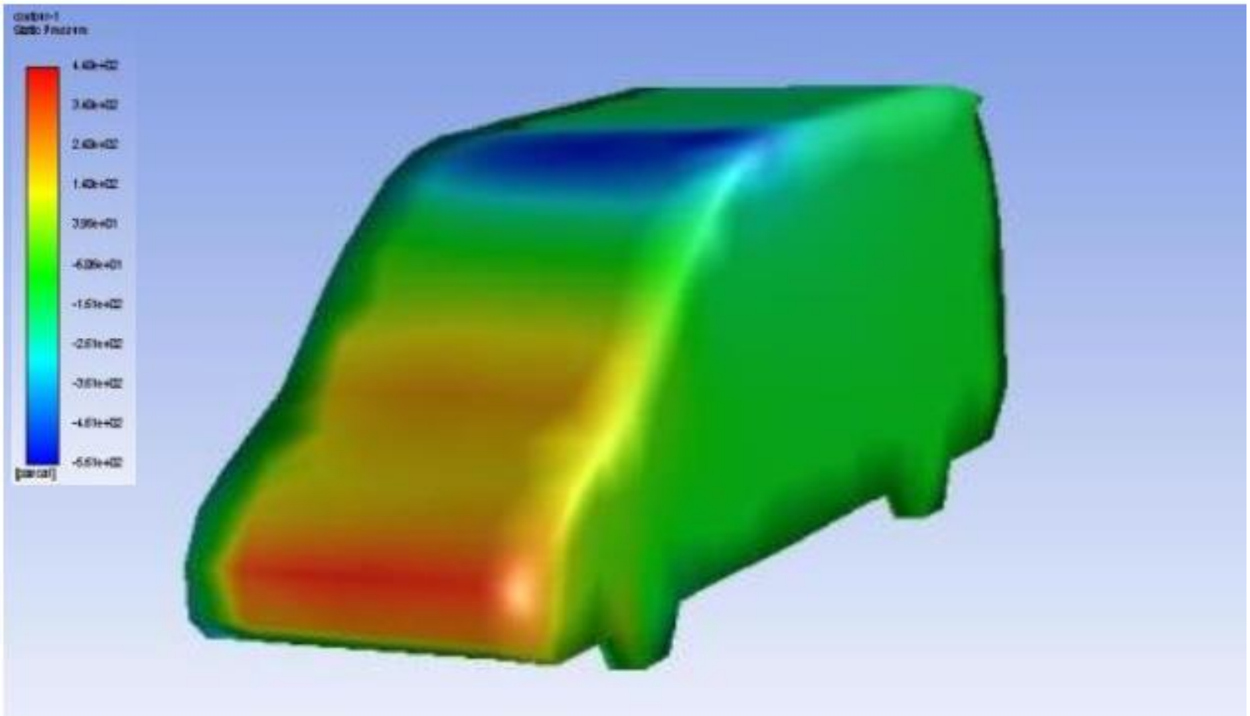

Figure 5.39. Pressure contour of model two at 100 kmph

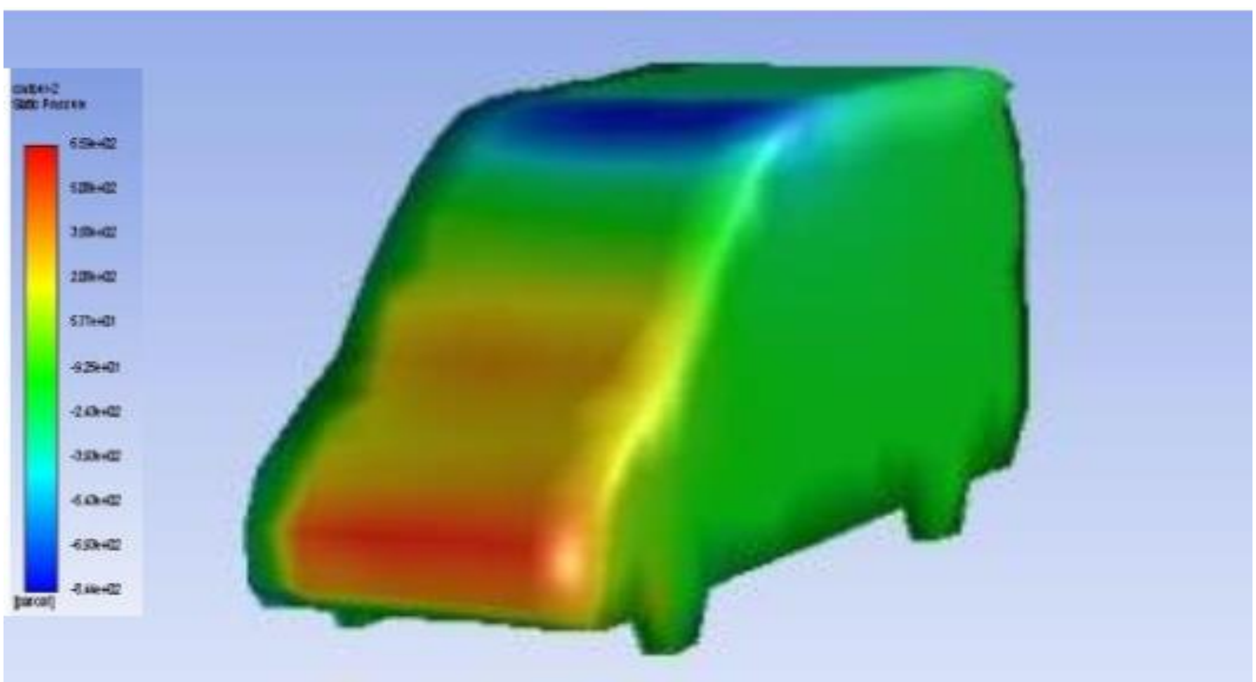

Figure 5.40. Pressure contour of model two at 120 kmph

Pressure contour Figures 5.38-5.40 show that the maximum pressure occurs at stagnation point colored by red on the grill of the vehicle. The second peak pressure occurs at the junction between the engine hood and the windshield. With increasing speed the maximum pressure increases. The increase in the surface pressure increases the drag coefficient which can be seen from Table 5.3.

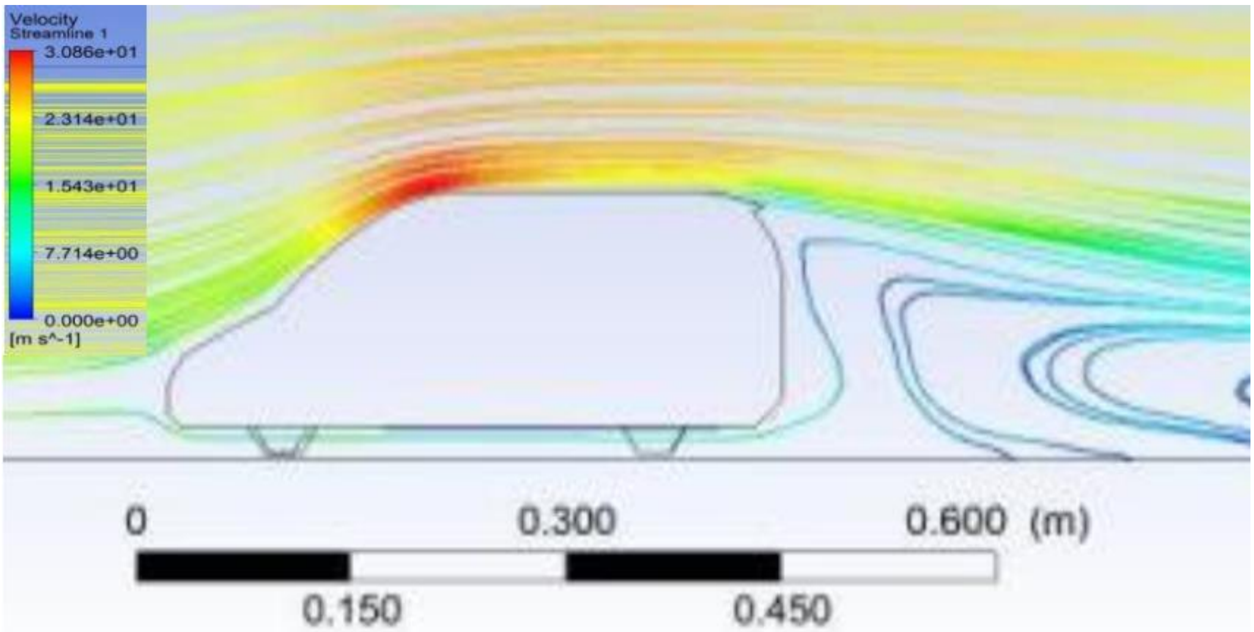

Figure 5.41. Velocity contour of model two at 80 kmph

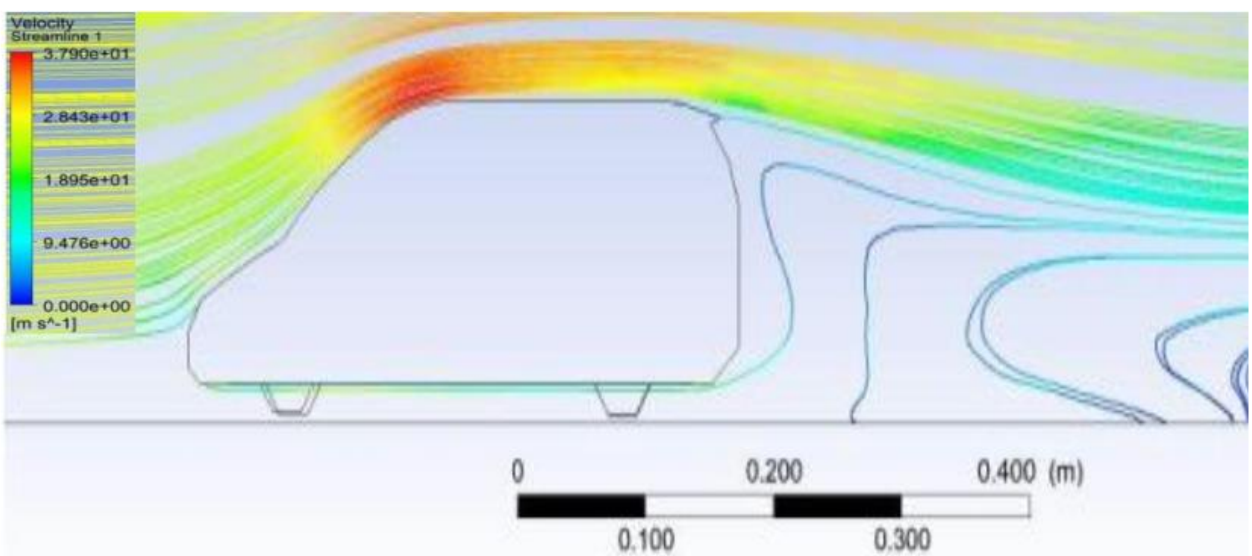

Figure 5.42. Velocity contour of model two at 100 kmph

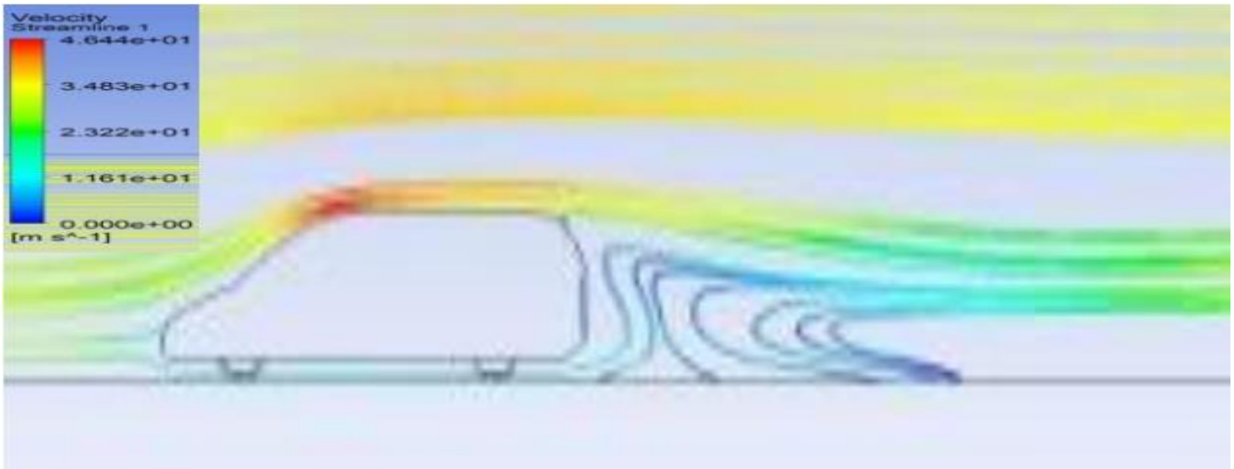

Figure 5.43. Velocity contour of model two at 120 kmph

This model is baseline model attached with 8-degree spoiler on its rear end of the roof. The test procedure was the same as model one and baseline model. The scaled residuals were similar with the baseline model and model one. And the surface pressure distribution is the same in shape and fashion for all speeds.

We can see from the lift coefficient figures (Figure 5.35-5.37) that the downward force decrease sufficiently at higher speeds. The decrease in lift coefficient is higher than that of the baseline model and model one. So, at higher speeds at the expense of drag model two is stable than the other models.

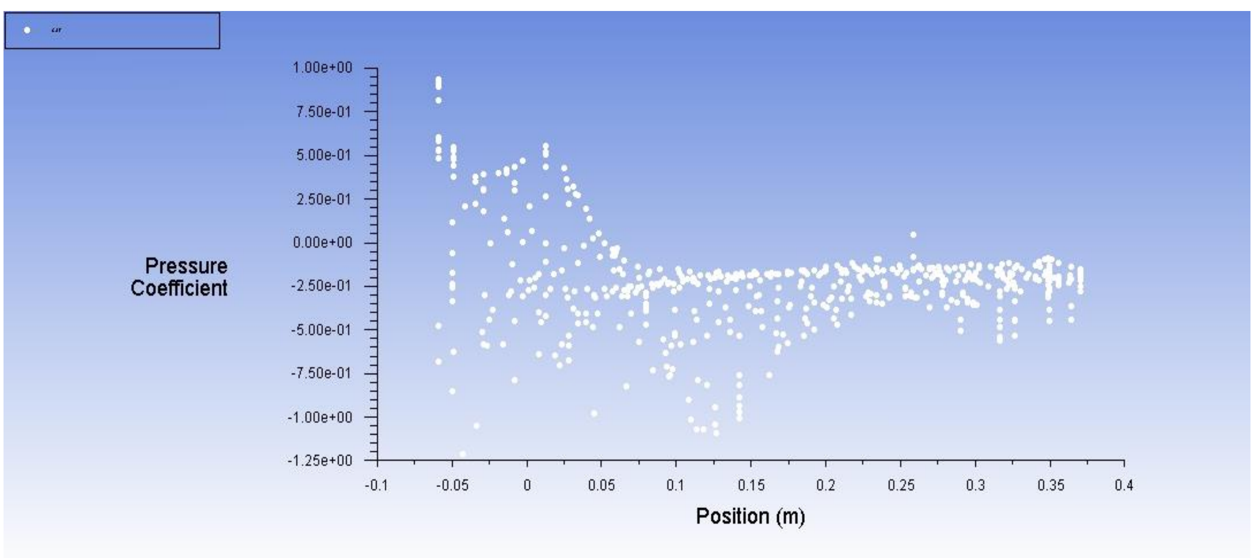

Figure 5.44. Surface pressure distribution for model two

Reduction in pressure on the surface of the spoiler can be seen from the pressure contour and surface pressure distribution figures (Figure 5.38-5.40 and figure 5.44). However, the reduction on model two is only limited to the rear tip of the spoiler. The amount in reduction is low that its influence on the downward force is reduced, which can be seen at lift coefficient decrement which is higher than that of model one.

5.2.3. Model Three

Result of scaled residuals, drag and lift coefficient, pressure and velocity contour at speed of 80 kmph 100 kmph and 120 kmph for model three are depicted here.

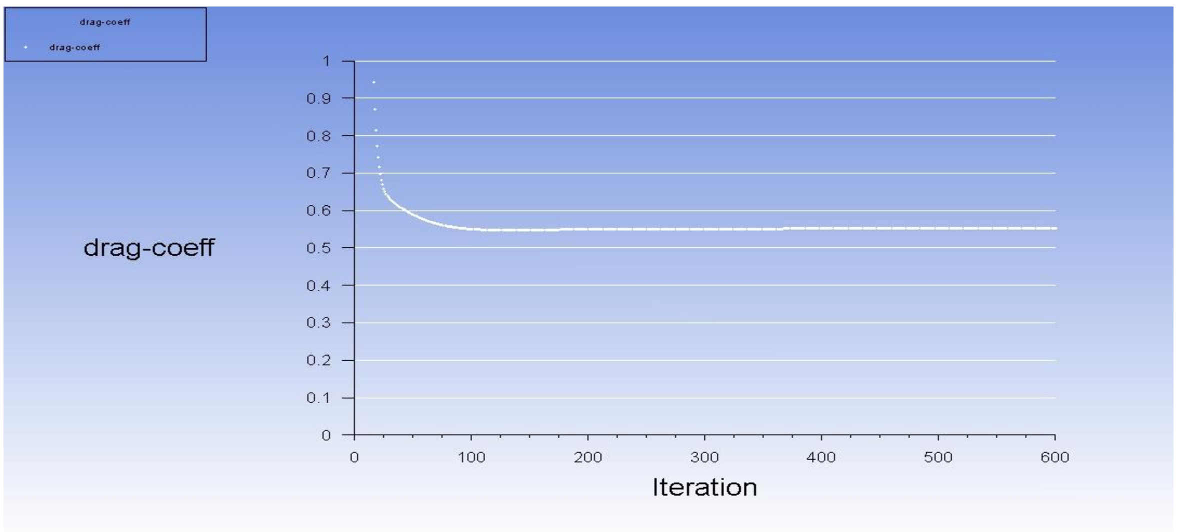

Figure 5.45. Drag coefficient of model three at 80 kmph

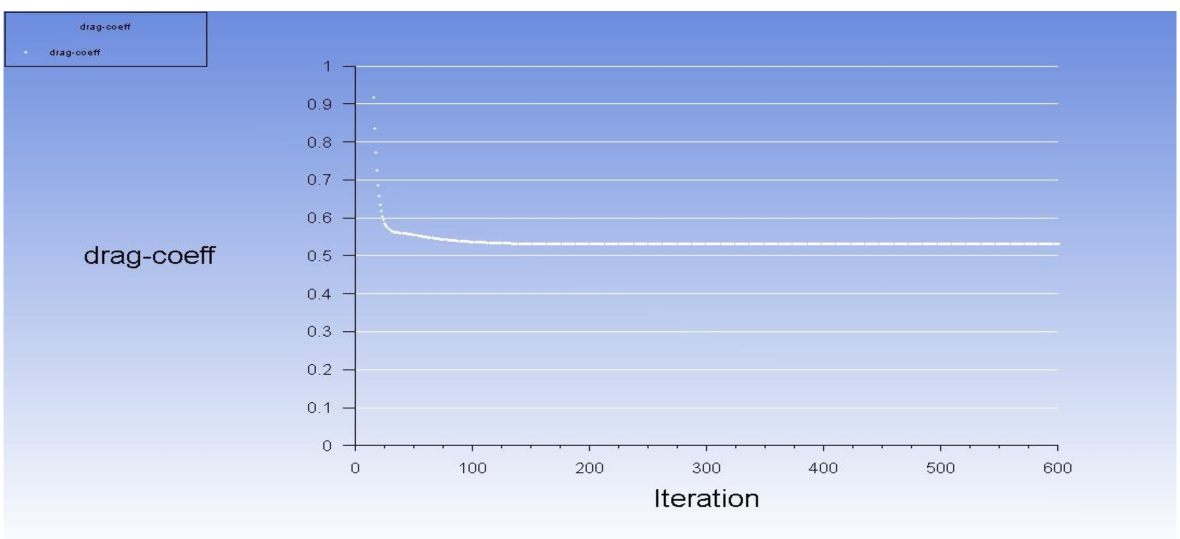

Figure 5.46. Drag coefficient of model three at 100 kmph

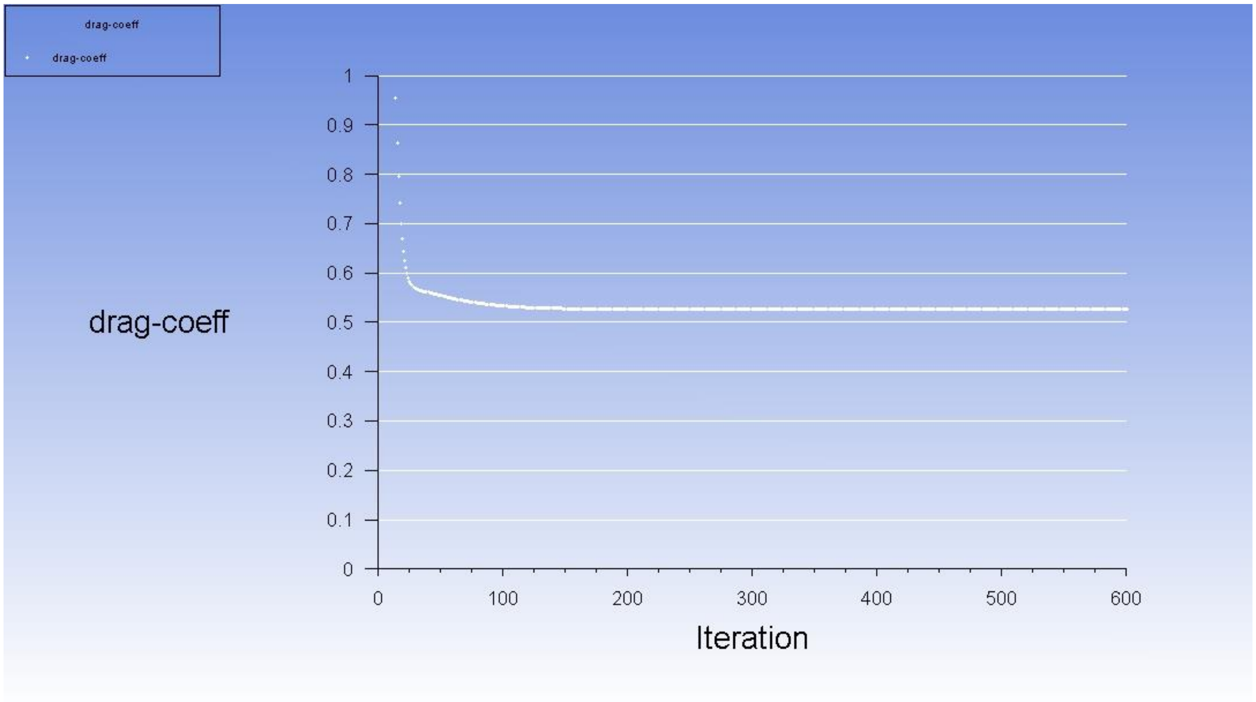

Figure 5.47. Drag coefficient of model three at 120 kmph

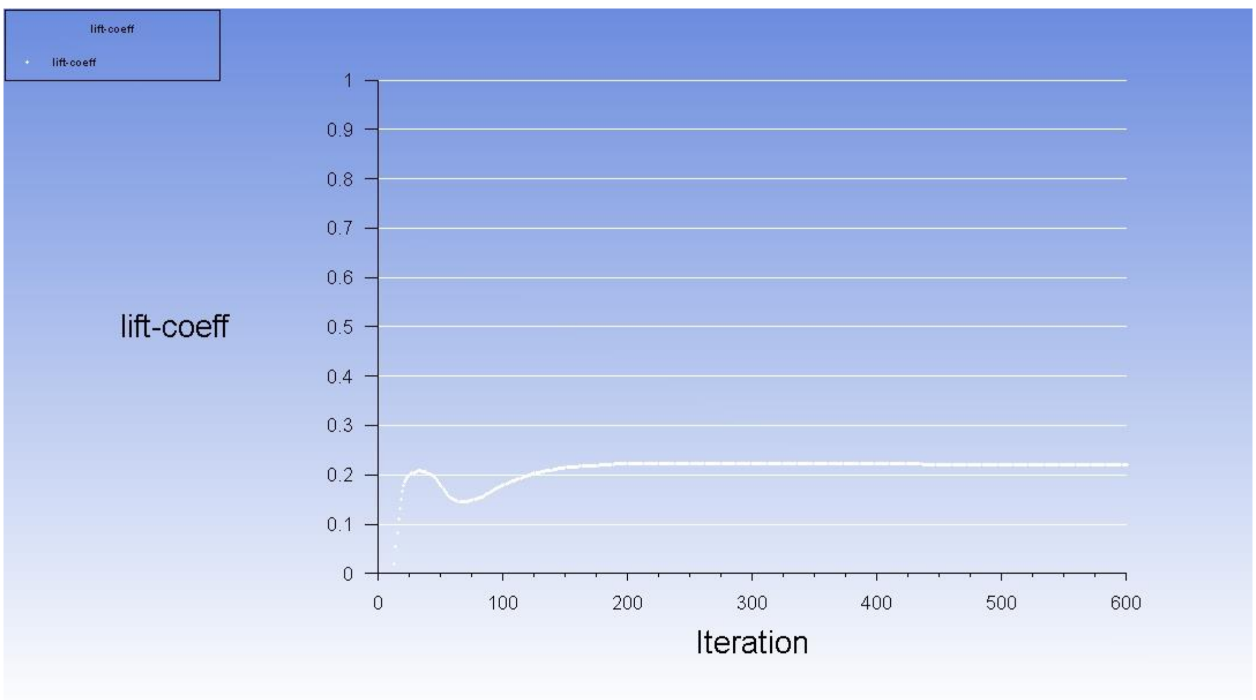

Figure 5.48. Lift coefficient of model three at 80 kmph

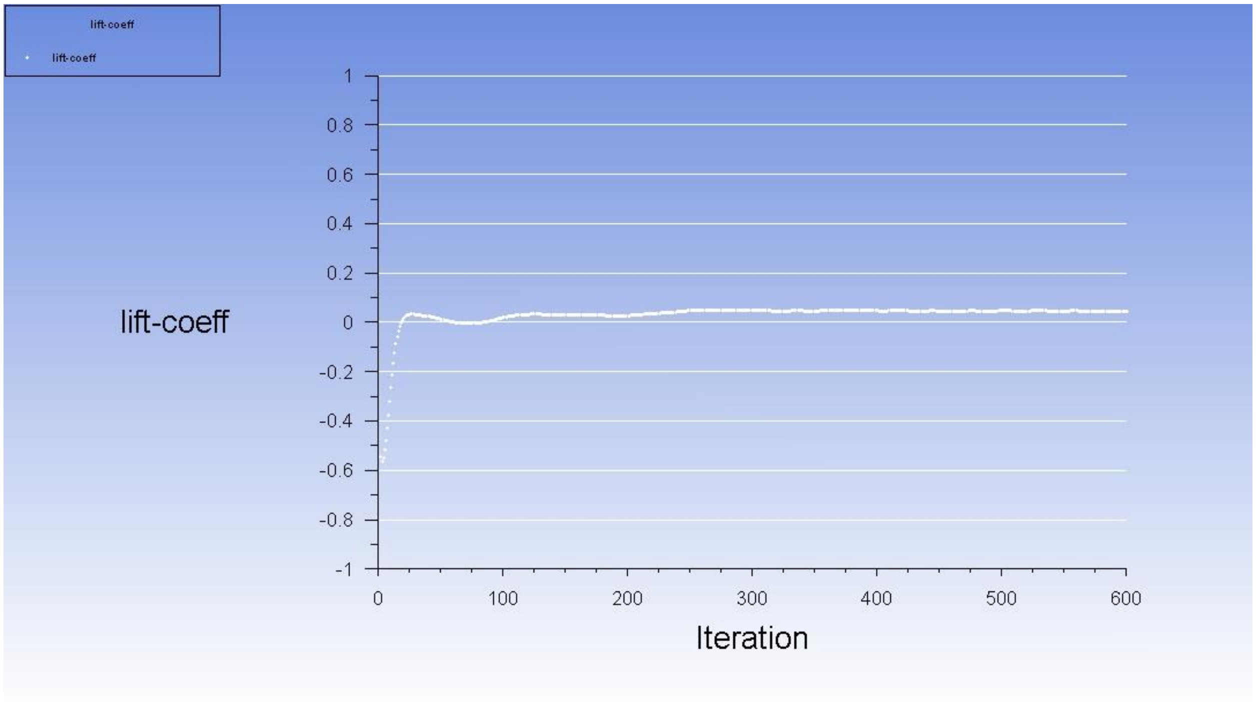

Figure 5.49. Lift coefficient of model three at 100 kmph

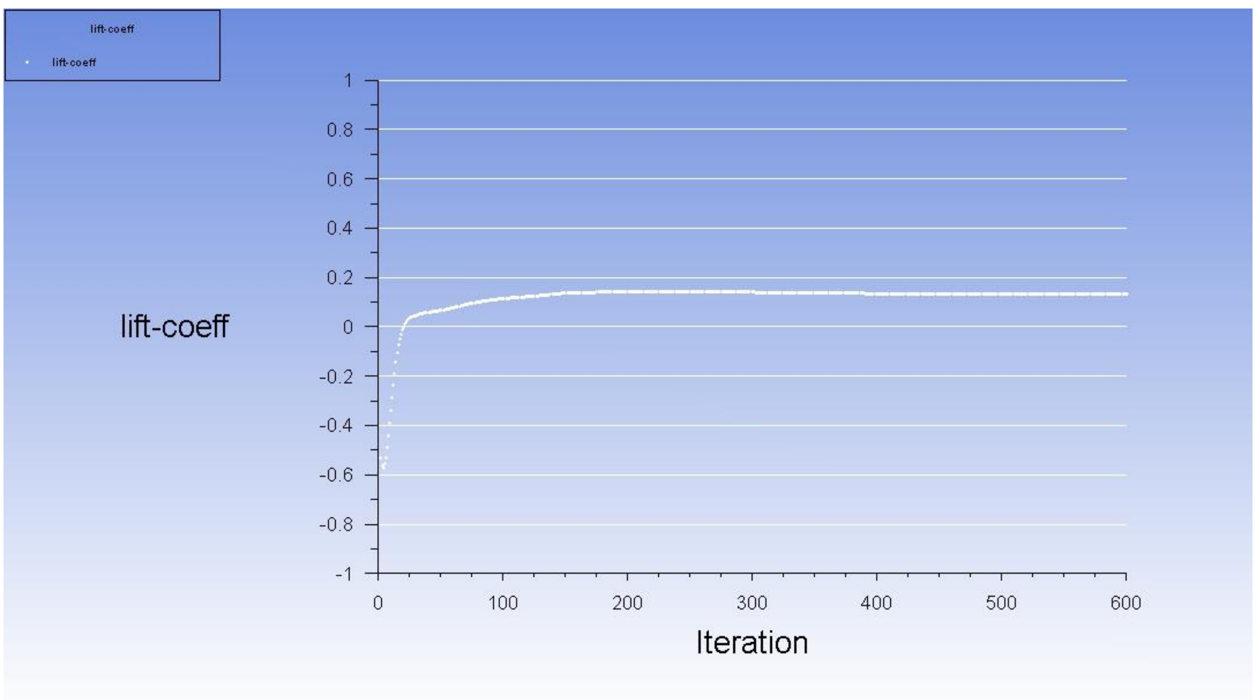

Figure 5.50. Lift coefficient of model three at 120 kmph

Table 5.4, explains the drag and lift coefficient of model three at different speed of the vehicle.

Table 5.4. Drag and lift coefficient for model three at different speeds

Model	Speed(kmph)	*Cd*	Cl
Model Three	80	0.53974	0.24691
	100	0.53089	0.04249
	120	0.52504	0.12901

Here also the drag coefficient is reduced than the baseline model, and also lower than model one and greater than model two (Figure 5.45 -5.47). And the drag decreases with increasing speed. The reduction in lift coefficient from the baseline model as the speed increases is greater than that of model one but lower than model two (Figure 5.48 -5.50). The figures of lift coefficient show how the amount of lift converges with each iteration. The converged values are shown in Table 5.4 This means that the model two has higher stability at higher speed and reduced drag than model one, model three and the baseline model.

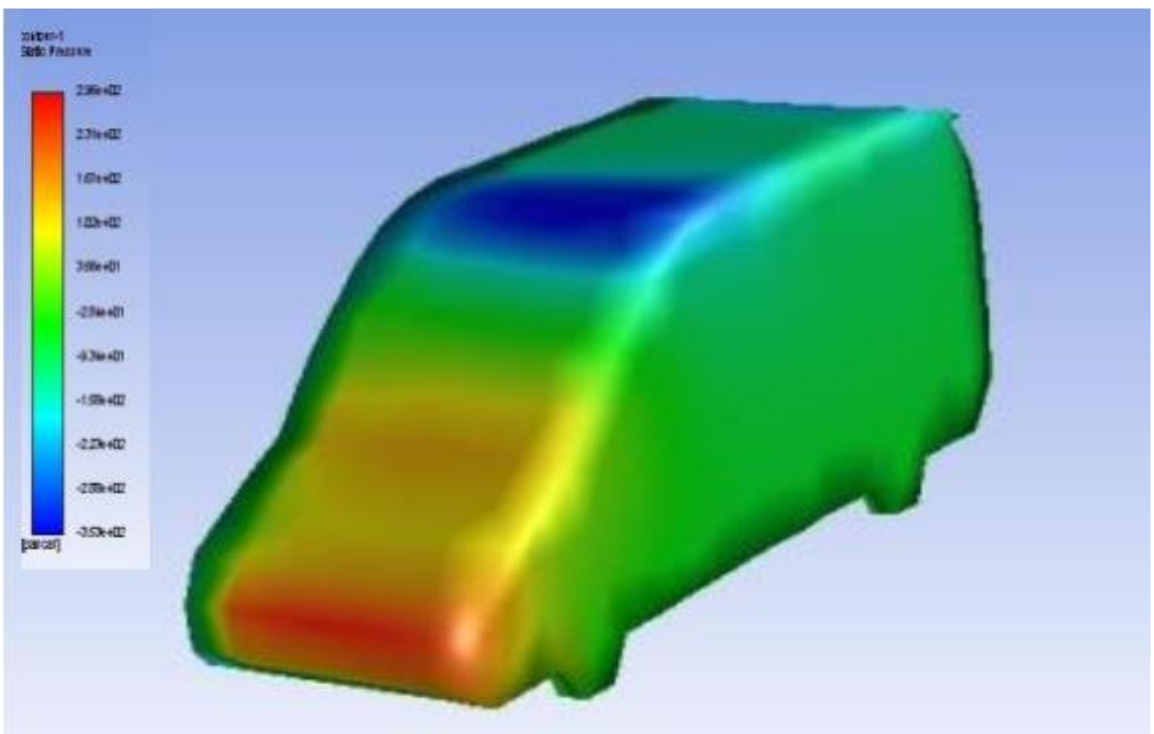

Figure 5.51. Pressure contour of model three at 80 kmph

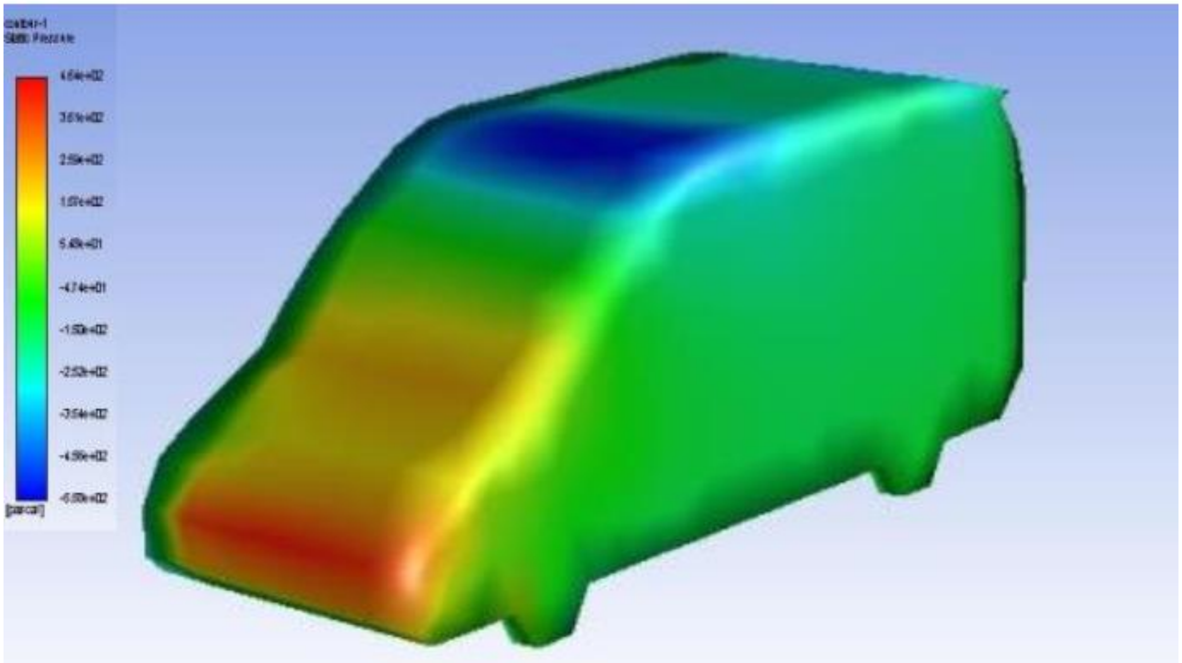

Figure 5.52. Pressure contour of model three at 100 kmph

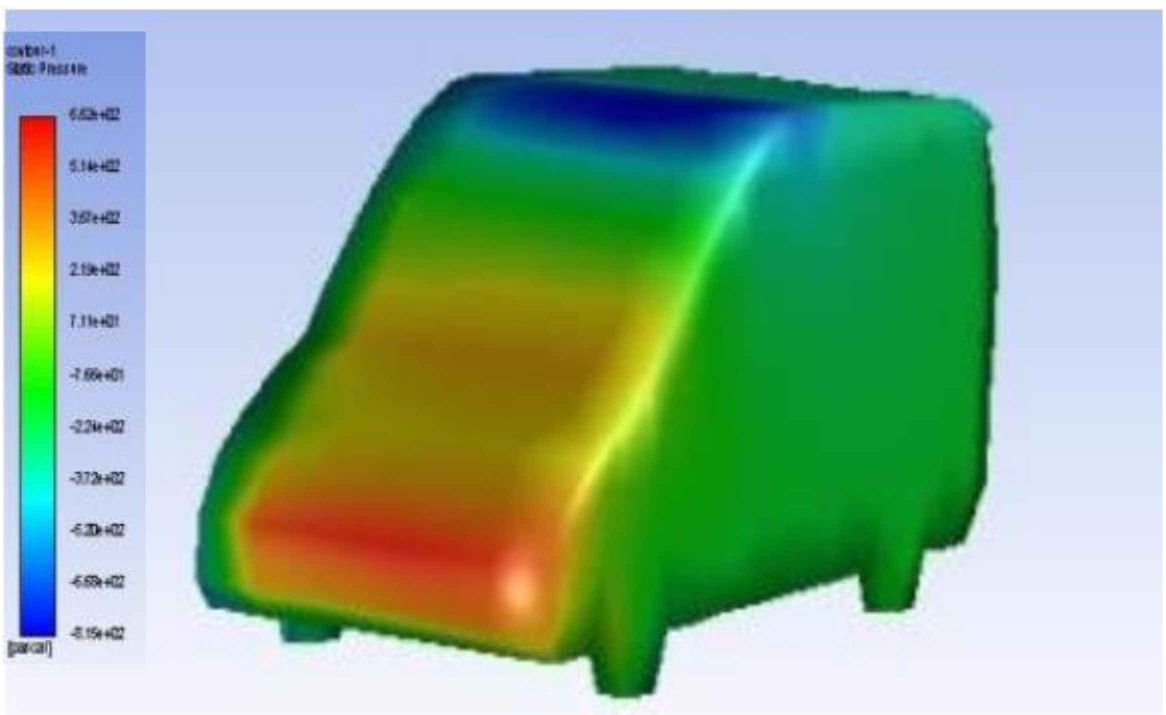

Figure 5.53. Pressure contour of model three at 120 kmph

Pressure contour Figures 5.51 -5.53 show that the maximum pressure occurs at stagnation point colored by red on the grill of the vehicle. The second peak pressure occurs at the junction between the engine hood and the windshield. With increasing speed the maximum pressure increases. The increase in the surface pressure increases the drag coefficient which can be seen from Table 5.4.

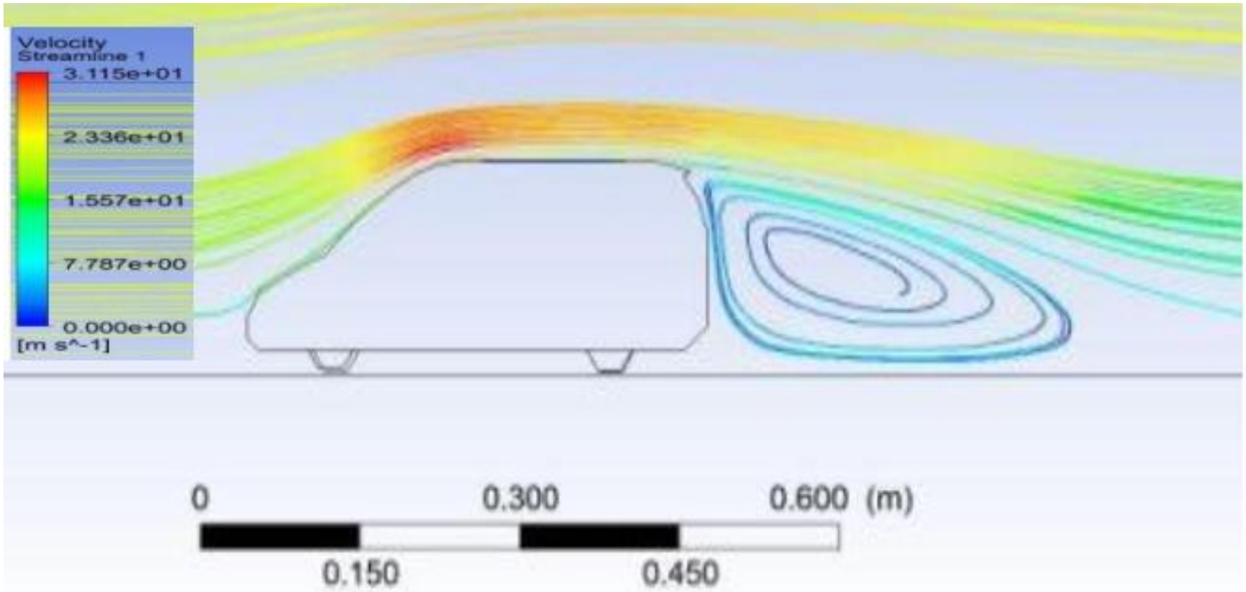

Figure 5.54. Velocity contour of model three at 80 kmph

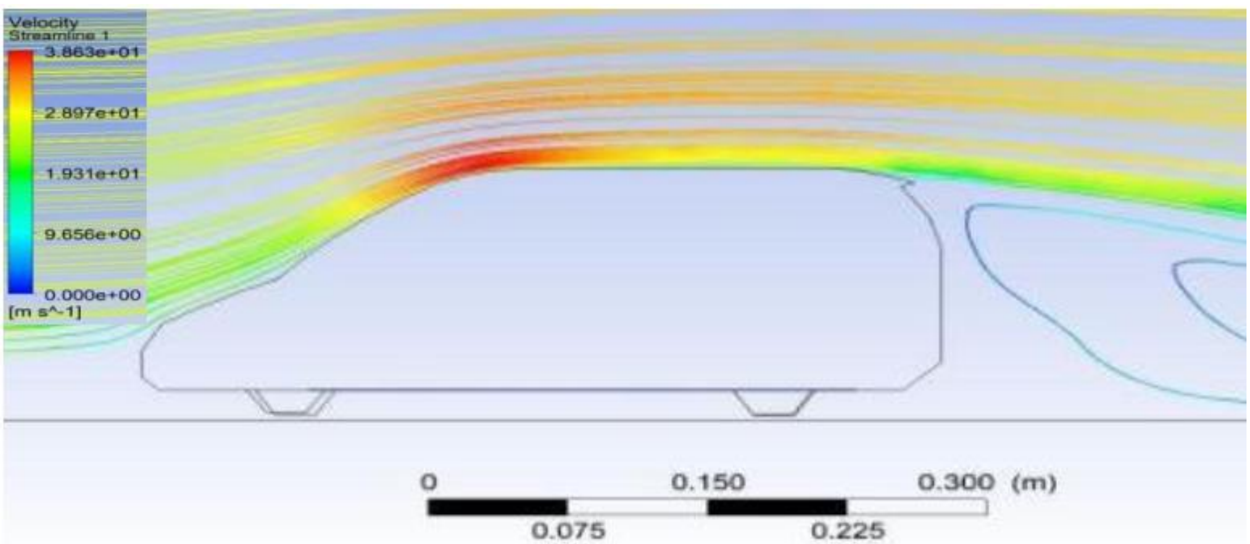

Figure 5.55. Velocity contour of model three at 100 kmph

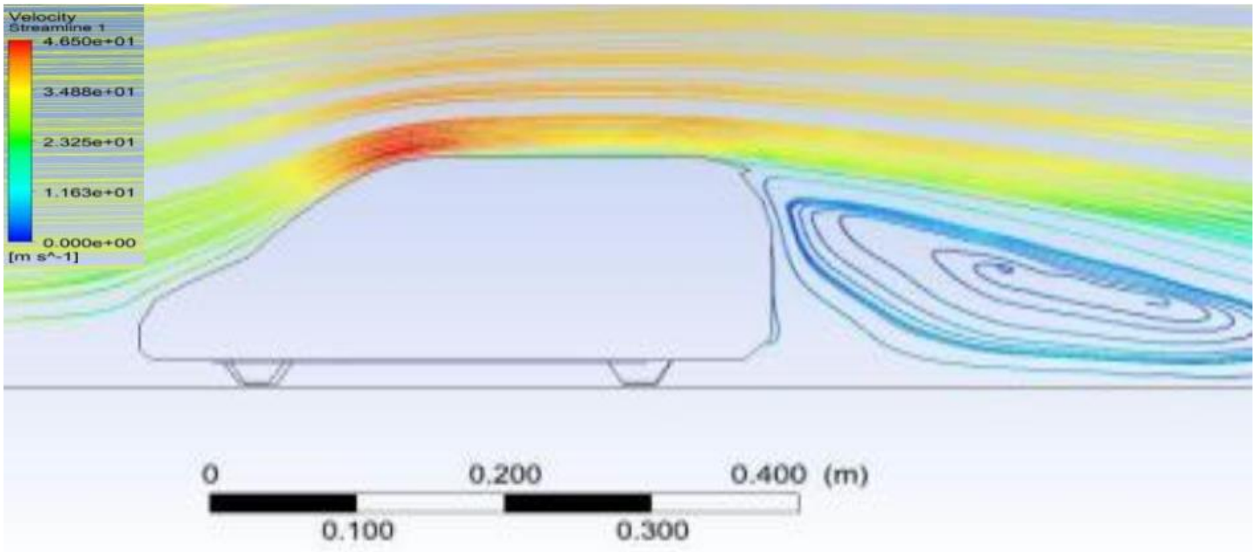

Figure 5.56. Velocity contour of model three at 120 kmph

This model is baseline model attached with 12 degree spoiler on its rear end of the roof. The test procedure was the same as model one , model two and baseline model. The scaled residuals were similar with the baseline model and model one and model two. And the surface pressure distribution is the same in shape and fashion for all speeds.

We can see from the lift coefficient figures (Figure 5.48-5.50) that the downward force decrease sufficiently at higher speeds. The decrease in lift coefficient is higher than that of the baseline model and model one but lower than model two. So, at higher speeds at the expense of drag model two is stable than the other models.

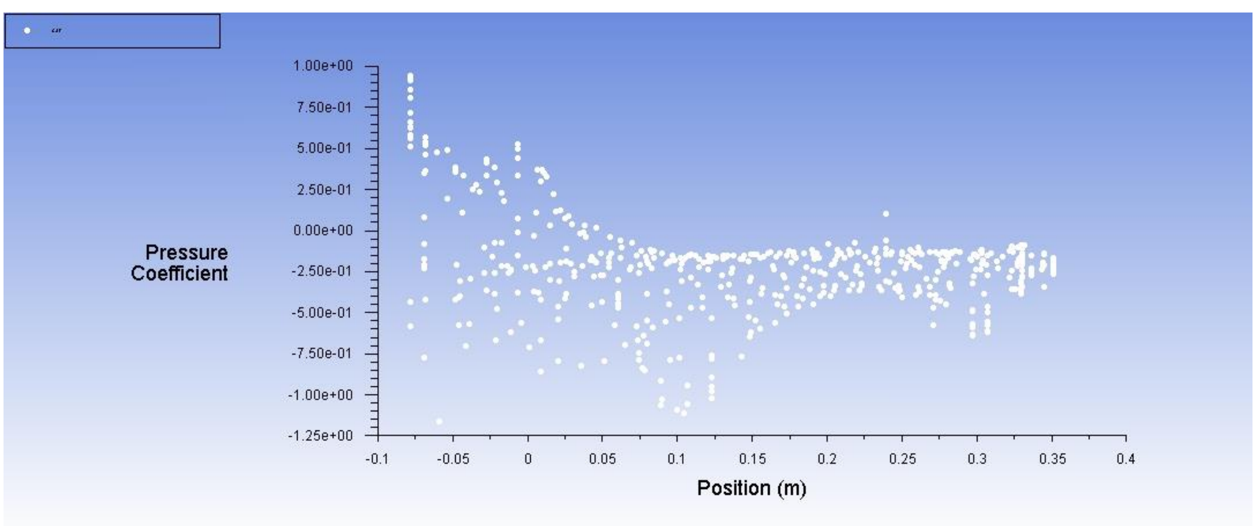

Figure 5.57. Surface pressure distribution for model three

Reduction in pressure on the surface of the spoiler can be seen from the pressure contour and surface pressure distribution figures (Figure 5.51-5.53 and Figure 5.57). However, the reduction on model two is only limited to the rear tip of the spoiler. The amount in reduction is low that its influence on the downward force is reduced, which can be seen at lift coefficient decrement which is higher than that of model one but lower than model two.

5.3. Comparison Between Models

From the graphs below the difference in drag and lift coefficient at 80 kmph, 100 kmph and 120 kmph between all four models can be seen.

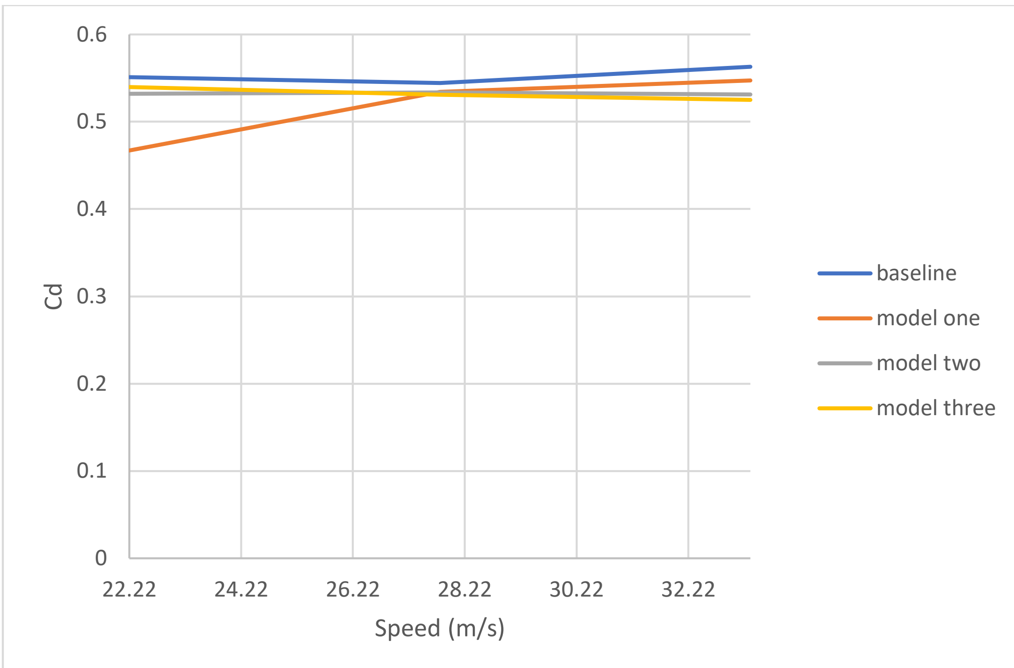

Figure 5.58. Drag coefficient of models at different speed

Generally, when we see from the graph above (Figure 5.58) the drag coefficients decreases with increasing speed of the vehicle. From the slope the quick rise in model one of the vehicle is due to increase in drag when the vehicle approaches 100 kmph but still its below the baseline model. When we see model two the drag reduces as the vehicle speed increases and it has the low drag coefficient when compared with the baseline model and model one. Model three on the other hand, the drag decreases as the speed increases and it has the lowest drag compare with the other models. So, because of the reduced drag coefficient at both low and high-speed model three saves more fuel and has less environmental effect because of its reduced fuel consumption and reduced emission.

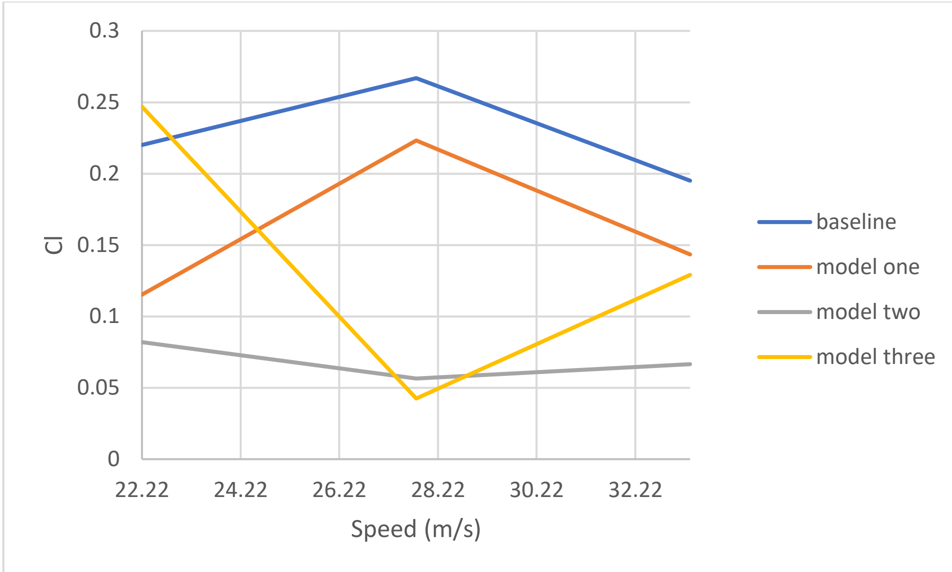

Figure 5.59. Lift coefficient of Models at different speed

For improved stability of vehicle at higher speeds the downward force should be high which is the result of reduced lift coefficient. From the Figure 5.59, model two has the least lift coefficient which makes it the most stable of all model at high speeds. Least stable is baseline model with the highest lift force. The lift coefficient of all models decreases with increasing speed. Hence, based on the result of the lift coefficient of all model's model two is the most stable model and the comparison of drag between the baseline model and the selected models are shown in table 5.5.

Table 5.5. Comparison of drag

	Models						
Speed(m/s)	Baseline Cd	Model one Cd	%diff. from Baseline	Model two Cd	%diff. from Baseline	Model three Cd	%diff. from Baseline
22.22	0.550895	0.46708	-15.2143	0.53193	-3.4425	0.53974	-2.024
27.78	0.544352	0.53410	-1.8833	0.53354	-1.9862	0.53089	-2.473
33.33	0.532913	0.54728	-2.7873	0.53122	-5.6400	0.52504	-6.737

Table 5.5, above summarizes the drag coefficient for the studied configuration along with the percentage difference from the Baseline case. Compared to the Baseline model, the entire studied configuration reduces the drag which is represented as drag coefficient. At 80kmph model one has the maximum improvement in drag reduction of 15.2% followed by model two and three with a drag-reduction improvement of 3.44% and 2.02% respectively.

At 100 kmph model three has the best drag reduction of 2.47% and model one has drag reduction of 1.88% and model two has 1.98% from the baseline model.

At speed of 120 kmph model three has the maximum improvement in drag reduction by 6.73% followed by model one with a drag reduction improvement of 2.78% and model two 5.64%. At this speed the drag coefficient of all models are below baseline drag coefficient. So, driving the models at this speed will not increase the drag coefficient because of lower drag coefficient than the baseline model and comparison of lift coefficient of baseline and the models are shown on table 5.6.

Table 5.6. Comparison of Lift

	Models						
Speed(m/s)	Baseline Cl	Model one Cl	%diff. from Baseline	Model two Cl	%diff. from Baseline	Model three Cl	%diff. from Baseline
22.22	0.220021	0.11525	-47.6186	0.08197	-62.7444	0.24691	12.22
27.78	0.266892	0.22325	-16.3519	0.05648	-78.8378	0.04249	-84.07
33.33	0.243112	0.14352	-40.9654	0.06651	-65.9089	0.12901	-33.87

Table 5.6, summarizes the lift coefficient of all models along with the percentage difference from the baseline model which were studied in this thesis. Model three has the maximum improvement in lift coefficient by 84.07% at 100 kmph. At this speed the lift improvement for model one is 16.35% and model two is 78.83%. The least lift improvement at 80kmph is 47.61% which corresponds to model one, for the same speed the percentage lift coefficient difference

from the baseline model is 62.75% for model two and for model three the lift increase and passes baseline model. It is shown in the table above that model one has reduced the baseline lift by 16.35% at 100 kmph. Whereas, model two has improved the amount of lift by 78.83% and model three improved by 84.07%.

From the table above model one and two when driven at all speed will not compromise the stability of the vehicle but driving model three when it approaches 100 kmh will result in best lift reduction of corresponding models and the stability of the vehicle is better improved at this speed.

5.4. Calculation of Fuel Consumption

Fuel saving of the given model relative to baseline model can be calculated. Percentage fuel reduction is 3/5 of percentage of total drag reduction [40]. The calculated values are given in the Table 5.7. below.

Table 5.7. Fuel Consumption Reduction

Models	Speed(m/s)	%diff. from baseline	%of fuel saving
Baseline	22.22		
	27.78		
	33.33		
Model one	22.22	-15.2143	9.12858
	27.78	-1.8833	1.12998
	33.33	-2.7873	1.67238
Model two	22.22	-3.4425	2.0655
	27.78	-1.9862	1.19172
	33.33	-5.6400	3.384
Model Three	22.22	-2.024	1.2144
	27.78	-2.473	1.4838
	33.33	-6.737	4.0422

From Table 5.7, we can see that maximum fuel amount of 9.12% can be reduced in model one travelling at 80 kmph. Model one reduces 1.12% and 1.67% of fuel when compared to baseline model at speed of 100 kmph and 120 kmph respectively. Model two has the least fuel reduction. The other better reduction is from model two with 2.06%, 1.19% and 3.38% at speed of 80 kmph, 100 kmph and 120 kmph respectively. Model three reduces fuel by 1.21%, 1.48% and 4.04% at the speed of 80 kmph, 100 kmph and 120 kmph respectively and Model three as a general i.e., in terms of reducing drag, lift and fuel consumption has better aerodynamic effect compared to the baseline model.

CHAPTER SIX
CONCLUSION AND RECOMMENDATIONS

6.1. Summary

Computational fluid dynamics was used to analyze flow around a 1/12 scaled down Toyota Dolphin vehicle. A steady state formulation was used in the present analysis. The objective of the present study was to reduce aerodynamic drag and lift of Dolphin vehicles using spoiler. The spoiler was attached to rear end of the baseline model at various arrangements. Model one had spoiler attached to the rear end of the baseline model at zero inclination angle. Model two was baseline model with spoiler attached at 8 degrees to its rear roof end, and finally model three was baseline model with spoiler attached at 12 degrees to its rear roof end. All models were modeled using SOLIDWORKS. Analysis was completed in ANSYS using realizable k-epsilon turbulence modeling. It was found that the large circulation region was formed in the back of the baseline vehicle and it created large pressure difference between the front and the rear of the vehicle, causing high drag and lift. Different arrangements of spoilers were attached and analyzed which were meant to push the flow separation a bit rearward and reduce the amount of drag by minimizing the wake region, and by throwing the turbulent air behind the vehicle. Comparison of streamlines and contour was made between the results from [39] and the present study. It was seen that the present study was able to capture the flow structure around the vehicle as accurately as [39]. Hence, present CFD simulation is validated against the CFD simulation of the similar vehicle [39].

6.2. Conclusions

Analysis using computational fluid dynamics(CFD) for 1/12 scaled down Toyota passenger midibus(dolphine) to analyze flow around the vehicle. Steady state formulation was used in the present analysis. The objective of the present study was to analyze aerodynamic effect of spoiler on the vehicle. The spoiler was attached at different arrangement. Model one has spoiler which is attached at the rear end of the roof of the vehicle with 0 degree angle inclination. Model two spoiler was attached at the same place with model one which is at the rear end of the roof of the vehicle with 8 degree angle inclination and Model three has spoiler which is attached at the rear end of the roof of the vehicle with 12 degree angle inclination.

All models were modeled using SOLIDWORKS. Analysis was completed in ANSYS using realizable k-epsilon turbulence modeling. It was found that large circulation region was formed at the back of the baseline model and created large pressure difference between the front and the rear of the vehicle, causing high drag. Different arrangements of spoilers were attached and analyzed which were meant to push the flow separation a bit rearward and reduce the amount of drag by minimizing the wake region, and by throwing the turbulent air behind the vehicle.

After the analysis on all models, the spoiler minimized the amount of swirling air at the back of the vehicle and hence reduced the amount of drag coefficient compared to baseline model. 15.2% aerodynamic drag reduction were found for model one. The reduction in drag for model one , model two and three significantly affects for reducing fuel consumption specially model one by 9.12%. On all three models, with increasing vehicle speed the drag and lift coefficient were reduced. So, with respect to the angle of inclination, spoiler with 0 degree angle decreases the drag while spoiler with 12 degree angle reduces the lift. Model three as a general i.e., in terms of reducing drag, lift and fuel consumption has better aerodynamic effect compared to the baseline model. From the analysis we can say adding add-on device greatly helped the vehicle in reducing the drag and lift, which in return reduces fuel consumption on the vehicle and also increases the vehicle stability when travelling at higher speed.

6.3. Recommendations

- ✓ Further improvement in drag and lift coefficients can be made possibly using optimization software and/or using synergetic effect of different aerodynamic add-on devices such as Airdam, vortex generators, roof garnish and/or combination of them and any other.
- ✓ For more accurate results a computer with high processing speed and capacity is recommended. This kind of computer will help in improving mesh quality and reducing processing time.

6.4. Future Research

In the future work could be testing of other add-on devices and different modification that reduce the aerodynamics of the vehicle. Also The aerodynamics of the vehicle can be changed by different position of add-on devices.

Further turbulence models could be applied to the parameter studies that were run to check the different model and see the effect.

REFERENCES

Abegaz, T., & Gebremedhin, S. (2019). Magnitude of road traffic accident related injuries and fatalities in Ethiopia. *PLoS ONE*, *14*(1), 1–10. https://doi.org/10.1371/journal.pone.0202240

Bansal, R., & Sharma, R. B. (2014). Drag Reduction of Passenger Car Using Add-On Devices. *Journal of Aerodynamics*, *2014*, 1–13. https://doi.org/10.1155/2014/678518

Bhalerao, S., Bari, C., & Bhujbal, K. (2019). d*esign and Analysis of rear car spoiler for Drag reduction and fuel efficiency*. *10*(5), 98–102.

Cable, M. (2009). *An Evaluation of Turbulence Models for the Numerical Study of Forced and Natural Convective Flow in Atria*. *May*, 1–136.

Cakir, M. (2012). CFD study on aerodynamic effects of a rear wing/ spoiler on a passenger vehicle. *Santa Clara University Scholar Commons*, 1–72. http://scholarcommons.scu.edu/mech_mstr

Cheah, L., Evans, C., Bandivadekar, A., & Heywood, J. (2007). *cheah_factorTwo*. *October*.

Das, R. C., & Riyad, M. (2017). CFD analysis of passenger vehicleat various angle of rear end spoiler. *Procedia Engineering*, *194*, 160–165. https://doi.org/10.1016/j.proeng.2017.08.130

Eftekhari, H., Al-Obaidi, A. S. M., & Eftekhari, S. (2020). The effect of spoiler shape and setting angle on racing cars aerodynamic performance. *Indonesian Journal of Science and Technology*, *5*(1), 11–20. https://doi.org/10.17509/ijost.v5i1.22701

Ganesh, G., & Vasudevan, V. (2015). Analysis of Effects of Rear Spoiler in Automobile Using Ansys. *Scientific & Engineering Research*, *6*(6), 762–766.

Ghanegaonkar, P. M., & Hiwase, H. M. (2014). Aerodynamics: Basic Concept and Rear End Application in Small Vehicles – A Review. *International Journal of Engineering Research & Technology (IJERT)*, *3*(7), 1397–1403.

Hu, X. X., & Wong, E. T. T. (2011). A numerical study on rear-spoiler of passenger vehicle. *World Academy of Science*, *Engineering and Technology*, *81*, 636–641. https://doi.org/10.5281/zenodo.1075367

Ipilakyaa, T. D., Tuleun, L. T., & Kekung, M. O. (2018). Computational fluid dynamics modelling of an aerodynamic rear spoiler on cars. *Nigerian Journal of Technology*, *37*(4), 975. https://doi.org/10.4314/njt.v37i4.17

Jahanmiri, M. (2010). Active Flow Control : A Review. *Research Report 2010*, 1–33.

Kane, S. N., Mishra, A., & Dutta, A. K. (2016). Preface: International Conference on Recent Trends in Physics (ICRTP 2016). *Journal of Physics: Conference Series*, *755*(1). https://doi.org/10.1088/1742-6596/755/1/011001

Kazi, A., Acharya, P., Patil, A., & Noraje, A. (2016). Effect of Spoiler Design on Hatchback Car. *International Journal of Modern Trends in Engineering & Research*, *3*(9), 192–200. https://doi.org/10.21884/ijmter.2016.3065.thkr0

Konstantinidis, E., & Bouris, D. (2012). Bluff Body Aerodynamics and Wake Control.

Applied Aerodynamics, *May*. https://doi.org/10.5772/38684

Kumar, D. M. V. S. (2017). Design, Analysis and Manufacturing of a Car Rear Spoiler for Drag Reduction. *Iarjset*, *4*(6), 89–96. https://doi.org/10.17148/iarjset.2017.4617

LEE, T. Y. K. and S. H. (2012). Combustion and Emission Characteristics of Wood Pyrolysis Oil-Butanol Blended Fuels in a Di Diesel Engine. *International Journal of …*, *13*(2), 293–300. https://doi.org/10.1007/s12239

Mashud, M., Ferdous, M., & Omee, S. H. (2012). Effect of spoiler position on aerodynamic characteristics of an airfoil. *International Journal of Mechanical and Mechatronics Engineering*, *12*(6), 1–6.

Nawam, M. Z., Rosli, M. A. M., & Rosli, N. A. S. (2018). Simulation study on the effect of rear-wing spoiler on the open aerodynamic performance of sedan vehicle. *Journal of Advanced Research in Fluid Mechanics and Thermal Sciences*, *49*(2), 146–154.

Parab, A., Sakarwala, A., Paste, B., Patil, V., & Mangrulkar, A. (2014). Aerodynamic Analysis of a Car Model using Fluent- Ansys 14.5. *International Journal on Recent Technologies in Mechanical and Electrical Engineering*, *1*(4), 7–13.

Paulo. (2019). No Titיליle. ペインクリニック学会治療指針２, *September*, 1–9.

Pranav, R., Hitesh, T., & Vaghela, K. (2017). Design Optimization and Cfd Analysis of Car Using Active Mounting To Reduce Dreg Coefficient and Reduce Lift To Sleep of Car At Higher Speed. *International Research Journal of Engineering and Technology(IRJET)*, *4*(3), 1678–1684. https://irjet.net/archives/V4/i3/IRJET-V4I3468.pdf

Sarkar, S., Thummar, K., Shah, N., & Vagrecha, V. (2019). A Review paper on Aerodynamic Drag Reduction and CFD Analysis of Vehicles. *International Research Journal of Engineering and Technology*, *6*(1), 231–235. https://doi.org/10.13140/RG.2.2.31506.91849

Selvaraju, P. N., Parammasivam, K. M., Shankar, S., & Devaradjane, G. (2015). Analysis of drag and lift performance in sedan car model using CFD. *Journal of Chemical and Pharmaceutical Sciences*, *7*(7), 429–435.

Sharma, R., & Bansal, R. (2013). Drag and Lift Reduction on Passenger Car with Rear Spoiler. *Research and Development (IJAuERD)*, *3*(3), 13–22.

Shinde, S. S., & Shende, P. M. D. (2017). Enhancement of Aerodynamic Drag Reduction of Passenger Vehicle using CFD analysis-. *International Journal of Innovative Research in Science, Engineering and Technology An*, *6*(1), 437–448.

Siva, G., & Loganathan, V. (2016). Design and Aerodynamic Analysis of a Car to Improve Performance. *Middle-East Journal of Scientific Research*, *24*, 133–140. https://doi.org/10.5829/idosi.mejsr.2016.24.RIETMA121

Sivakumar, P., Rajalakshmi, N., Shalini, M., & Malathi, N. (2019). Vehicle Aerodynamic Analysis – A Primitive Approach. *International Research Journal of Engineering and Technology (IRJET)*, *6*(4), 4347–4351.

Sivanesh Prabhu. M, Arulvel. S, M. S. (2017). CFD Analysis of Automobile Rear Dynamic Spoiler. *International Journal of Scientific & Engineering Research*, *8*(8), 1431–1435.

http://www.ijser.org

Socrates, S., Prasath, M. N., Suryanand, S., Kishore, J., & suman Kumar, P. (2018). *Computational Investigations of Aerodynamic Drag Using Spoiler of an*. *119*(12), 14585–14592. http://www.ijpam.eu

Sodja, J. (2007). Turbulence models in CFD. *University of Ljubljana*, *March*, 1–18. http://mafija.fmf.uni-lj.si/seminar/files/2006_2007/Turbulence_models_in_CFD.pdf

Sudin, M. N., Abdullah, M. A., Shamsuddin, S. A., Ramli, F. R., & Tahir, M. M. (2014). Review of research on vehicles aerodynamic drag reduction methods. *International Journal of Mechanical and Mechatronics Engineering*, *14*(2), 35–47.

Suhendra, A. D., Asworowati, R. D., & Ismawati, T. (2020). No 主観的健康感を中心とした在宅高齢者における 健康関連指標に関する共分散構造分析Title. *Akrab Juara*, *5*(1), 43–54. http://www.akrabjuara.com/index.php/akrabjuara/article/view/919

Taha, T. R. (2005). An Introduction to Parallel Computational Fluid Dynamics. In *IEEE Concurrency* (Vol. 6, Issue 4). https://doi.org/10.1109/mcc.1998.736434

Tomar, A. S., Prajapati, A., Sharma, A., & Shrivastava, S. (2019). CFD analysis on the aerodynamic effects of spoiler at different angle on car body. *International Journal of Innovative Technology and Exploring Engineering*, *8*(7), 2845–2848.

Tousi, S. M. R., Bayat, P., & Bayat, P. (2015). Evaluating the Importance of Rear Spoiler on Energy Efficiency of Electric Vehicles. *International Journal of Automotive Engineering*, *5*(4), 2034–2053. http://www.iust.ac.ir/ijae/browse.php?a_id=333&sid=1&slc_lang=en

Varma, R., Scholar, Mt., & Professor, A. (2018). CFD Analysis of Aerodynamics of Car. *International Journal of Innovative Research in Science*, *7*(5), 4689–4693. https://doi.org/10.15680/IJIRSET.2018.0705037

Velagapudi, N. K., K., L. N., Rao, L. N. V. N., & Y., S. R. (2015). Investigation of Drag and Lift Forces over the Profile of Car with Rearspoiler using CFD. *International Journal of Advances in Scientific Research*, *1*(8), 331. https://doi.org/10.7439/ijasr.v1i8.2510

Wilcox, D. C. (2006). Turbulence Modelling for CFD 3rd Edition. In *Turbulence Modeling for CFD*. http://www.dcwindustries.com

Wolde, E. W. (2019). *CFD Analysis on Aerodynamic Drag Reduction of Pickup Vehicles Using Rear Spoiler By*.

Yakkundi, V., & Mantha, S. S. (2018). *Effect of Spoilers on Aerodynamic Properties of Car Effect of Spoilers on aerodynamic properties of a car*. *7*(March), 271–280.

APPENDICES

Appendix A: Models Inside Enclosure and Mesh

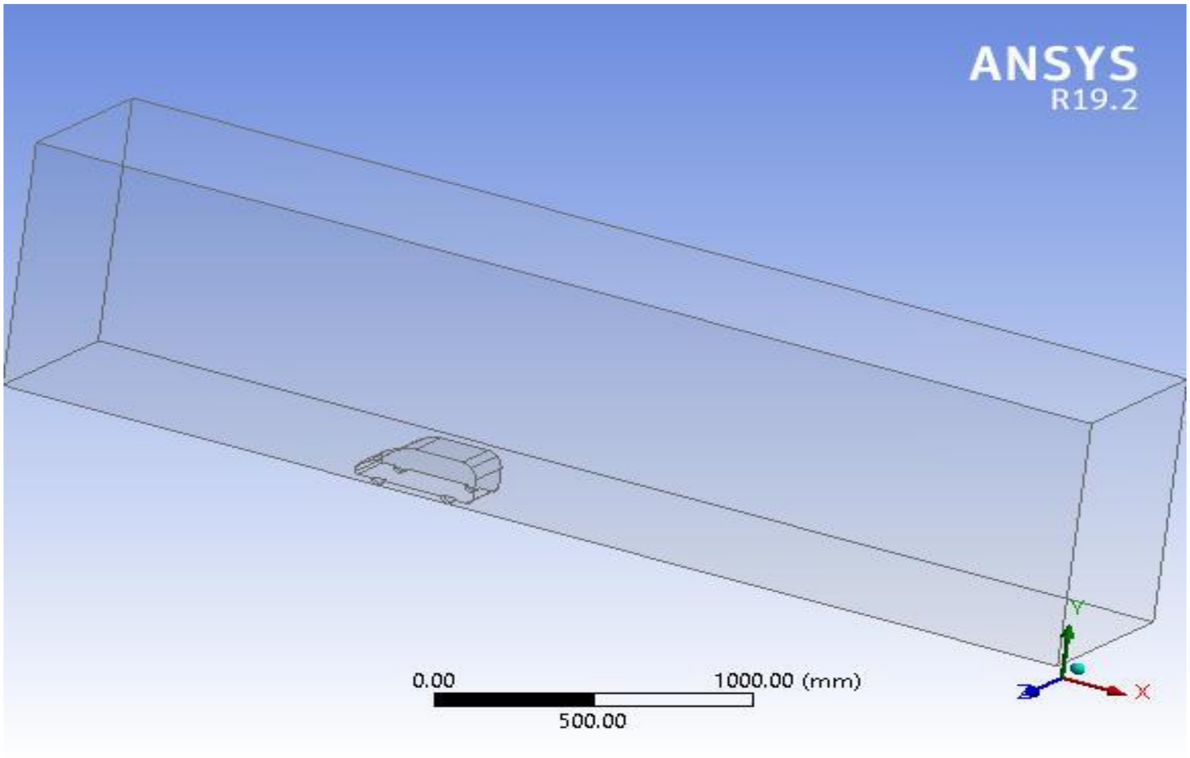

Figure A-1. Baseline model inside enclosure

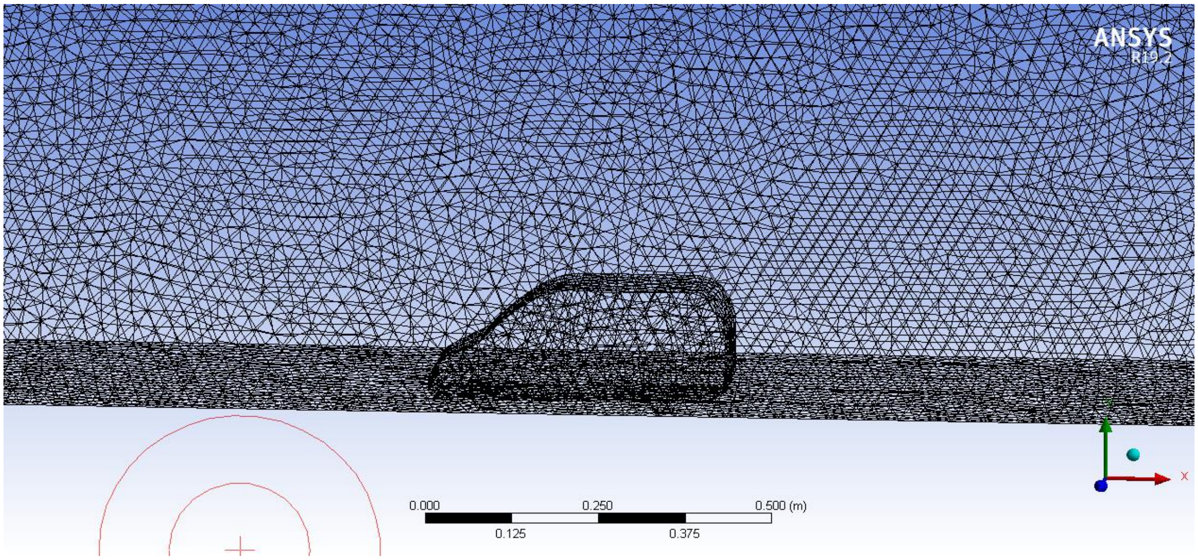

Figure A-2. Baseline model meshing

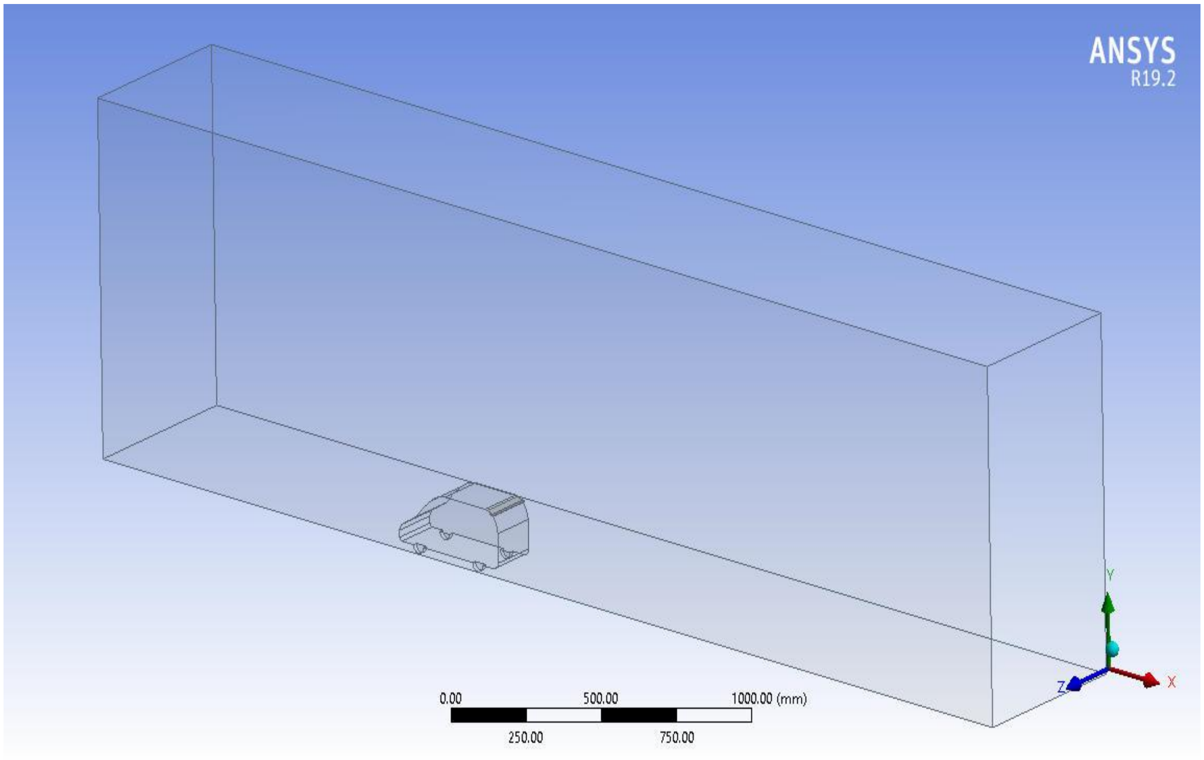

Figure A-3. Model one inside enclosure

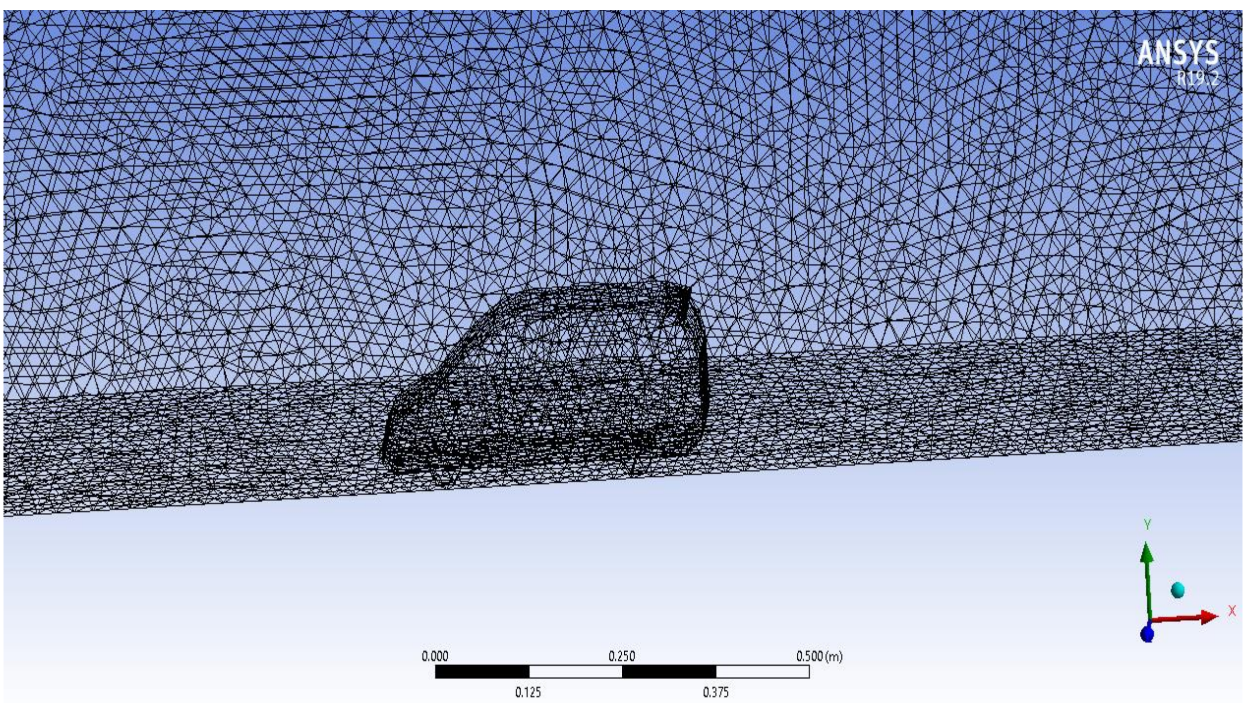

Figure A-4. Model one after meshing

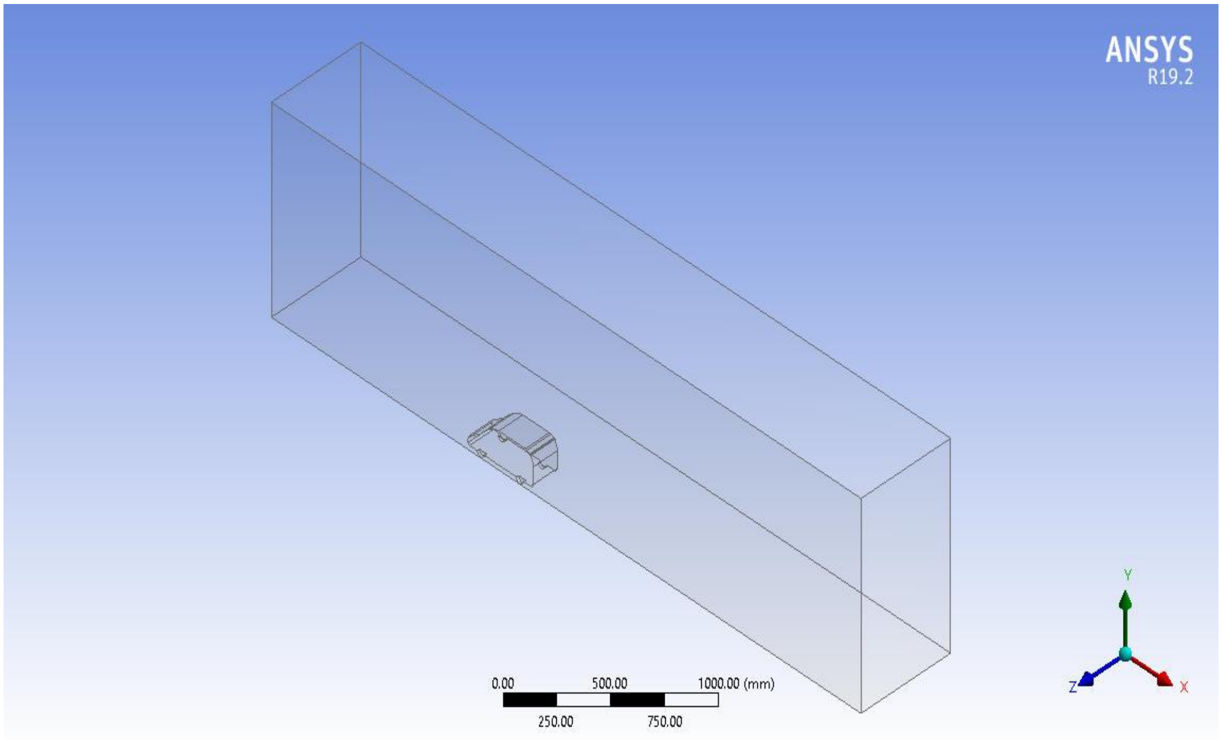

Figure A-5. Model two inside enclosure

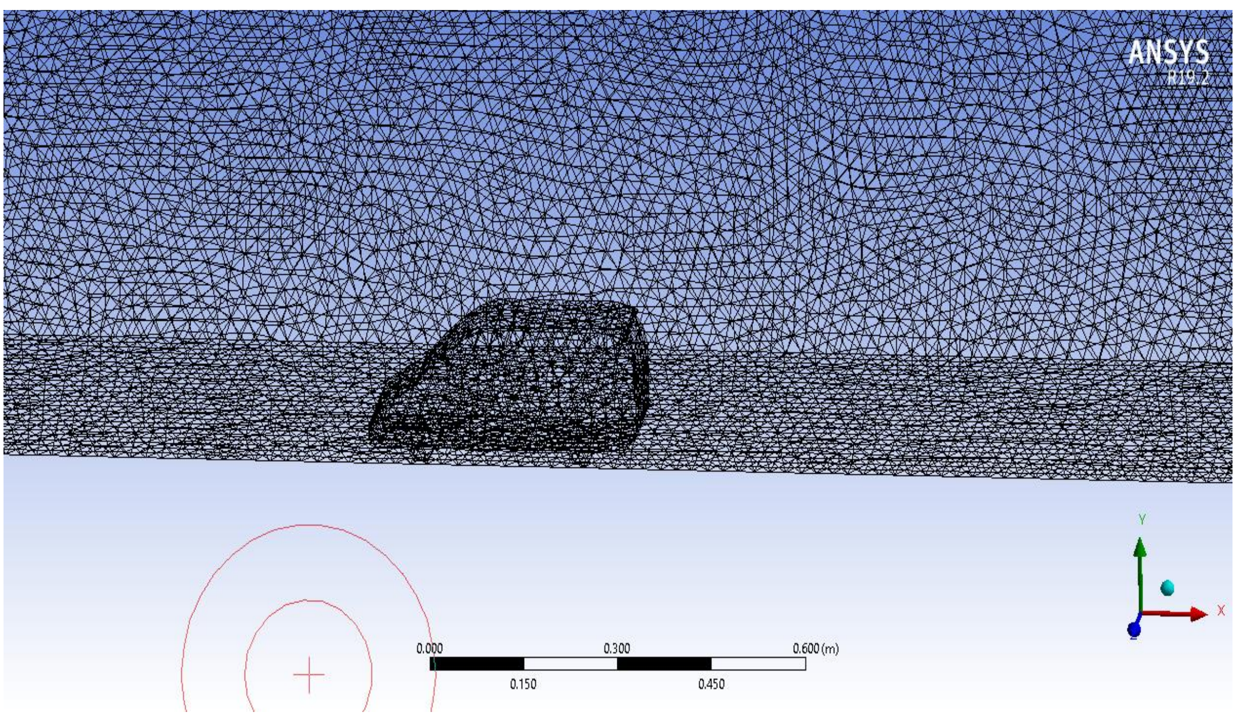

Figure A-6. Model two after meshing

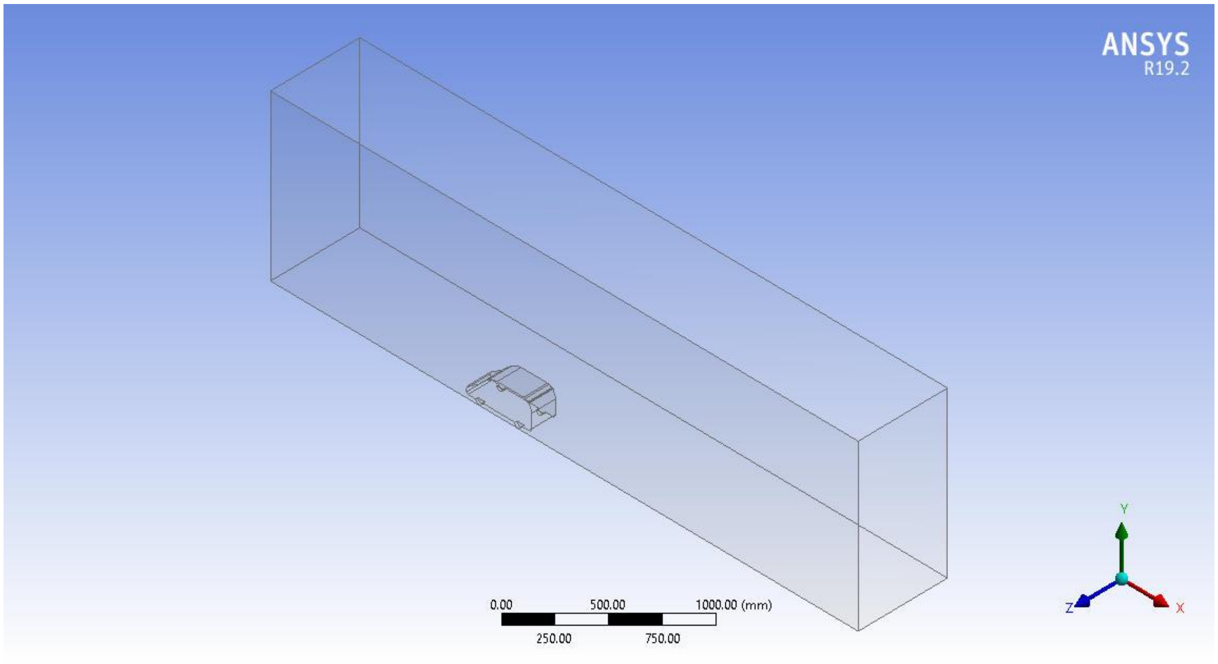

Figure A-7. Model three inside enclosure

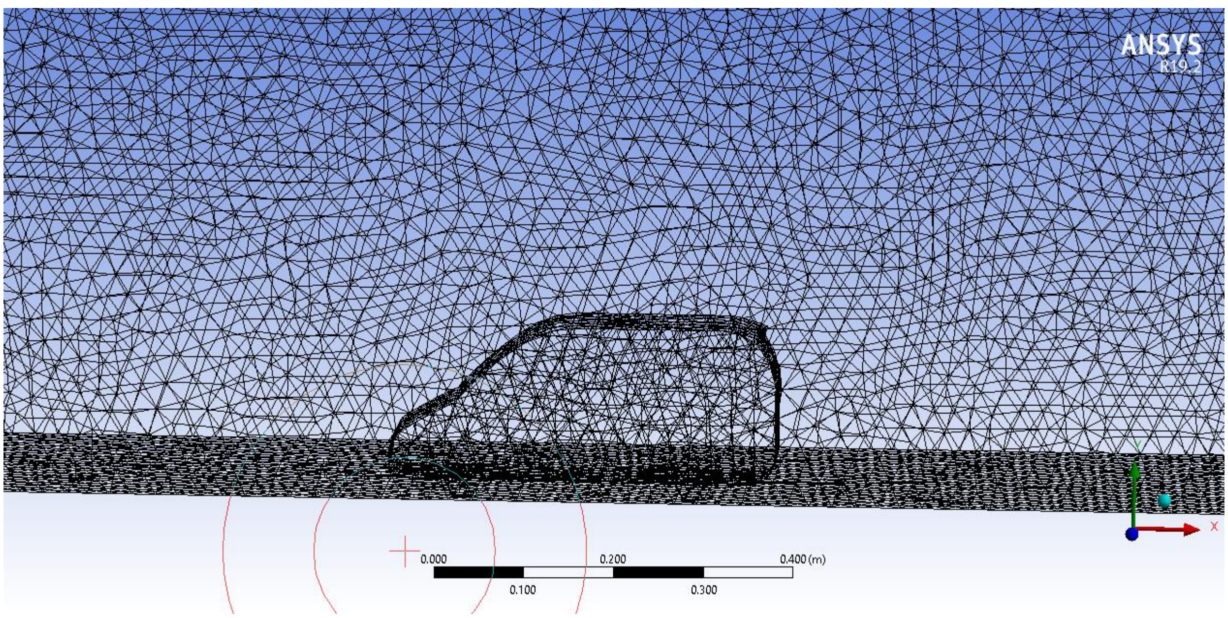

Figure A-8. Model three after meshing

Appendix B: SolidWorks Modelling

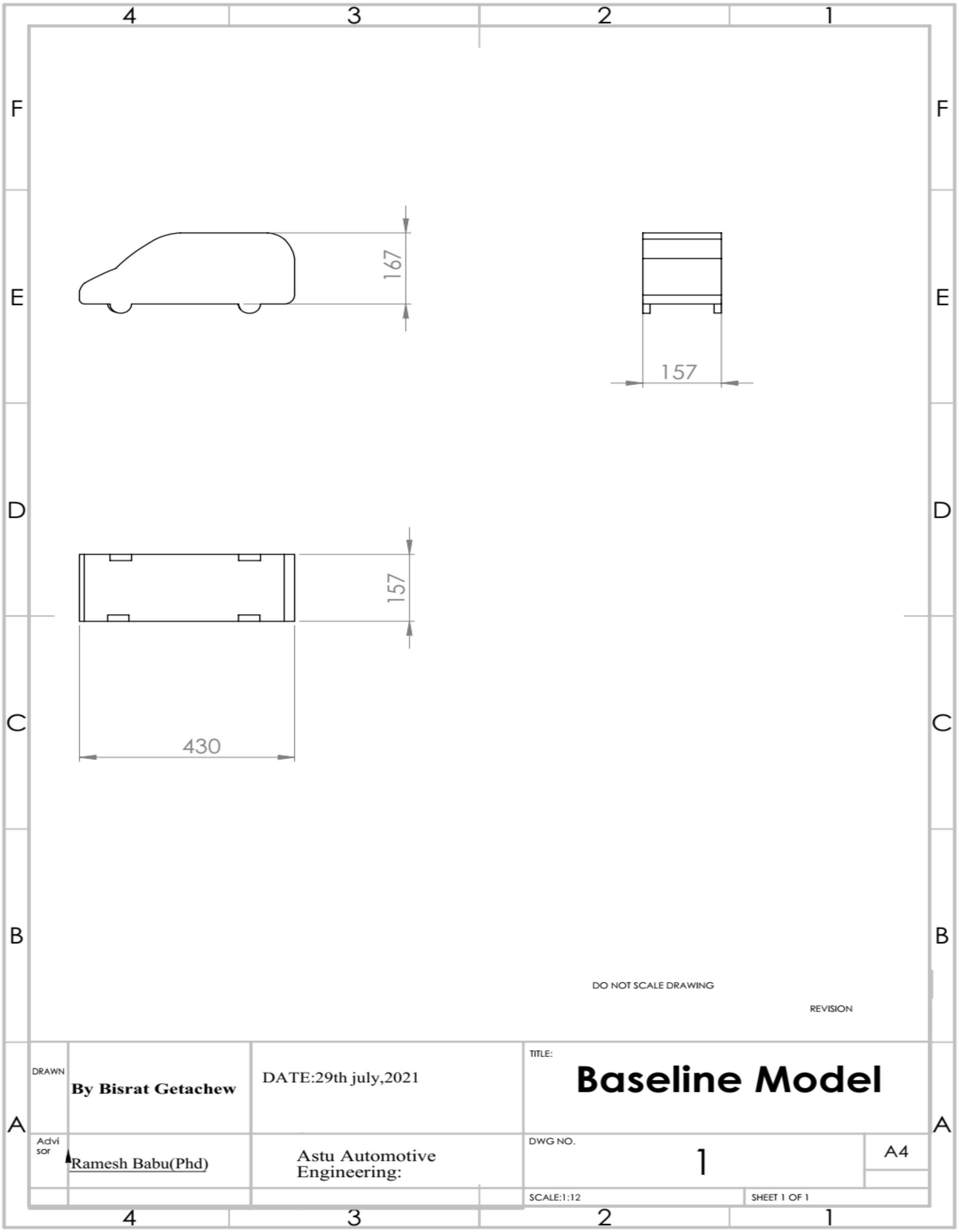

Figure B-1. Baseline model Multiview

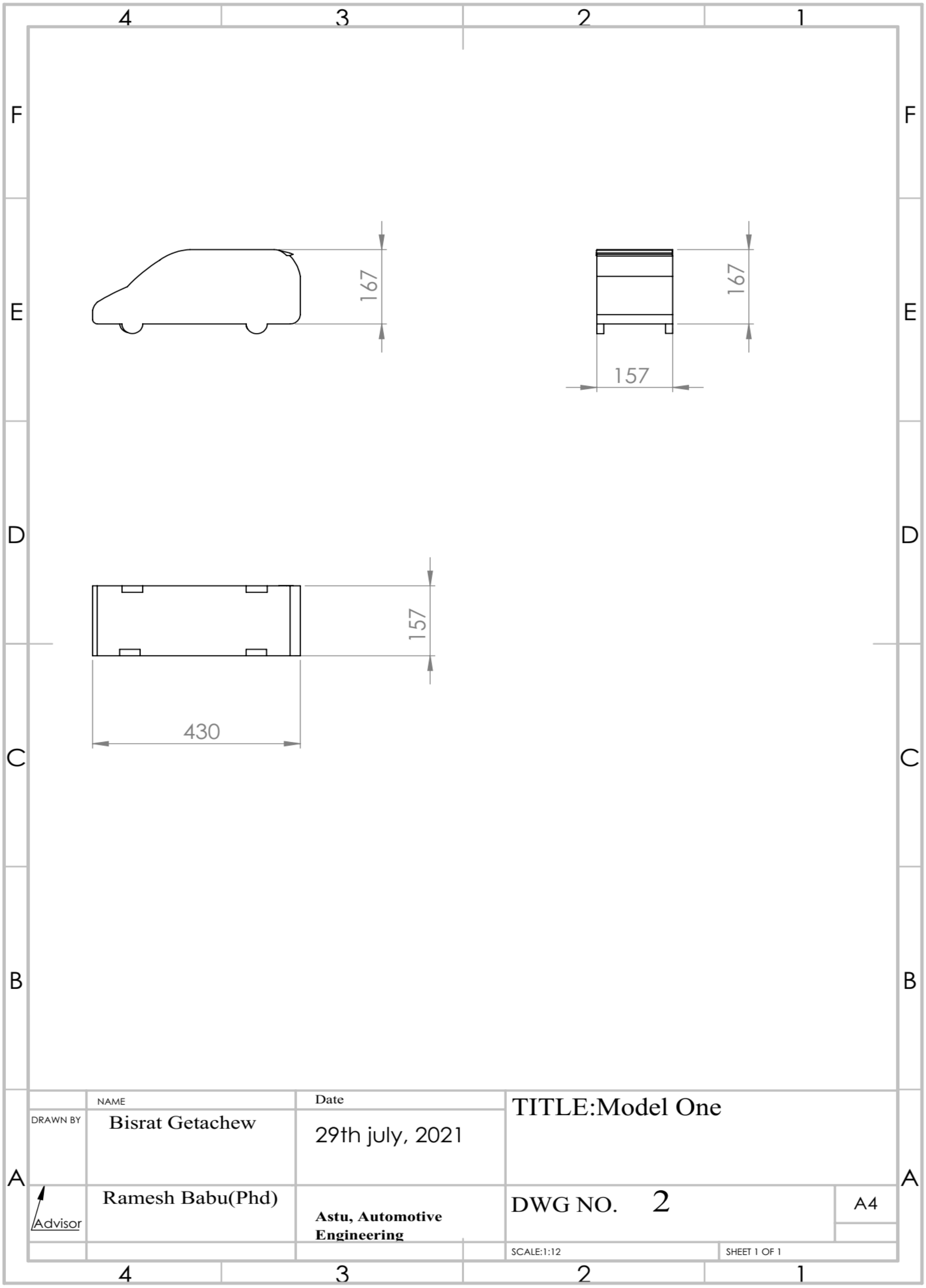

Figure B-2. Model one Multiview

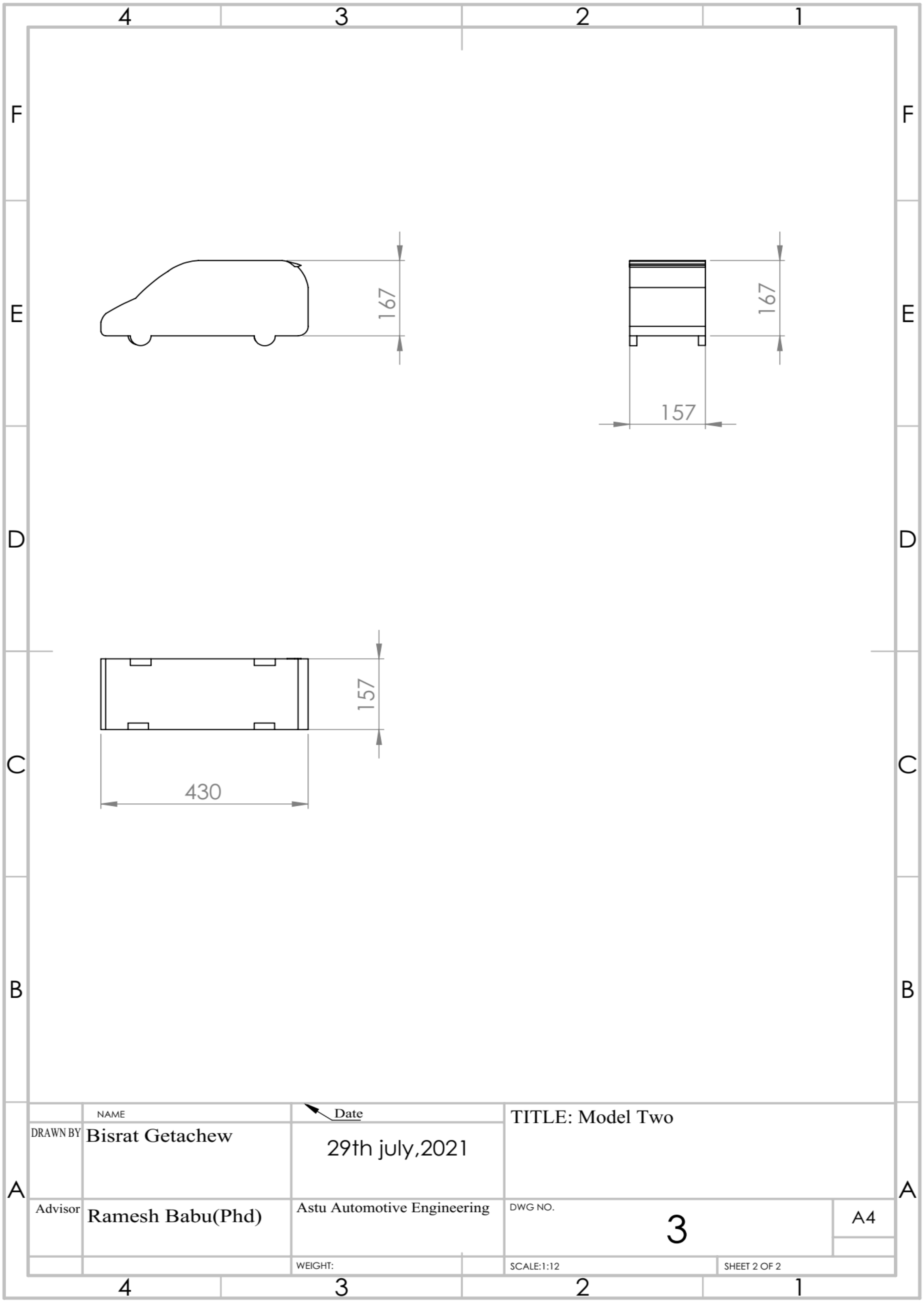

Figure B-3. Model two Multiview

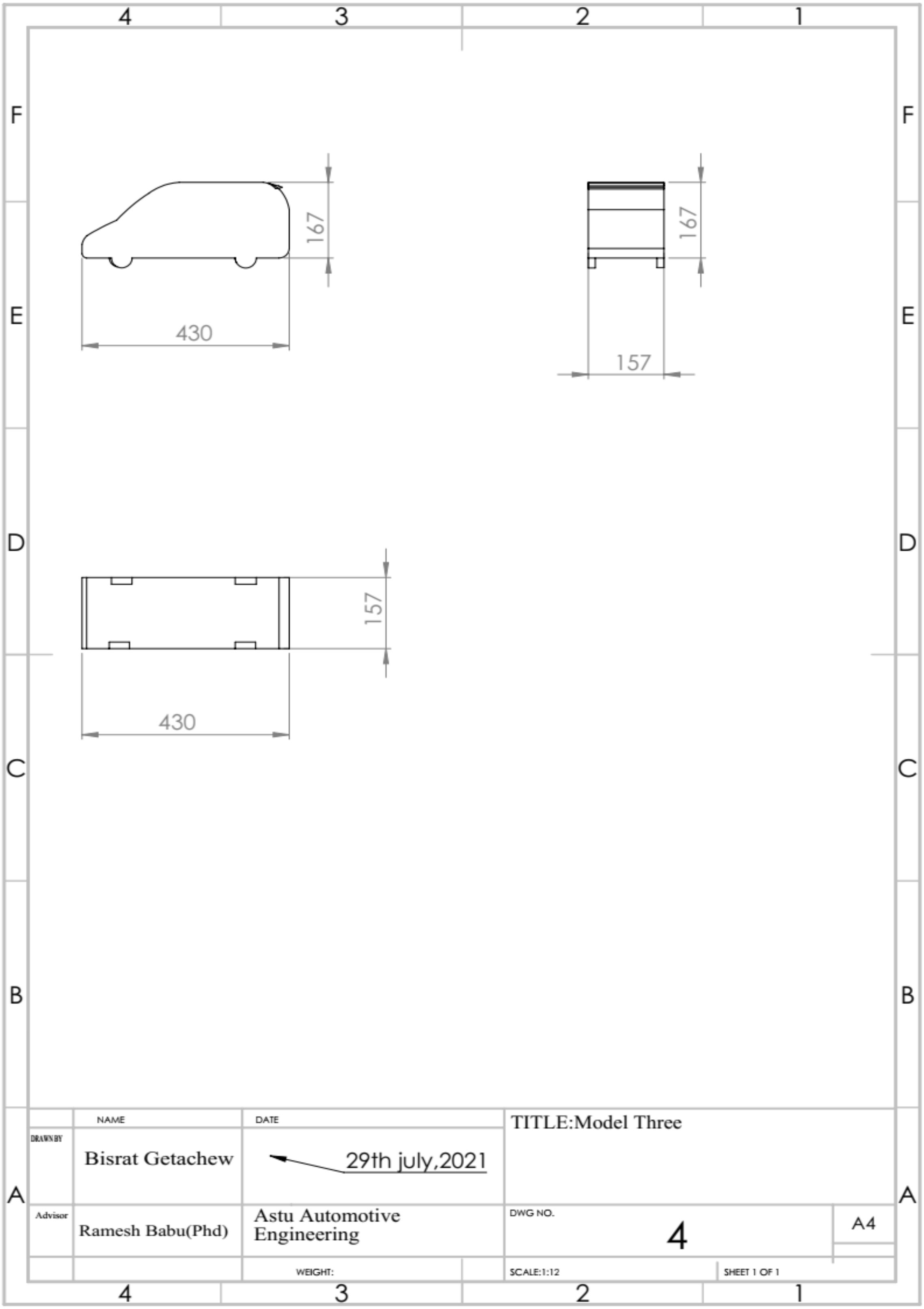

Figure B-4. Model three Multiview

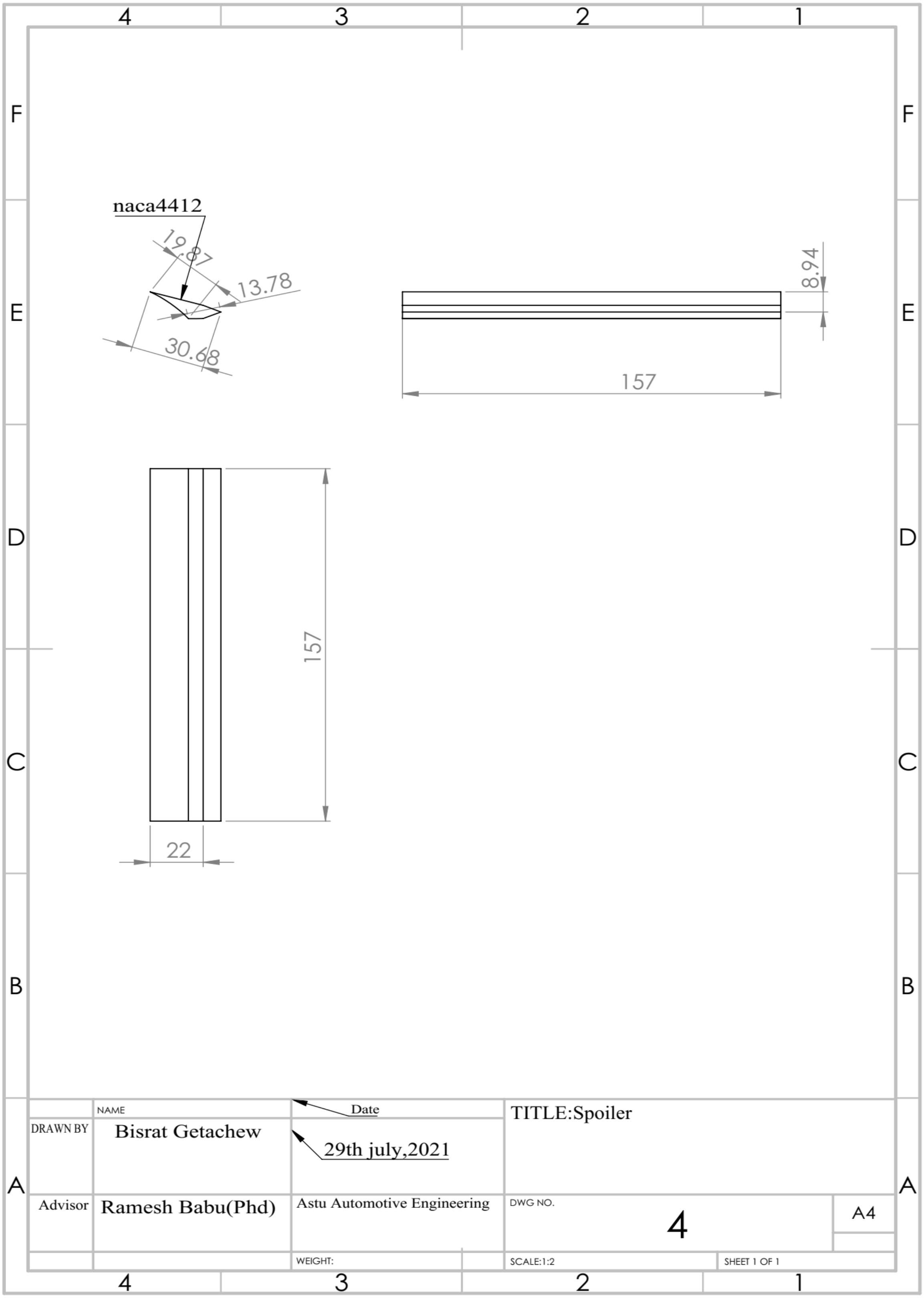

Figure B-5. Spoiler Multiview

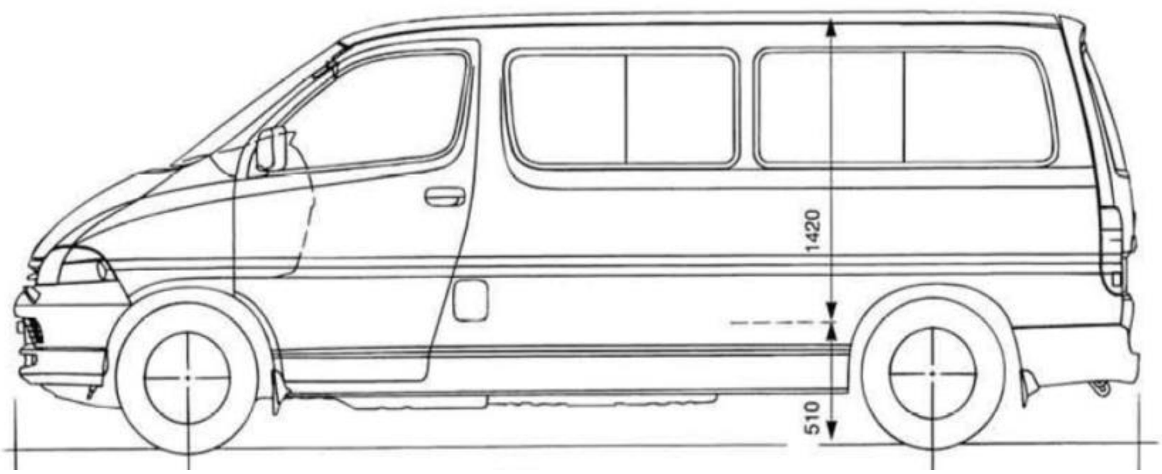

Figure B-6. Selected Toyota HIACE Model (Dolphin)

Basics	
Body style	**Panel Van**
Gearbox	**5/Manual**
Dimensions	
Length	**5240 mm**
Width	**1800 mm**
Height	**1995 mm**
Wheelbase	**3430 mm**
Load Space	
Loads pace Length	**2780 mm**
Load space Width	**1650 mm**

Width Between Wheel arches	**1225 mm**
Load space Height	**1420 mm**
Load space Volume	**5.4 m^3**
Doors	
Rear Door Width	**1650 mm**
Rear Door Height	**1405 mm**
Side Door Width	**1330 mm**
Side Door Height	**1000 mm**
Door Opening (degrees)	**180**
Miscellaneous	
Kerb Weight	**-**
Gross Weight	**3000 kg**
Warranty	**36/60,000**
Service Interval	**20,000/2 Years (Main)**
Fuel Tank Capacity	**75 L**
Maximum Towing Weight	**2000 kg**
Engine	
Engine Size	**2500.0**

Fuel	**Diesel**
Emissions Rating	**Euro 4**

Performance	
Power (bhp)	**117 bhp**
Torque	**294 Nm**

Appendix C: Mesh Details

Table C-1. Baseline Model Mesh Detail

Object Name	*Mesh*
State	Solved
Display	
Display Style	Use Geometry Setting
Defaults	
Physics Preference	CFD
Solver Preference	Fluent
Element Order	Linear
Element Size	Default (0.20264 m)
Export Format	Standard
Export Preview Surface Mesh	No
Sizing	
Use Adaptive Sizing	No
Growth Rate	Default (1.2)
Max Size	Default (0.40528 m)
Mesh Defeaturing	Yes
Defeature Size	Default (1.0132e-003 m)
Capture Curvature	Yes
Curvature Min Size	Default (2.0264e-003 m)
Curvature Normal Angle	Default (18.0°)
Capture Proximity	Yes
Proximity Min Size	Default (2.0264e-003 m)

Num Cells Across Gap	Default (3)
Proximity Size Function Sources	Faces and Edges
Bounding Box Diagonal	4.0528 m
Average Surface Area	0.50732 m²
Minimum Edge Length	1.4493e-002 m
Quality	
Check Mesh Quality	Yes, Errors
Target Skewness	Default (0.900000)
Smoothing	High
Mesh Metric	None
Inflation	
Use Automatic Inflation	None
Inflation Option	Smooth Transition
Transition Ratio	0.272
Maximum Layers	5
Growth Rate	1.2
Inflation Algorithm	Pre
View Advanced Options	No
Assembly Meshing	
Method	None
Advanced	
Number of CPUs for Parallel Part Meshing	Program Controlled
Straight Sided Elements	
Rigid Body Behavior	Dimensionally Reduced

Triangle Surface Mesher	Program Controlled
Topology Checking	Yes
Pinch Tolerance	Default (1.8237e-003 m)
Generate Pinch on Refresh	No
Statistics	
Nodes	246644
Elements	1347035

Table C-2. Model One Mesh Detail

Object Name	*Mesh*
State	Solved
Display	
Display Style	Use Geometry Setting
Defaults	
Physics Preference	CFD
Solver Preference	Fluent
Element Order	Linear
Element Size	Default (0.20264 m)
Export Format	Standard
Export Preview Surface Mesh	No
Sizing	
Use Adaptive Sizing	No
Growth Rate	Default (1.2)
Max Size	Default (0.40528 m)

Mesh Defeaturing	Yes
Defeature Size	Default (1.0132e-003 m)
Capture Curvature	Yes
Curvature Min Size	Default (2.0264e-003 m)
Curvature Normal Angle	Default (18.0°)
Capture Proximity	No
Bounding Box Diagonal	4.0528 m
Average Surface Area	0.33865 m²
Minimum Edge Length	8.5795e-006 m
Quality	
Check Mesh Quality	Yes, Errors
Target Skewness	Default (0.900000)
Smoothing	High
Mesh Metric	None
Inflation	
Use Automatic Inflation	None
Inflation Option	Smooth Transition
Transition Ratio	0.272
Maximum Layers	5
Growth Rate	1.2
Inflation Algorithm	Pre
View Advanced Options	No
Assembly Meshing	
Method	None

Advanced	
Number of CPUs for Parallel Part Meshing	Program Controlled
Straight Sided Elements	
Rigid Body Behavior	Dimensionally Reduced
Triangle Surface Mesher	Program Controlled
Topology Checking	Yes
Pinch Tolerance	Default (1.8238e-003 m)
Generate Pinch on Refresh	No
Statistics	
Nodes	233921
Elements	1324158

Table C-3. Model Two Mesh Detail

Object Name	*Mesh*
State	Solved
Display	
Display Style	Use Geometry Setting
Defaults	
Physics Preference	CFD
Solver Preference	Fluent
Element Order	Linear
Element Size	Default (0.20264 m)
Export Format	Standard
Export Preview Surface Mesh	No

Sizing	
Use Adaptive Sizing	No
Growth Rate	Default (1.2)
Max Size	Default (0.40528 m)
Mesh Defeaturing	Yes
Defeature Size	Default (1.0132e-003 m)
Capture Curvature	Yes
Curvature Min Size	Default (2.0264e-003 m)
Curvature Normal Angle	Default (18.0°)
Capture Proximity	No
Bounding Box Diagonal	4.0528 m
Average Surface Area	0.40601 m²
Minimum Edge Length	8.5795e-006 m
Quality	
Check Mesh Quality	Yes, Errors
Target Skewness	Default (0.900000)
Smoothing	High
Mesh Metric	None
Inflation	
Use Automatic Inflation	None
Inflation Option	Smooth Transition
Transition Ratio	0.272
Maximum Layers	5
Growth Rate	1.2

Inflation Algorithm	Pre
View Advanced Options	No
Assembly Meshing	
Method	None
Advanced	
Number of CPUs for Parallel Part Meshing	Program Controlled
Straight Sided Elements	
Rigid Body Behavior	Dimensionally Reduced
Triangle Surface Mesher	Program Controlled
Topology Checking	Yes
Pinch Tolerance	Default (1.8238e-003 m)
Generate Pinch on Refresh	No
Statistics	
Nodes	247078
Elements	1348589

Table C-4. Model Three Mesh Detail

Object Name	*Mesh*
State	Solved
Display	
Display Style	Use Geometry Setting
Defaults	
Physics Preference	CFD
Solver Preference	Fluent

Element Order	Linear
Element Size	Default (0.20264 m)
Export Format	Standard
Export Preview Surface Mesh	No
Sizing	
Use Adaptive Sizing	No
Growth Rate	Default (1.2)
Max Size	Default (0.40528 m)
Mesh Defeaturing	Yes
Defeature Size	Default (1.0132e-003 m)
Capture Curvature	Yes
Curvature Min Size	Default (2.0264e-003 m)
Curvature Normal Angle	Default (18.0°)
Capture Proximity	No
Bounding Box Diagonal	4.0528 m
Average Surface Area	0.40592 m^2
Minimum Edge Length	8.5795e-006 m
Quality	
Check Mesh Quality	Yes, Errors
Target Skewness	Default (0.900000)
Smoothing	High
Mesh Metric	None
Inflation	
Use Automatic Inflation	None

Inflation Option	Smooth Transition
Transition Ratio	0.272
Maximum Layers	5
Growth Rate	1.2
Inflation Algorithm	Pre
View Advanced Options	No
Assembly Meshing	
Method	None
Advanced	
Number of CPUs for Parallel Part Meshing	Program Controlled
Straight Sided Elements	
Rigid Body Behavior	Dimensionally Reduced
Triangle Surface Mesher	Program Controlled
Topology Checking	Yes
Pinch Tolerance	Default (1.8237e-003 m)
Generate Pinch on Refresh	No
Statistics	
Nodes	247514
Elements	1350619